AD-A147 471 THE DEVELOPMENT OF A HIGH AVERAGE POWER GLASS LASER SOURCE(U) KIGRE INC TOLEDO OH J D MYERS 31 MAY 84 N00014 81-C-2376 1/2

UNCLASSIFIED F/G 20/5 NL

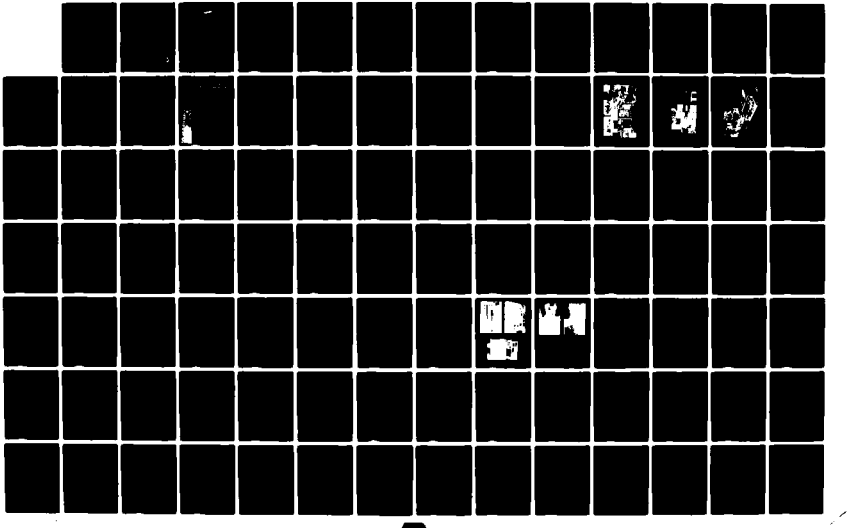

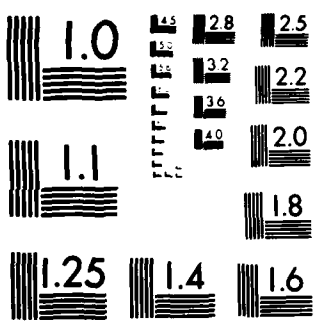

MICROCOPY RESOLUTION TEST CHART
NATIONAL BUREAU OF STANDARDS-1963-A

Report No: N00014-81-C-2376-0002-A003

(12)

THE DEVELOPMENT OF A HIGH AVERAGE POWER GLASS LASER SOURCE

John D. Myers
Kigre, Inc.
5333 Secor Road
Toledo, Ohio 43623
(419) 473-3157

May 31, 1984

Final Report, Period of July 13, 1981 through March 31, 1984
Contract Number N00014-81-C-2376

Approved for Public Release
Distribution Unlimited

Prepared For
Naval Research Laboratory
Washington, DC 20375

DCASMA Detroit
McNamara Federal Building
477 Michigan Ave.
Detroit, MI 48226

SECURITY CLASSIFICATION OF THIS PAGE (When Data Entered)

REPORT DOCUMENTATION PAGE	READ INSTRUCTIONS BEFORE COMPLETING FORM
1. REPORT NUMBER N00014-81-C-2376-0002-A003	2. GOVT ACCESSION NO. / 3. RECIPIENT'S CATALOG NUMBER A147471
4. TITLE (and Subtitle) The Development of A High Average Power Glass Laser Source.	5. TYPE OF REPORT & PERIOD COVERED Final report period of July 13, 1981 thru March 31, 1984 6. PERFORMING ORG. REPORT NUMBER
7. AUTHOR(s) John D. Myers	8. CONTRACT OR GRANT NUMBER(s) N00014-81-C-2376
9. PERFORMING ORGANIZATION NAME AND ADDRESS Kigre, Inc. 5333 Secor Road Toledo, Ohio 43623	10. PROGRAM ELEMENT, PROJECT, TASK AREA & WORK UNIT NUMBERS
11. CONTROLLING OFFICE NAME AND ADDRESS Naval Research Laboratory Washington, D.C. 20375	12. REPORT DATE March 31, 1984 13. NUMBER OF PAGES 146
14. MONITORING AGENCY NAME & ADDRESS(if different from Controlling Office) DCASMA Detroit McNamara Federal Building/477 Michigan Avenue Detroit, Michigan 48226	15. SECURITY CLASS. (of this report) Unclassified 15a. DECLASSIFICATION/DOWNGRADING SCHEDULE
16. DISTRIBUTION STATEMENT (of this Report) Approved for public release Distribution unlimited	
17. DISTRIBUTION STATEMENT (of the abstract entered in Block 20, if different from Report)	
18. SUPPLEMENTARY NOTES	
19. KEY WORDS (Continue on reverse side if necessary and identify by block number) Laser glass, Ion Exchange, Flourescent Conversion, Clad Laser Glass, Phosphate Laser Glass, Silicate Laser Glass, Energy Transfer.	

20. ABSTRACT (Continue on reverse side if necessary and identify by block number)

Objective:
The subject contract has as its objective the development of a high average power glass laser by systematically improving the factors which influence the ability of a laser glass to handle large power levels. Based upon the availability of the athermal laser glass composition Q-100, the rationale used was toward the improvement of the efficiency of a glass laser by developing methods to increase the pumping efficiency and toward the improvement of the

DD FORM 1 JAN 73 1473 EDITION OF 1 NOV 65 IS OBSOLETE

SECURITY CLASSIFICATION OF THIS PAGE (When Data Entered)

(20)
power handling capability of the glass laser rod itself. These incremental developments were broken down as follows:

Task	Objectives
(1)	Characterization of Q-100 Laser Glass:....The measurement of its thermo-physical and thermo-optical properties to better define its engineering design parameters.
(2)	Improve Pumping Efficiency or Q-100:...Primarily by cladding Q-100 with a matching cladding glass which would act as a lense and improve the transfer of pumping energy from the flashlamp.
(3)	Reduce thermal loading of Q-100 by selective filtering of the flashlamp radiation and/or use energy transfer schemes to increase that portion of the flashlamp radiation corresponding to the neodymium pump bands.
(4)	Increase the rupture strength of Q-100 to directly increase its power-handling capability.
(5)	Investigate alternate pump sources to improve efficiency.

Report No: N00014-81-C-2376-0002-A003

THE DEVELOPMENT OF A HIGH AVERAGE POWER GLASS LASER SOURCE

John D. Myers
Kigre, Inc.
5333 Secor Road
Toledo, Ohio 43623
(419) 473-3157

May 31, 1984

Final Report, Period of July 13, 1981 through March 31, 1984
Contract Number N00014-81-C-2376

Approved for Public Release
Distribution Unlimited

Prepared For
Naval Research Laboratory
Washington, DC 20375

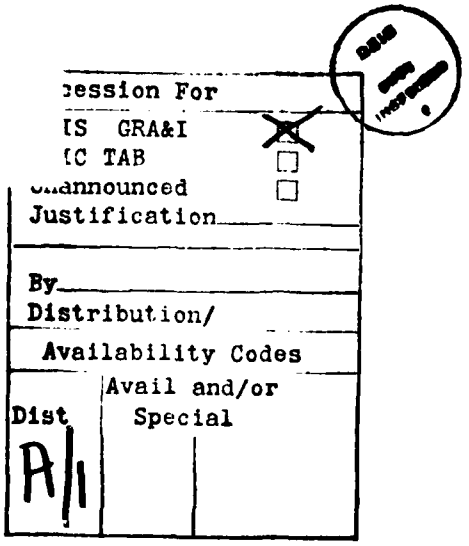

DCASMA Detroit
McNamara Federal Building
477 Michigan Ave.
Detroit, MI 48226

Report No: N00014-81-C-2376-0002-A003

THE DEVELOPMENT OF A HIGH AVERAGE POWER GLASS LASER SOURCE

John D. Myers
Kigre, Inc.
5333 Secor Road
Toledo, Ohio 43623
(419) 473-3157

May 31, 1984

Final Report, Period of July 13, 1981 through March 31, 1984
Contract Number N00014-81-C-2376

Approved for Public Release
Distribution Unlimited

Prepared For
Naval Research Laboratory
Washington, DC 20375

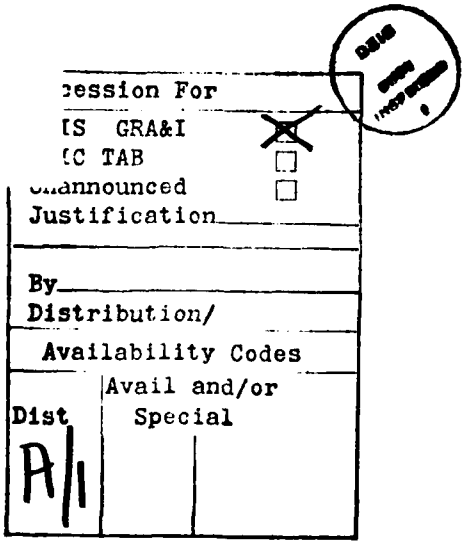

DCASMA Detroit
McNamara Federal Building
477 Michigan Ave.
Detroit, MI 48226

ABSTRACT AND INTRODUCTION

The Development of a High Average Power Glass Laser Source

Objective

The subject contract has as its objective the development of a high average power glass laser by systematically improving the factors which influence the ability of a laser glass to handle large power levels. Based upon the availability of the athermal laser glass composition Q-100, the rationale used was toward the improvement of the efficiency of a glass laser by developing methods to increase the pumping efficiency and toward the improvement of the power handling capability of the glass laser rod itself. These incremental developments were broken down as follows:

Task	Objectives
I	Characterization of Q-100 Laser Glass:....The measurement of its thermo-physical and thermo-optical properties to better define its engineering design parameters.
II	Improve Pumping Efficiency of Q-100:...Primarily by cladding Q-100 with a matching cladding glass which would act as a lense and improve the transfer of pumping energy from the flashlamp.
III	Reduce thermal loading of Q-100 by selective filtering of the flashlamp radiation and/or use energy transfer schemes to increase that portion of the flashlamp radiation corresponding to the neodymium pump bands.
IV	Increase the rupture strength of Q-100 to directly increase its power-handling capability.
V	Investigate alternate pump sources to improve efficiency.

Results

Each of these tasks were designed to add an element necessary to the success of the overall program. A summary of the results of each task is as follows:

Task I Measurement of Q-100's static physical properties were performed by the Thermophysical Properties Research Laboratory at Purdue University and the National Bureau of Standards. The dynamic characterization was carried out by the Naval Research Laboratory and the Naval Weapons Center at China Lake, California. These reports provide a sufficient data base for the design of new systems or retrofitting of existing Nd:YAG systems with laser glass. These reports can be found in Task I.

Task II The Cladding of Q-100.

Q-100 was successfully cladded with a lanthanum phosphate glass, resulting in a 23% increase in efficiency and a lasing threshold reduced by 35%. Extensive research was done into the development of a silicate cladding glass for Q-100 which would maintain cladded Q-100's improved efficiency, while facilitating an ion-exchange process to increase the rupture strength several fold. Although two silicate glasses, SL-8 and SL-11, have properties that are close to the desired specifications, further research is necessary to achieve a practical silicate cladding glass for Q-100.

Task III Selective Filtering and/or Energy Transfer to Reduce Thermal Loading.

Past attempts to reduce thermal loading have, for the most part, involved ideas to limit heating of the laser rod by either modifying the flashlamp radiation or increasing the efficiency of the laser rod. Task III led to the development of a filter glass hereafter designated L-386. Not only does L-386 filter out unusable radiation, but it also transforms a part of the unusable UV radiation into wavelengths that are in the Nd-pump bands via fluorescence, thereby reducing thermal loading and increasing efficiency at the same time. A complete report of research and findings are given in Task III.

Task IV Ion Exchange of Phosphate Glass.

Although some improvement was made in the rupture strength of Q-100 using ion-exchange methods to produce a compression layer, further research needs to be done into this area. A report of methods attempted and their results are given in Task IV along with promising avenues of further investigation.

Task V. Alternative Pump Sources

Although a cerium doped Krypton flashlamp appeared to have a longer life with less fall-off than a Xenon flashlamp, there was no improvement in overall efficiency. A synopsis of our research into this area is given in Task V.

The appendicies have been placed at the end of their respective tasks in order to facilitate convenient reference of research material. Each task is denoted by a colored sheet to provide for quick location.

TASK I

Characteristics of Q-100

TASK I

Characteristics of Q-100

Introduction and Summary

Task I of the referenced contract, was charged with characterizing Q-100 glass in terms of its static and dynamic properties, thereby establishing a base line against which future improvements can be measured.

Static Characterization

The measurement of Q-100's physical properties was carried out by two laboratories. Thermal conductivity and specific heat data (Appendix A) was measured by R. E. Taylor and H. Groat of the Thermophysical Properties Research Laboratory at Purdue University. The data on Young's Modulus, Poisson Ratio, Refractive Index, Viscosity, Thermal Expansion, Temperature Coefficient of Refractive Index, and Photoelastic Constants was collected by Albert Feldman of the National Bureau of Standards (Appendix B). Non-linear Index, Thero-optic Coefficient, Stress-optic Coefficient, and Abbe Number Data was derived at Kigre, Inc. by William Zhong from data submitted by the National Bureau of Standards.

Dynamic Characterization

Five (5) Q-100 rods were sent to Naval Research Laboratory in February, 1982 for testing and evaluation. The same rods were previously sent to the Naval Weapons Center, China Lake, California for evaluation (Appendix C). In an effort to optimize the dynamic thermo-optic properties of Q-100, small compositional adjustments were made in each of the five rods....resulting in the small differences in operating characteristics.

Evaluation of Q-100 Physical Properties

The physical properties of Q-100 laser glass have been measured by NBS recently. The original data list is as follows:

Young's Modules	$E = 5.3 \times 10^{10} Pa$
Poisson Ratio	$\mu = 0.271$

Refractive Index	λ (nm)	n
	486.1	1.5788 = n_F
	546.1	1.5745
	589.3	1.5721 = n_D
	656.3	1.5695 = n_C
	632.8	1.5705
	1152	1.5600

Linear Thermal Expansion Coefficient (0-100°C) $\alpha = 112 \times 10^{-7}/^{o}C$

Thermo-optic Constant (dn/dt) (0-100°C)

$\lambda = 632.8nm$ $\quad B = (^{dn}/_{dT}) = -5.6 \times 10^{-6}/^{o}K$

$\lambda = 1152nm$ $\quad B = (^{dn}/_{dT} = -5.7 \times 10^{-6}/^{o}K$

Piezo-optic Constants

$\lambda = 632.8nm$ $\quad q11 = 1.35 \times 10^{-12} Pa^{-1}$

$q12 = 2.07 \times 10^{-12} Pa^{-1}$

$\lambda = 1152nm$ $\quad q11 = 1.47 \times 10^{-12} Pa^{-1}$

$q12 = 2.17 \times 10^{-12} Pa^{-1}$

* Note 1 Pa (Pascal) = 1 Newton/M^2 = $1.02 \times 10^{-6} Kg/mm^2$

Direct Derivation of Other Properties:

Abbe number $\upsilon_D = \frac{n_{D-1}}{n_F - n_C} = 61.52$

Stress-optical Coefficient

$$C_1 = \Delta n1/p = \frac{n^3}{2} \times q_{12}$$

$$C_2 = \Delta n11/p = \frac{n^3}{2} \times q_{11}$$

$$B = C_1 - C_2$$

At $\lambda = 632.8nm$

$$C_1 = -4.01\times10^{-12}Pa^{-1} = -3.93nm/cm/Kg/cm^2$$

$$C_2 = -2.61\times10^{-12}Pa^{-1} = -2.56nm/cm/Kg/cm^2$$

$$B = -1.40\times10^{-12}Pa^{-1} = -1.37nm/cm/Kg/cm^2$$

At λ = 1152nm

$$C_1 = -4.12\times10^{-12}Pa^{-1} = -4.04nm/cm/Kg/cm^2$$

$$C_2 = -2.79\times10^{-12}Pa^{-1} = -2.74nm/cm/Kg/cm^2$$

$$B = -1.33\times10^{-12}Pa^{-1} = -1.30nm/cm/Kg/cm^2$$

Derivation of Other Thermo-optic and Stress-optic Coefficients

The Thermal-optical Coefficients W P and Q

The thermal-optical coefficient W designates the change of glass in optical pathlength in a unit length with increasing temperature for 1°C (suppose the temperature is evenly distributed throughout the glass):

$$W = B + \alpha (n-1)$$

Thus at λ = 632.8nm

$$W = 0.79\times10^{-6}/^{o}K$$

at λ = 1152nm

$$W = 0.60\times10^{-6}/^{o}K$$

With the coexistance of temperature gradient and stress, the pathlength, difference or wave distortion through a laser glass can be evaluated by a factor P.

$$P = B - \frac{\alpha E}{2(1-\mu)}(C_1+3C_2)$$

The stress-induced optical distortion:

$$Q = \frac{\alpha E}{2(1-\mu)}(C_1-C_2)$$

For Q-100 laser glass, the values of P and Q are:

at 632.8nm $P = -0.78 \times 10^{-6}/^{o}K$

$Q = +0.57 \times 10^{-6}/^{o}K$

at 1152nm $P = -0.62 \times 10^{-6}/^{o}K$

$Q = +0.54 \times 10^{-6}/^{o}K$

Note: For comparison, the W P Q of phosphate laser glasses are in the region of:

$W = -0.25$ to $+1.75 \times 10^{-6}/^{o}K$

$P = -0.6$ to $+1.4 \times 10^{-6}/^{o}K$

$Q = +0.1$ to $+1.1 \times 10^{-6}/^{o}K$

(See V.P. Kravchenko and Yu. P. Rudnitskii, Sov. J. Quantum Electron, V9, 1979, pp. 399-415).

Athermalization Analysis

According to McMahon (private communication) the athermalization would result if:

(1) Both P and Q are small.
(2) $|P| = Q$.

The Q-100 laser glass satisfies these conditions, especially (2).

In addition, as a laser glass is heated up by multipulse pumping, the athermalization condition can be achieved when:

$P = Q/2$ for rods

$P = Q$ for slabs

Assuming that $\frac{dP}{dt} = 1.5 \times 10^{-8}/^{o}C$

and $\frac{dQ}{dt} = 0$

The athermal temperatures of Q-100 are:

$$\Delta Ta = T \text{ oper.} - T \text{ room} = (P - Q/2)/\frac{dP}{dt} \text{ for rods;}$$

$$\text{and } \Delta Ta = (P-Q)/\frac{dP}{dt} \text{ for slabs}$$

we get: (at 1152nm, which is close to 1.05 μm)

$$\Delta Ta = 59^{o}C \text{ for rods}$$

$$\text{and } \Delta Ta = 77^{o}C \text{ for slabs}$$

These athermal temperatures approximate practical operating temperatures for repetitively pulsed glass laser materials quite well.

Nonlinear Refractive Index

The nonlinear refractive index, n_2, can be estimated from the equation derived by A. Glass (LLL UCRL, 1974 p. 259)

$$n_2 = \frac{68(n_D-1)(n_D^2+2)^2 \times 10^{-13}}{\nu D(1.517+((n_D^2+2)(n_D+1)\nu D)/6n_D)^{1/2}} \text{ cgs. esu.}$$

Substituting the value of n_D and ν_D of the Q-100 glass in the equation, we get the estimated nonlinear refractive index of Q-100:

$$n_2 = 1.45 \times 10^{-13} \text{ cgs. esu.}$$

The optical divergence under high-intensity laser pumping can be characterized by the ratio $^{n2}/n$. According to the data from Krevchenko, V.B. et.al. (1979), they are ranging from 0.69 to 1.06 for phosphate glasses. The estimated value of $^{n2}/n$ for Q-100 is:

$$^{n2}/n = 1.45/1.57 = 0.92$$

APPENDIX A

TPRL

THERMOPHYSICAL PROPERTIES RESEARCH LABORATORY

TPRL 317

THERMOPHYSICAL PROPERTIES OF A GLASS

A Report to Kigre, Inc.

by

R.E. Taylor and H. Groot

February 1983

School of Mechanical Engineering

Purdue University, West Lafayette, Indiana

TABLE OF CONTENTS

LIST OF TABLES

LIST OF FIGURES

THERMOPHYSICAL PROPERTIES OF A GLASS

INTRODUCTION

Samples of a Nd-doped phosphate glass designated as Q-100 were submitted by Kigre, Inc. for thermal diffusivity (α), specific heat (C_p), and density (ρ) determinations. Thermal conductivity values were calculated as the product of these three quantities, i.e., $\lambda = \alpha C_p \rho$.

Thermal diffusivity measurements were made using the laser flash technique. The flash method, in which the front face of a small disc-shaped sampled is subjected to a short laser burst and the resulting rear face temperature rise is recorded, is used in over 80% of the present thermal diffusivity measurements throughout the world. The method is shown schematically in Figure 1, which includes a visual display of the rear face temperature rise curve. The half-time ($t_{1/2}$) is determined as the time required for this rise to reach one-half of its maximum value (Figure 1). Thermal diffusivity (α) is calculated from the half-time and sample thickness (ℓ) according to the equation $\alpha = 0.13885\ \ell^2/t_{1/2}$. Actually values of α are calculated at other rise times as well, for example 20%, 25%, 30%, 33 1/3%, 40%, etc., in addition to the 50% (half-time) rise. The equation then is $\alpha = K_x\ \ell^2/t_x$ where x is the percent rise, K_x are constants calculated from the theoretical model, and t_x is the time required to reach x% rise.

A highly developed apparatus exists at TPRL (Figure 2) and we have been involved in an extensive program to evaluate the technique and broaden its uses. The apparatus consists of a Korad K2 laser, a high vacuum system including a bell jar window for viewing the sample, a tantalum or stainless steel tube heater surrounding a sample holding assembly, a spring-loaded thermocouple and an IR detector, appropriate biasing circuits, amplifiers, A-D converters, crystal clocks, and a minicomputer-based digital data acquisition system (Figure 3) capable of accurately taking data in the 40 microsecond and longer time domain. The computer controls the experiment, collects the data, calculates the results, and compares the raw data with the theoretical model. For a transparent material, such as the present material, a thin disk of graphite is bonded to the front surface and a very thin coating of high temperature black

paint is applied to the rear surface. The thermophysical properties of the graphite layer are known and the effects of this layer are taken into account using a data analysis based on two layers in series subjected to a short energy flash on the surface of one layer. The purpose of the graphite layer is to absorb the laser beam and to prevent large temperature gradients in the sample. The very thin layer of paint on the rear surface is to provide an opaque surface for the IR detector monitoring the resulting rear surface temperature rise.

Specific heat (C_p) was measured using a standard Perkin-Elmer Model DSC-2 Differential Scanning Calorimeter (Figure 4) using sapphire as the reference material. The standard and sample, both encapsulated in aluminum pans were subject to the same heat flux and the differential power required to heat the samples at the same rate was recorded using the same digital data acquisition system. From the mass of the sapphire standard, sample and aluminum pans, the differential power, and the known specific heat of sapphire, the specific heat of the sample is computed.

The thermal conductivity values for the materials were determined at even temperature intervals using the realtion $k = \alpha C_p d$, where d is the bulk density. Smoothed values of α and C_p were used. The data are not corrected for thermal expansion. All measured quantitites are directly traceable to NBS standards.

RESULTS AND DISCUSSION

The specific heat results at 25°C intervals are given in Table 1 and are plotted in Figure 5. Actually, these data are only one-fifth of the data taken as values were obtained at 5°C intervals. The material begins to soften above 400°C and the specific heat determination was terminated at this temperature.

The thermal diffusivity sample was 0.0870 inches thick, 0.4910 inches diameter and weighed 0.8656 gms. Therefore its bulk density was 3.207 gms cm^{-3}. To this sample a 0.0003 inch layer of paint was applied to the rear surface and a 0.0115 inch thick graphite disk was bonded to the front surface using a 0.0037 inch layer of E-solder. The diffusivity and conductivity values

were calculated simultaneously from the experimental data. These data are the thicknesses of the front graphite layer and the sample, the density and specific heat of each layer, the diffusivity of the graphite layer and the measured half-time. The results are given in Table 2. Thermal diffusivity values are plotted in Figure 6 and thermal conductivity values are plotted in Figure 7. Above 400°C, we have evidence that the specific heat results increase rapidly and the thermal diffusivity results decrease rapidly. However, the results are not accurate enough to calculate thermal conductivity values above 400°C.

TABLE 1

SPECIFIC HEAT RESULTS

TEMP. (°C)	TEMP (°F)	C_p (W sec $gm^{-1}K^{-1}$)
57	134	0.6242
77	170	0.6414
102	215	0.6599
127	260	0.6784
152	305	0.6949
177	350	0.7105
202	395	0.7258
227	440	0.7400
252	485	0.7559
277	530	0.7678
302	575	0.7829
327	620	0.7976
352	665	0.8123
377	710	0.8285
402	755	0.8543

TABLE 2

THERMAL DIFFUSIVITY AND CONDUCTIVITY RESULTS

TEMP. (°C)	DENSITY ($gm\ cm^{-3}$)	SPECIFIC HEAT ($Ws\ gm^{-1}K^{-1}$)	DIFFUSIVITY ($cm^2\ sec^{-1}$)	CONDUCTIVITY ($W\ cm^{-1}K^{-1}$)	CONDUCTIVITY (BTU in $hr^{-1}ft^{-2}F^{-1}$)	TEMP. (°F)
23	3.207	0.590	0.00282	0.00534	3.70	73
103	3.207	0.660	0.00266	0.00563	3.90	217
200	3.207	0.724	0.00271	0.00629	4.36	392
309	3.207	0.787	0.00244	0.00616	4.27	588
400	3.207	0.852	0.00233	0.00637	4.41	752

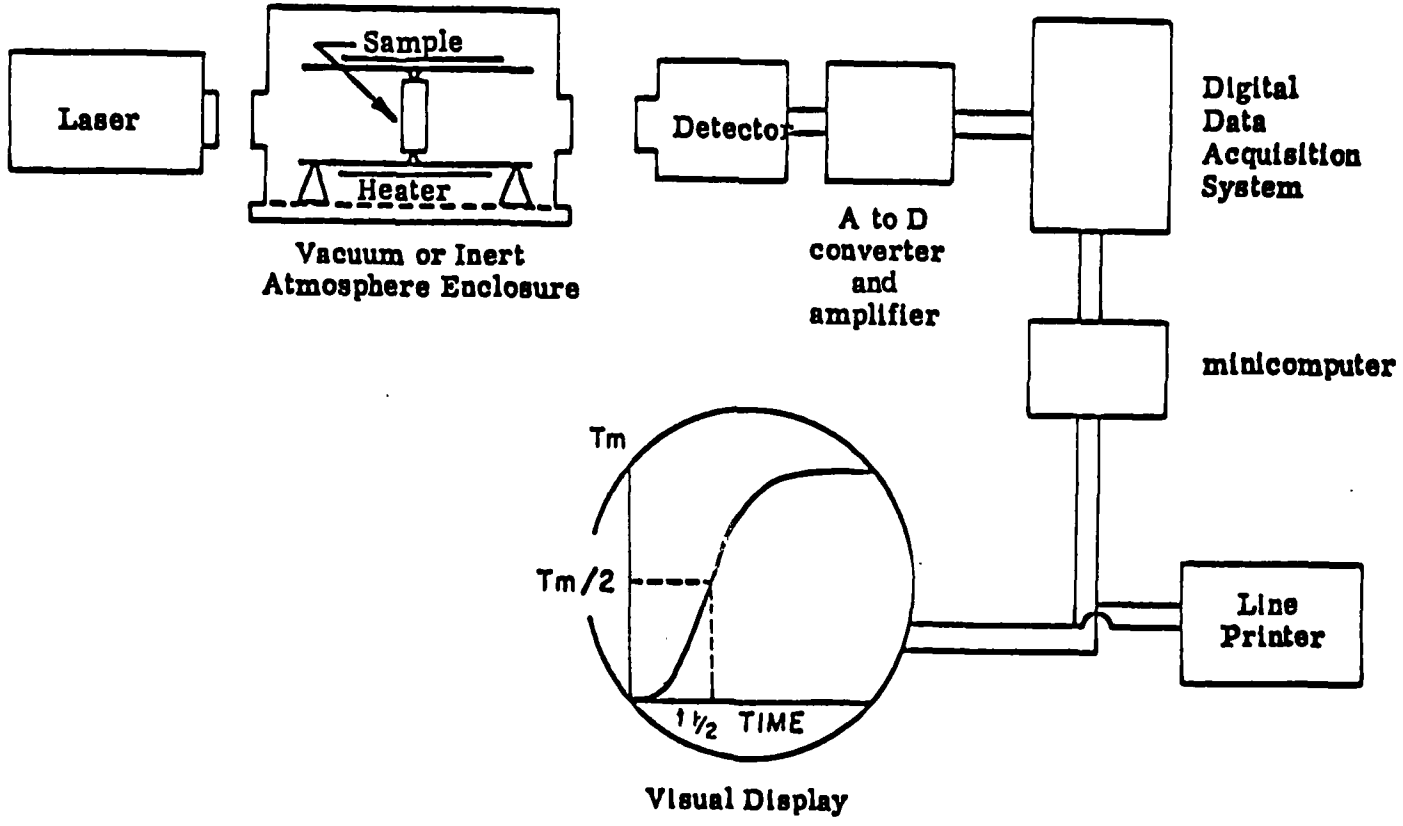

FIGURE 1. Laser Flash Diffusivity (Schematic)

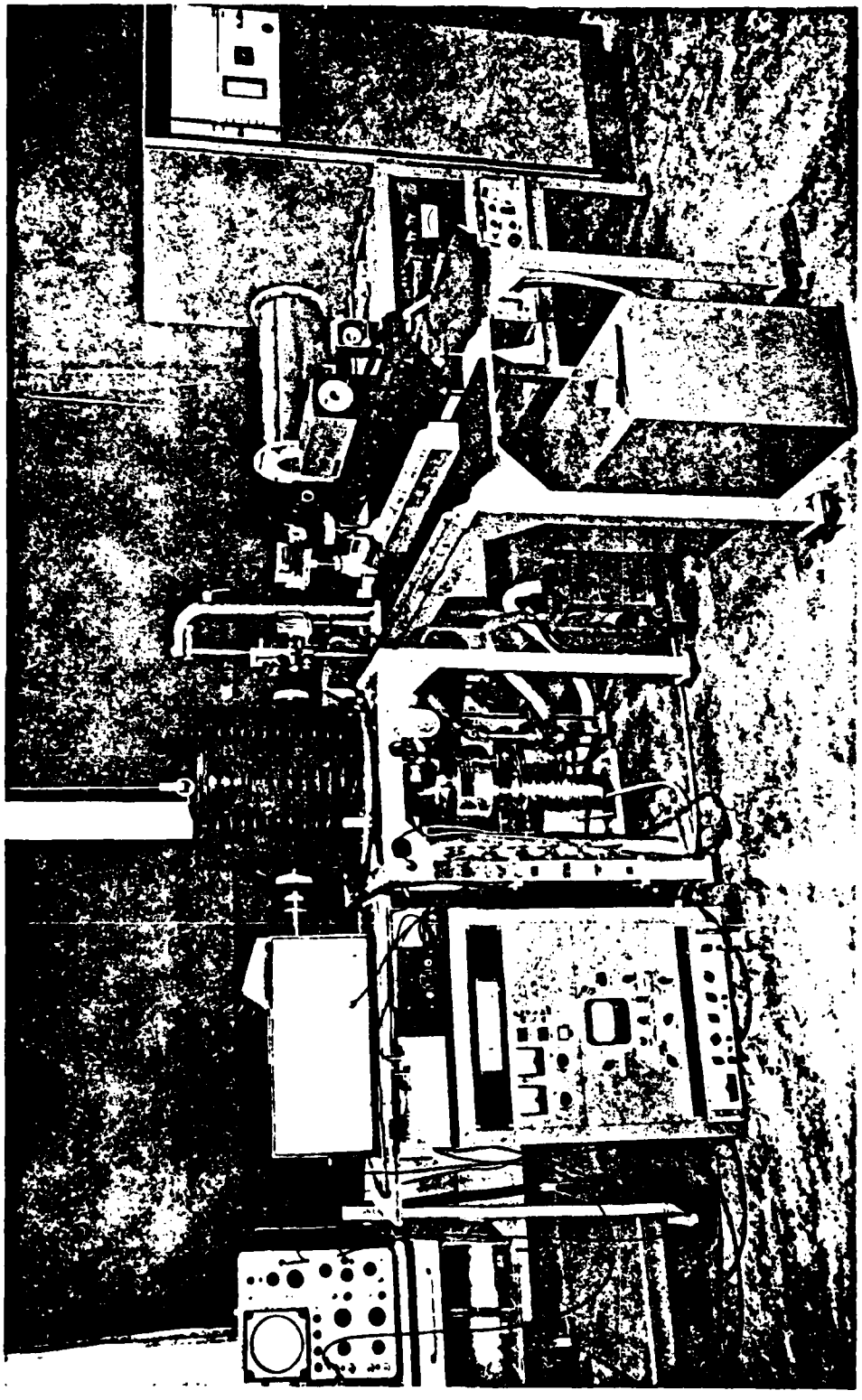

Figure 2. Laser Flash Diffusivity Apparatus

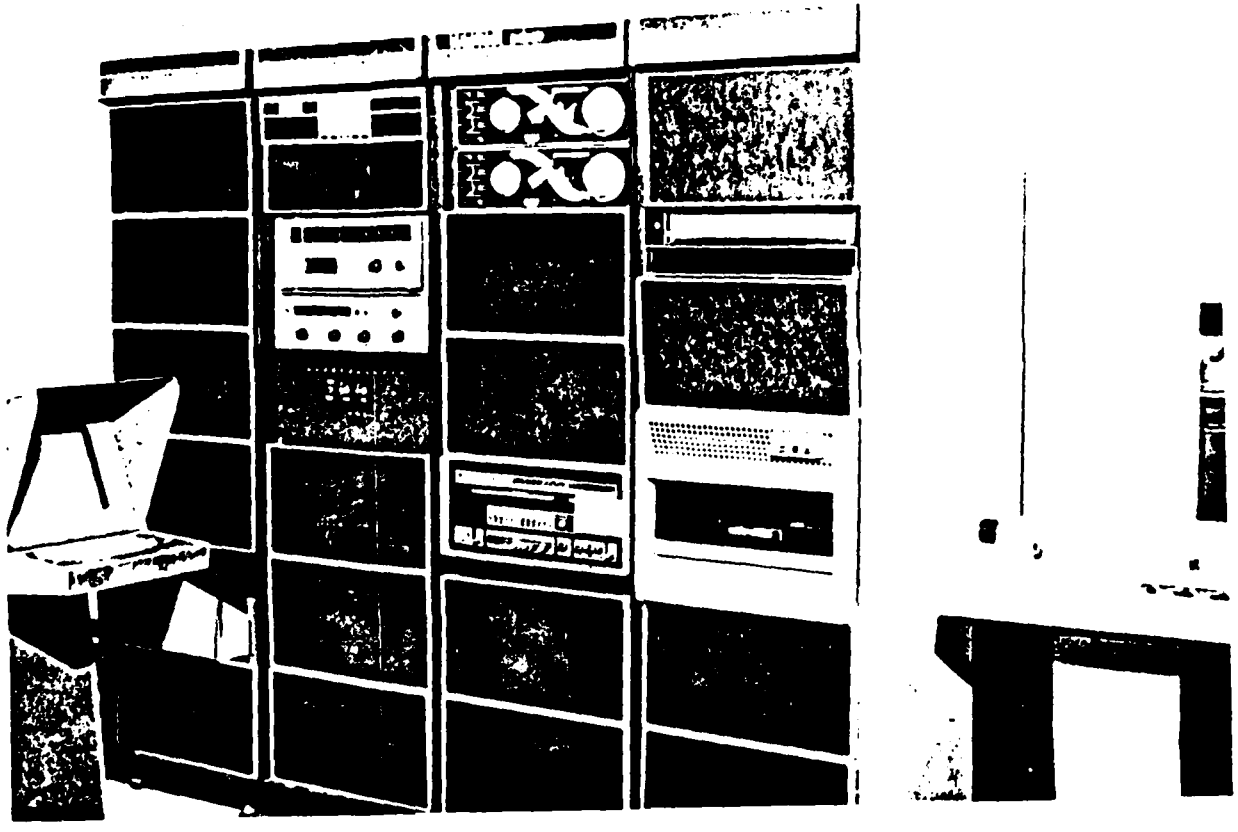

Figure 3. Digital Data Acquisition System

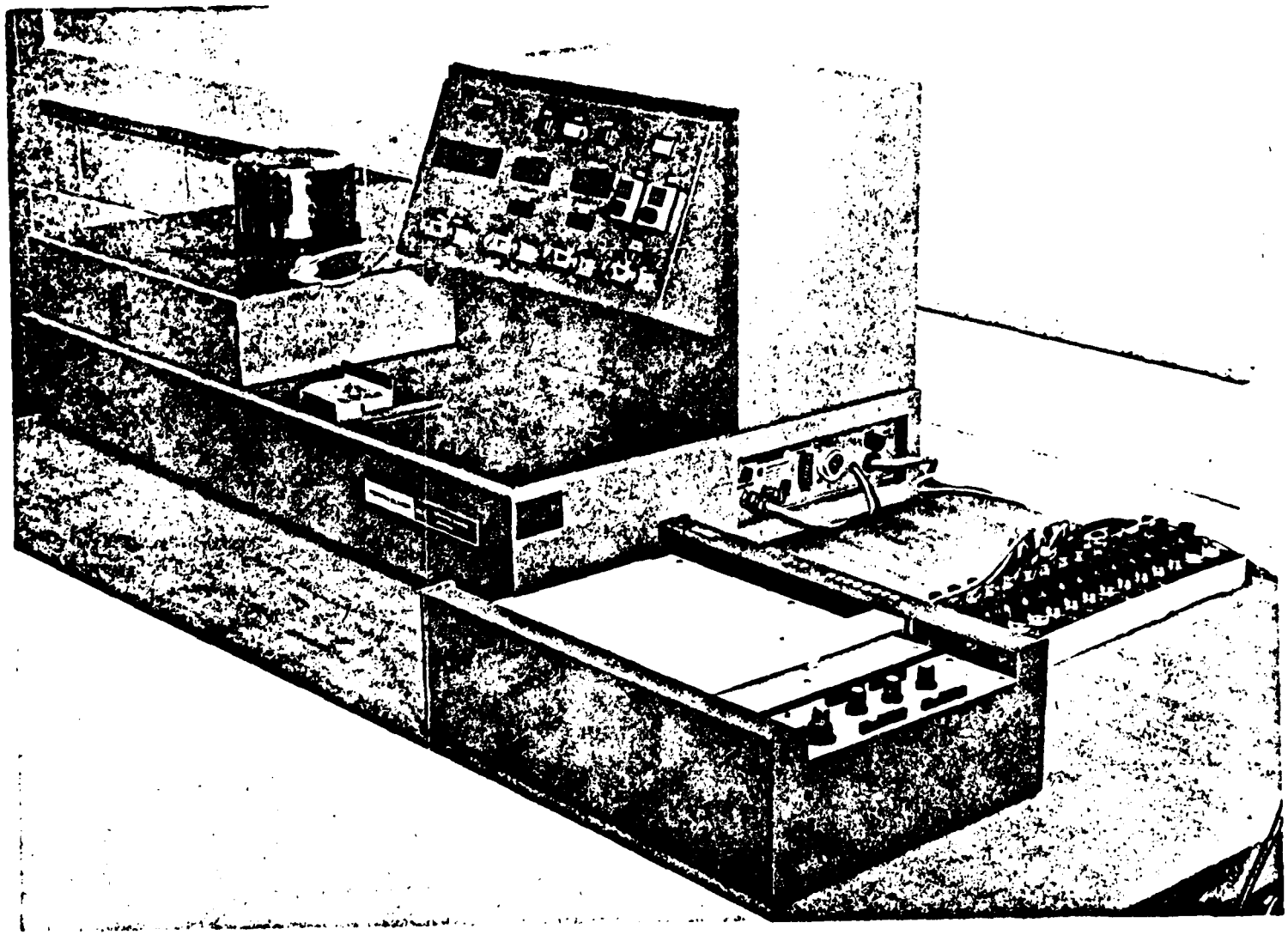

Figure 4. Differential Scanning Calorimeter

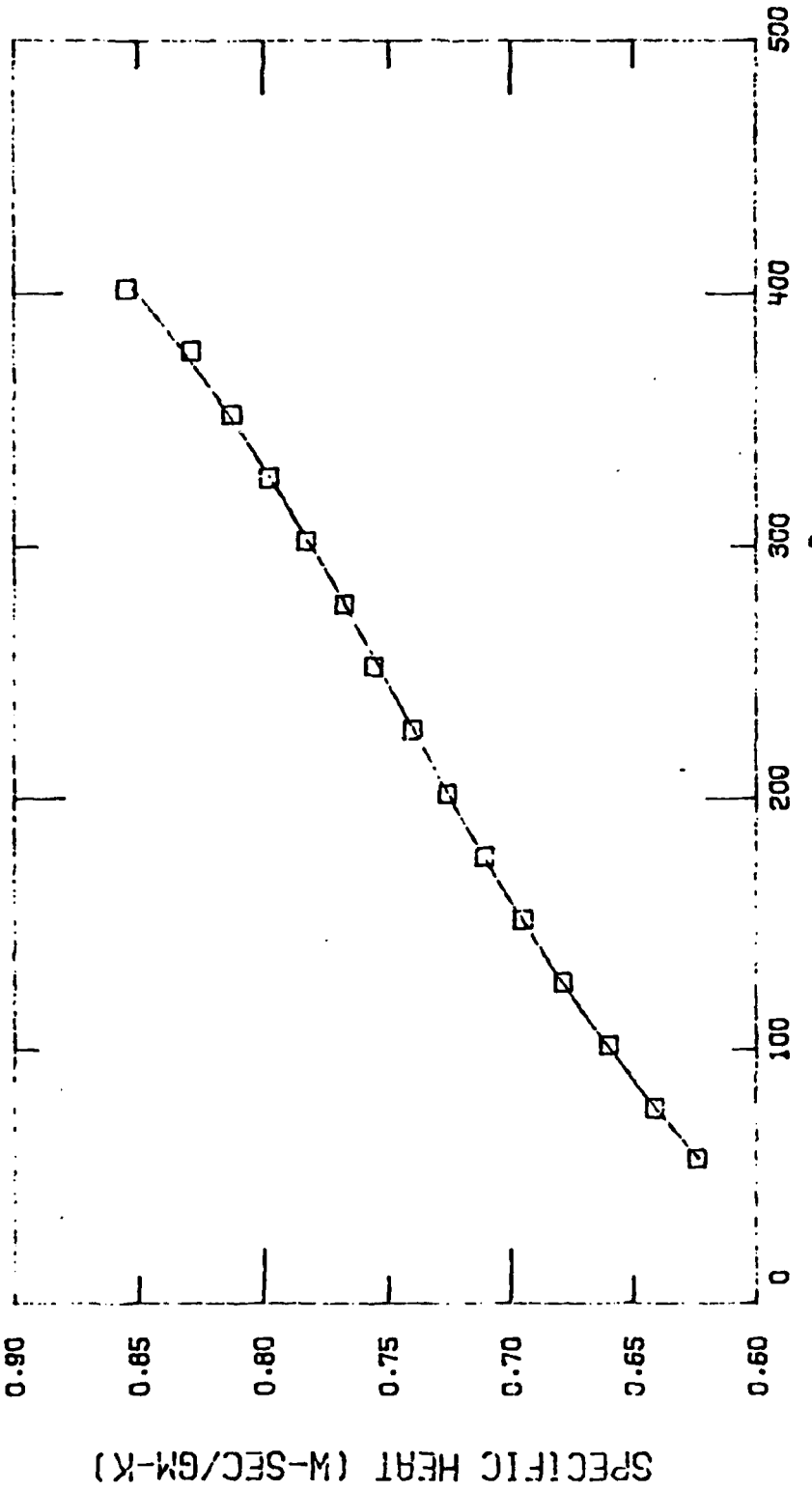

Figure 5. Specific Heat

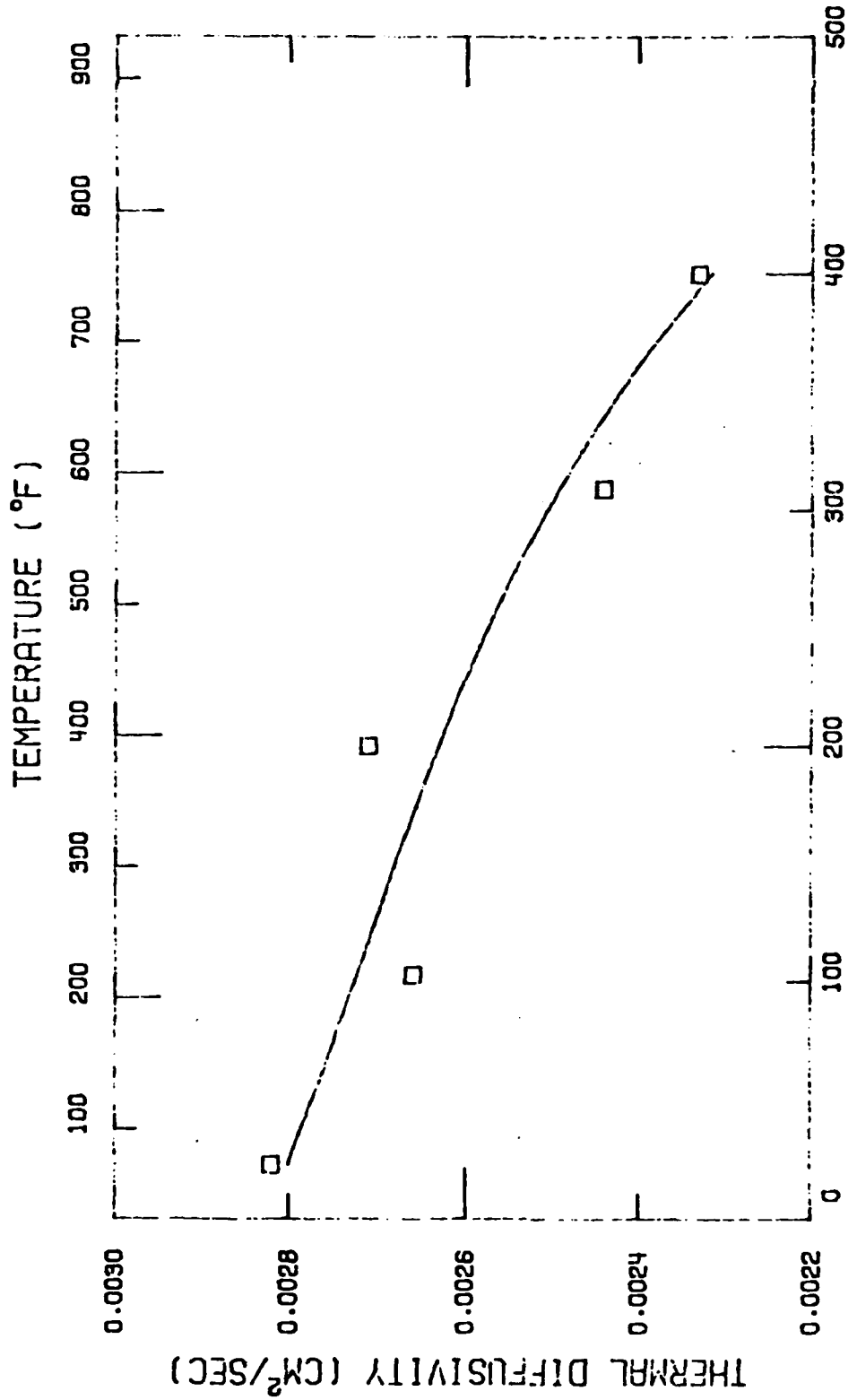

Figure 6. Thermal Diffusivity

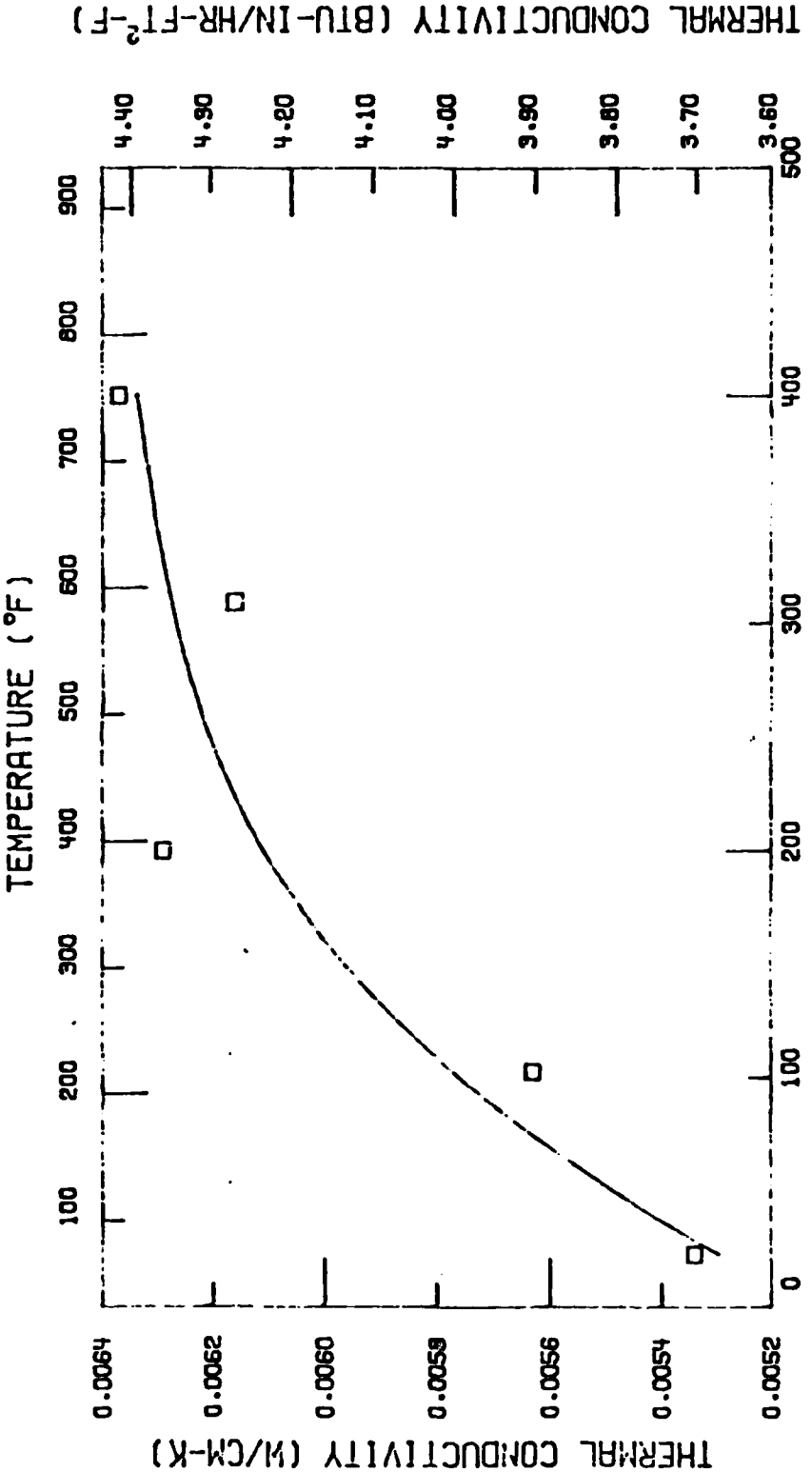

Figure 7. Thermal Conductivity

APPENDIX B

NBS DATA

Kigre Q-100 Glass

Young's Modulus $E = 5.3 \times 10^{10}$ Pa

Poisson Ratio $\mu = 0.271$

Refractive Index

Measurements of the refractive index of Q-100 were conducted on two precision spectrophotometers by the method of minimum deviation and measured relative to the refractive index of air, n_a, which is about 1.0003 over the full wavelength of measurement.

Using the minimum deviation technique, collimated radiation is passed through a specimen which is in the form of a triangular prism. The prism is rotated about an axis parallel to the prism apex until a position is found where the angular deviation of the beam at a chosen wavelength is a minimum. In terms of the minimum deviation angle D, the angle between the emergent beam and an undeviated beam, and the prism angle A, the refractive index is given by

$$n = \frac{\text{Sin } \frac{D+A}{2}}{\text{Sin } \frac{A}{2}}$$

λ(nm)	n
486.1	1.5788
546.1	1.5745
589.3	1.5721
656.3	1.5695
632.8	1.5705
1152	1.5600

Linear Thermal Expansion Coefficient (0-100°C) $\alpha = 112 \times 10^{-7}/^{\circ}C$

The linear Thermal expansion coefficient of Q-100 was measured by an interferometric technique. In this technique a specially prepared specimen is placed between two optic flats, Fizeau interference figures are observed when monochromatic radiation from a helium-neon laser is

reflected from the two surfaces in contact with the specimen. These fringes are observed to shift as a function of temperature due to thermal expansion of the specimen.

Thermo-optic Constant (dn/dT) (0-100°C)

The thermo-optic constant is measured by an interferometric technique at discrete laser wavelengths over the temperature range of 0°C to 100°C. Observations are made of the shift of Fizeau interference fringes formed from reflections off the surfaces of an optical specimen polished plane parallel as a function of temperature.

λ = 632.8 nm (dn/dT) = -5.6×10^{-6}/K

λ = 1152 nm (dn/dT) = -5.7×10^{-6}/K

Piezo-optic Constants

Measurements of piezo-optic constants at λ=632.8nm and λ=1152nm were carried out using a modified Dyson Interfermeter and a Twyman-Green Interferometer respectively. A complete explanation of methods used can be found in an article by Albert Feldman, Measurement of the Photoelastic Constants of Optical Materials in the September-October, 1978 issue of Optical Engineering, Volume 17, Number 5, Page 453.

λ = 632.8 nm $q_{11} = 1.35 \times 10^{-12}$ Pa^{-1}

$q_{12} = 2.07 \times 10^{-12}$ Pa^{-1}

λ = 1152 nm $q_{11} = 1.47 \times 10^{-12}$ Pa^{-1}

$q_{12} = 2.17 \times 10^{-12}$Pa^{-1}

Thermal Expansion

Static measurements from room temperature to 150°C give a thermal expansion coefficient of 113.9×10^{-7}/°C using a pushrod dilatometer.

Also included are plots of $\Delta L/L$ on heating and cooling at rates of approximately 2°C/min. The line through the points on the heating curve are described by a fourth degree polynomial.

$$\Delta L/L = -2.985 \times 10^{-4} + 1.1996 \times 10^{-5}\, T - 3.2334 \times 10^{-9}\, T^2 + 2.0994 \times 10^{-11}\, T^3 - 2.6930 \times 10^{-14}\, T^4$$

The lines through the points on the cooling curve are described by a fifth degree polynomial:

$$\Delta L/L = -2.4812 \times 10^{-3} + 5.8583 \times 10^{-5}\, T - 4.8104 \times 10^{-7}\, T^2 + 2.3337 \times 10^{-9}\, T^3 - 5.3791 \times 10^{-12}\, T^4 + 4.7785 \times 10^{15}\, T^5 .$$

Thermal expansion coefficients between two points may be calculated using the following expression:

$$\alpha = \frac{(\Delta L/L)_1 - (\Delta L/L)_2}{T_1 - T_2} - 5.4 \times 10^{-7}/°C.$$

Viscosity

The softening point, annealing and strain points were determined using ASTM procedures C336 and C338 respectively.

Softening Point	492 °C
Annealing Point	399 °C
Strain Point	376 °C

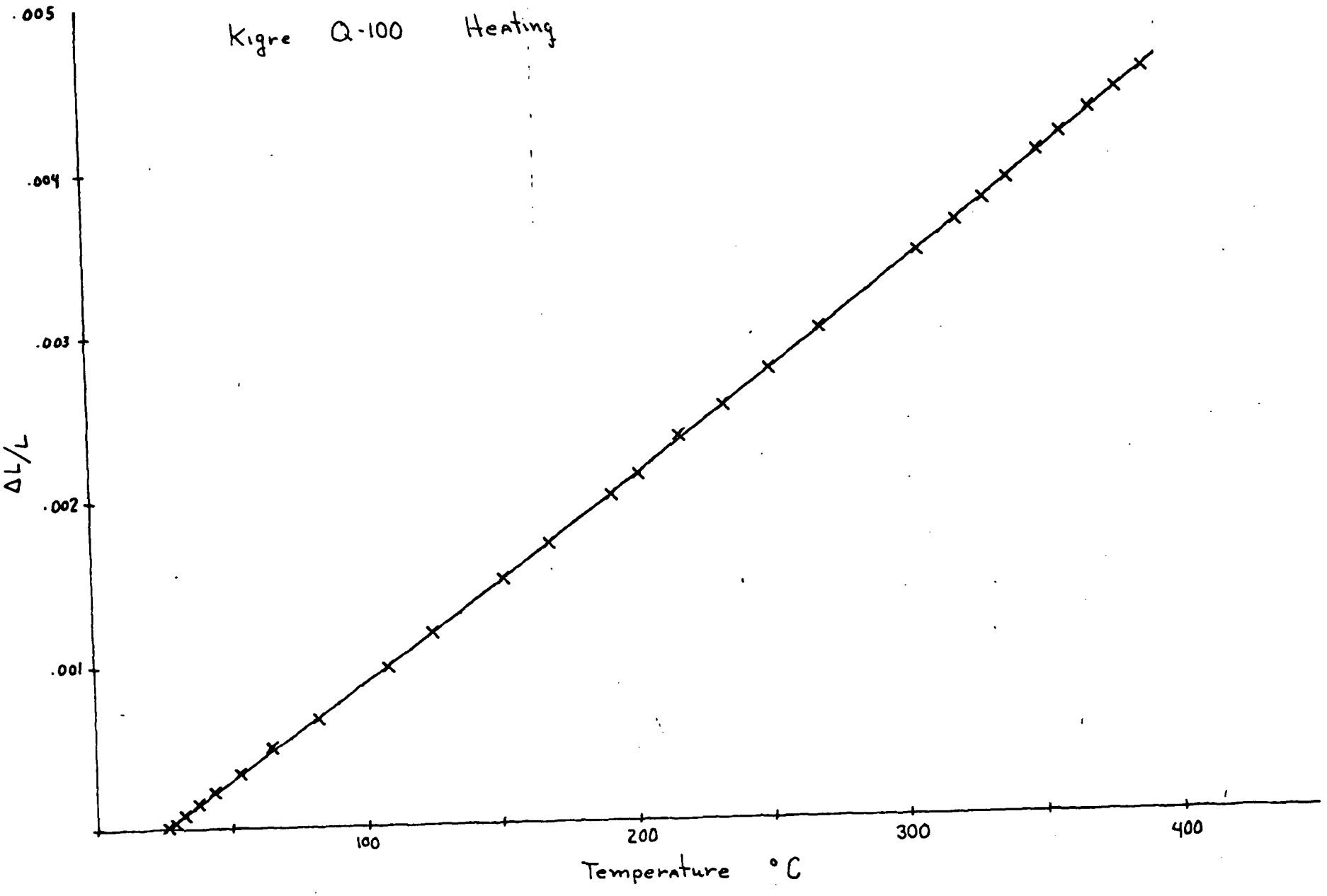
Kigre Q-100 Heating
.005
.004
.003
.002
.001
ΔL/L
100
200
300
400
Temperature °C

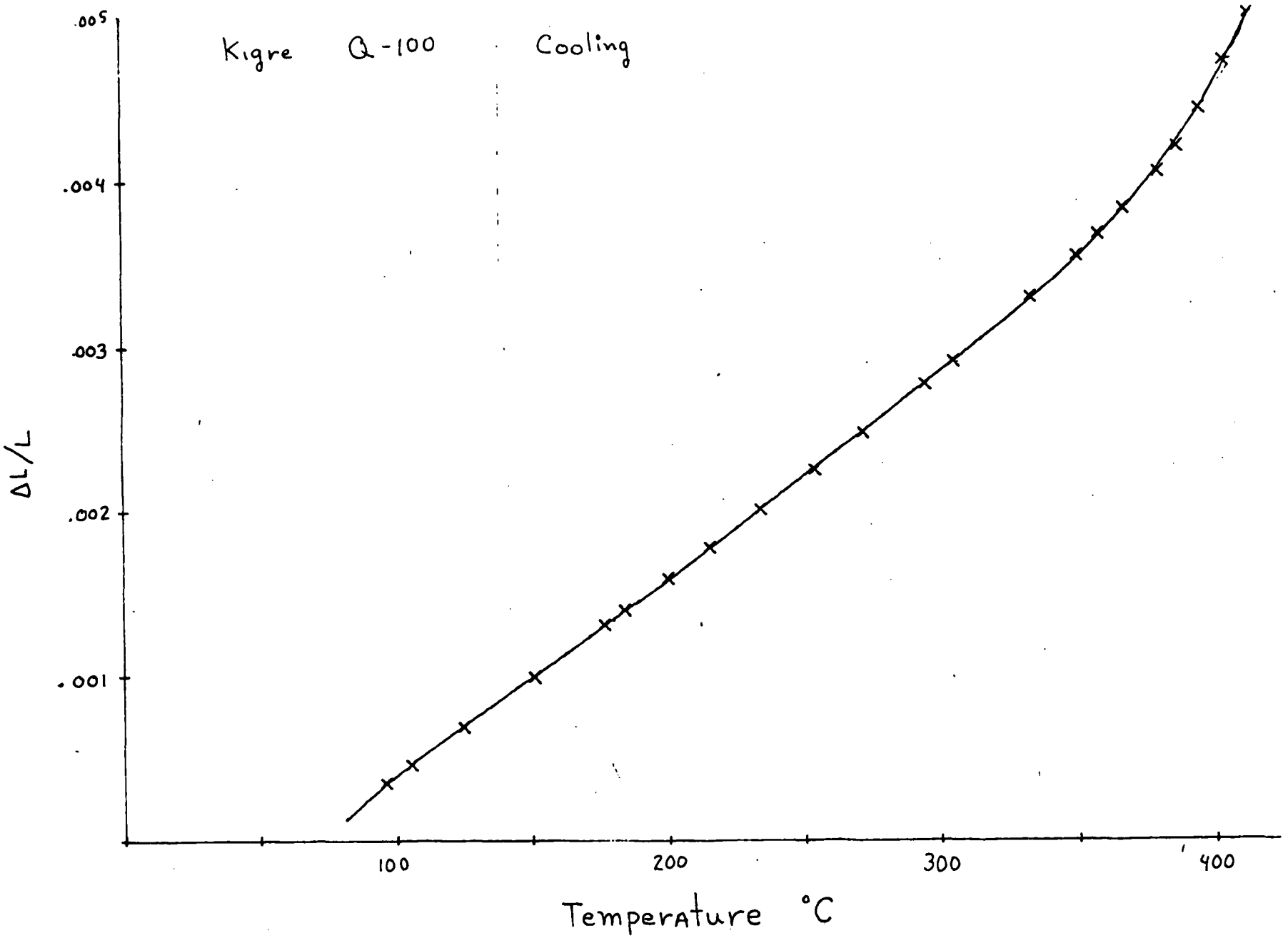
Kigre Q-100 Cooling
.005
.004
.003
.002
.001
ΔL/L
100
200
300
400
Temperature °C

APPENDIX C

DEPARTMENT OF THE NAVY
NAVAL WEAPONS CENTER
CHINA LAKE, CALIFORNIA 93555

IN REPLY REFER TO:
3151/DWR:gb
Reg 3151-118
13 Nov 1981

MEMORANDUM

From: D.W. Ricks, Laser Systems Branch (Code 3151)
To: Head, Laser Systems Branch (Code 3151)

Subj: Evaluation of new Q-100 Glass Rods from Kigre

Ref: (a) "Q-88* Glass vs Nd:YAG for P-ELI;performance of" by R.D, Anderson, Reg momo 3151-16-79, dtd 7 Mar 1979,

(b) "Evaluation of a Q-100 Glass Laser Rod and Comparison to Q-88* and YAG", by Harry W. Holloway, Reg memo 3151-18-81 dtd 19 Feb 1981.

1. Introduction. Kigre, Inc. has been tasked by DARPA to develop a laser glass with higher efficiency and better thermo-optics properties. The results of the present evaluation show that Kigre has made significant progress and is possibly close to being competitive with Nd:YAG rods in many applications. Since glass rods are cheaper, and more quickly manufactured they may provide a way to ease the critical shortage of Nd:YAG. I have determined in this evaluation the efficiency, divergence and wavefront distortion of five (5) glass rods which differ slightly from each other in composition.

2. Apparatus. The rods were placed in a water-cooled, ceramic-wrapped cavity designed for 3" rods. The glass rods themselves are 3 1/4' by 1/4" diameter. I used a simmered krypton flashlamp. The pulse forming network consisted of a 25 μ Farad capacitor and a 43 μ Henry inductor. One end mirror was flat and 100% reflective, the output mirror was a variable. The cavity was not Q-switched.

3. Efficiency - comparison of output mirrors. With rod P-667 I measured the output energy as a function of input energy using 65%, 75% and 85% reflectivity output mirrors. At each input energy level I carefully adjusted the mirrors and the orientation of the laser cavity to maximize the output. The output was extremely sensitive to alignment, probably because the glass rods were not anti-reflective coated. The results are shown in figure 1. These results are similar to those of reference (a) and reference (b).

4. Efficiency - comparison of Rep rate. I measured the output energy of rod P-667 at both 10 pps and 15 pps. The results, shown in figure 2 demonstrate that efficiency falls off rapidly with pulse rate.

5. Efficiency - comparison of rods. The output versus input energy for the various glass rods are shown in figure 3. Also shown in the figure are the efficiency curves for Nd:YAG rods 7750 and 4864. From previous data taken under the RODS program these two YAG rods were known to represent the most efficient and the least efficient in the collection of 36 YAG rods. Note that at high input energy the glass rods are as good as the worst YAG rod. The data was taken with a 75% output mirror at 10pps.

Subj: Evaluation of new Q-100 Glass Rods from Kigre

6. In figure 4 I compared the efficiency of the previous measurements (reference (a) and (b)) with the measurements I made. Apparently these latest rods from Kigre have a lower threshold energy and higher slope efficiency than the previous rods. However the test conditions were not precisely the same. In reference (a) Anderson used a pulse forming network of a 124 μ H inductor and a 19.3 μ F capacitor. The pulse forming network of reference (b) is not specified. Futhermore I used a new model 401 General Photonics closed loop cooler with a better designed pump that does not introduce bubbles in the water, as the old one (used in reference (a) and (b)) occasionally did. My rod mounting structure also had several degrees of freedom to optimize alignment while the rod holder of reference (a) and (b) was fixed.

7. Divergence. Divergence was determined by measuring the ratio of energy through an aperture to the total energy. The apertures are placed in the focal plane of a 100 cm lens. The flashlamp was pulsed at 10 pps with 9.0 Joules. This corresponds to an output energy of between 110 mJ and 130 mJ. The output mirror reflectivity was 75%. The results, plotted in figure 5 show that these glass rods have low divergence. If we take the divergence as the aperture size where 90% of the energy is transmitted then the divergence is between 2.2 and 2.5 mrad. Anderson (reference (a)) found the divergence of a Q-88* glass rod to be about 4.5 mrad (using an 85% output mirror and only 7.0 Joule input energy).

8. Because the pulse width is about 20 n sec for Nd:YAG (shorter than it is for Nd:Glass), the output mirror for a YAG system is usually chosen to be 55% or less reflective to reduce high power densities. The beam divergence of a YAG rod with a 55% reflective mirror is usually between 2.2 and 2.5 mrad, the same as these glass rods with a 75% mirror.

9. Figure 6 shows that with an 85% output mirror the divergence for rod P-667 is about the same as with the 75% mirror. The divergence increases to about 3.0 mrad at 15 pps.

10. Wavefront Distortion. I used the Jaman interferometer to observe the wavefront distortion of the glass rods. This distortion was then analyzed by ZAPP with FRINGE. The isometric plots of the wavefront distortion are shown in figures 7,8,9,10 and 11. There is very little distortion. Table 1 shows the 4th-order aberrations, in waves, along with the peak-to-valley (P-V) and average (RMS) distortion. In terms of wavefront error these glass rods are an improvement over YAG rods. Rods 7750 and 4864 are shown for comparison.

11. Conclusion. The glass rods tested show beam divergence as low as that of Nd:YAG rods. This is a considerable improvement over the previous glass rods. The efficiency has also improved to the point that glass rods are as efficient as some Nd:YAG rods. Further evaluation of these rods to determine the extent of thermally induced misalignment and distortion is recommended. Measurements of pulse width and efficiency Q-switched should also be performed.

D. W. Ricks

D. W. Ricks

Copy to:
315
3151 (Dobberpuhl, Wee)

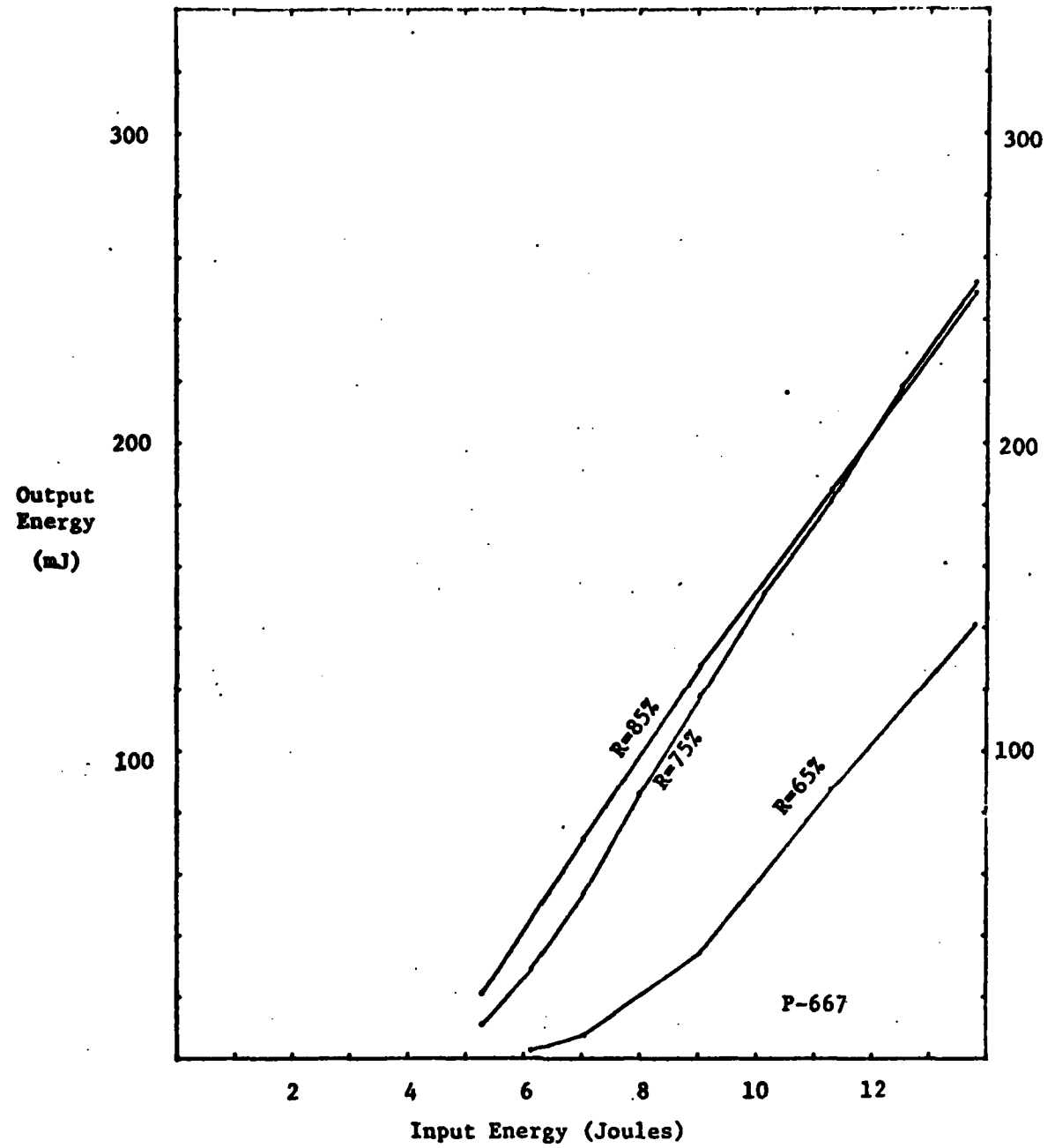

Figure 1. Comparison of efficiency for Nd:glass rod P-667 at 65%, 75%, and 85% output mirror reflectivities.

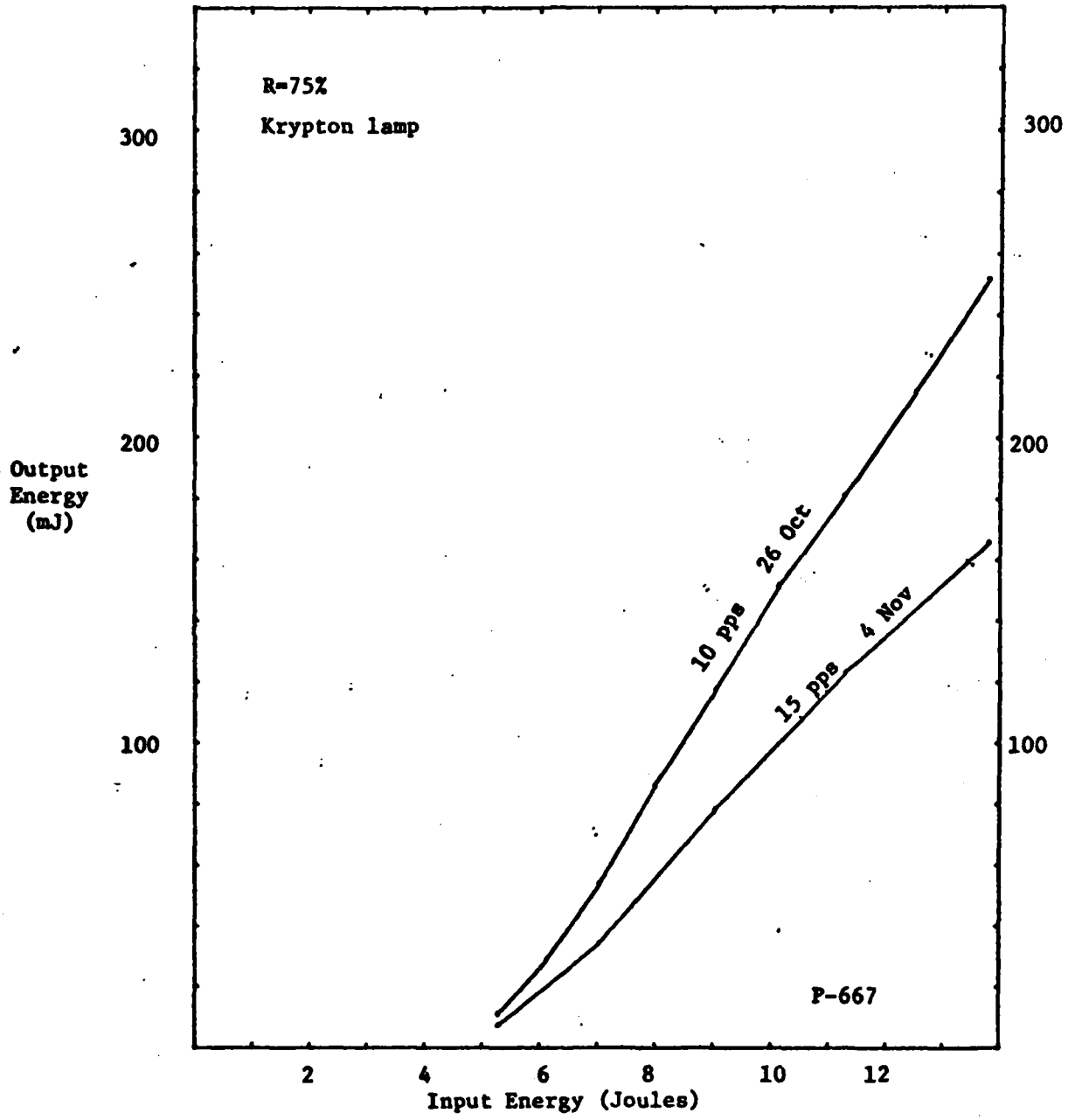

Figure 2. Comparison of efficiency in Nd:glass rod P-667 at 10pps and 15pps.

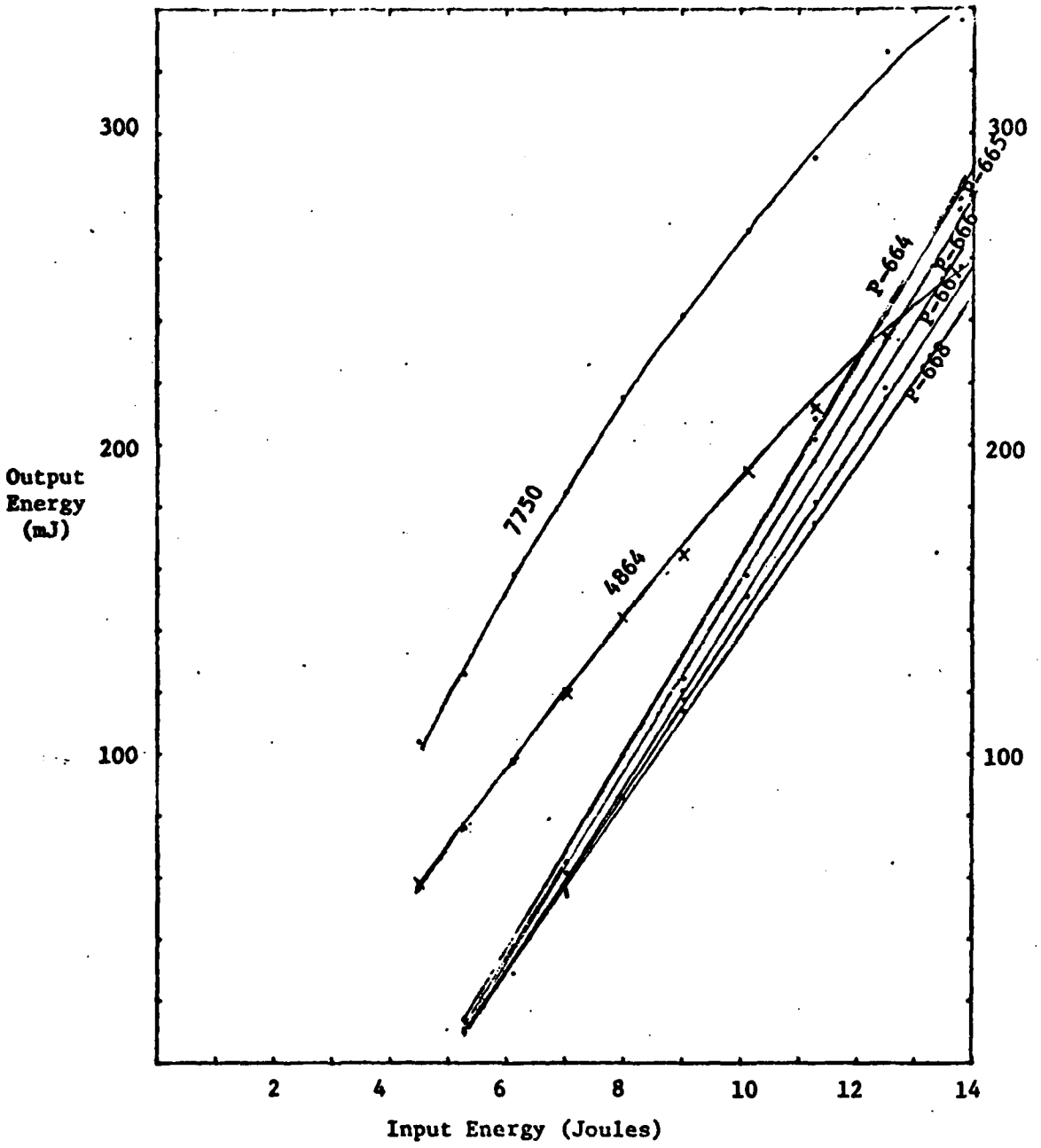

Figure 3. Comparison of efficiency; two Nd:YAG rods (7750 and 4864) and 5 Nd:glass rods. 10 pps and 75% output mirror.

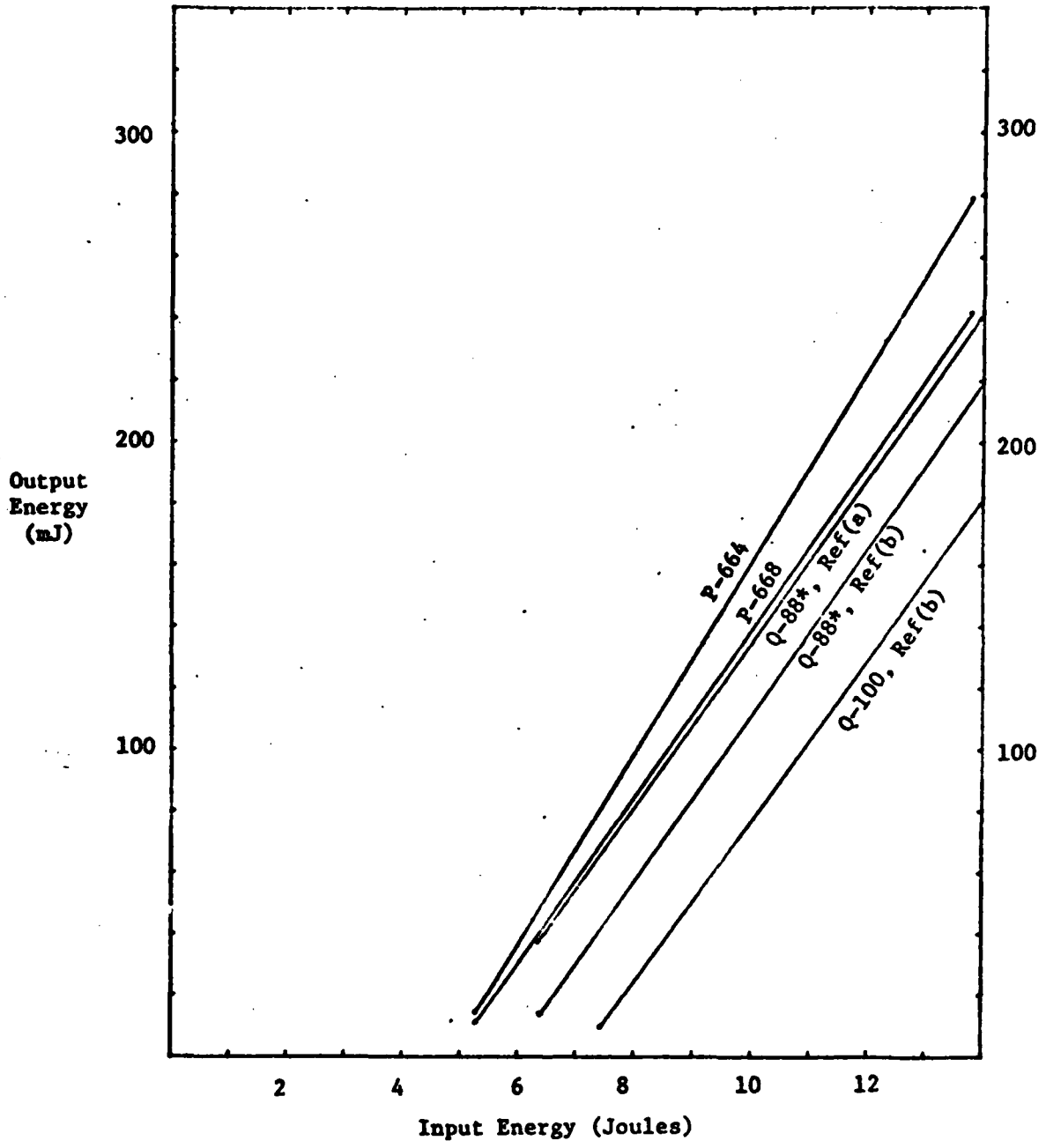

Figure 4. Comparison of efficiency in recent and previously tested glass rods. 10 pps and 75% output mirror.

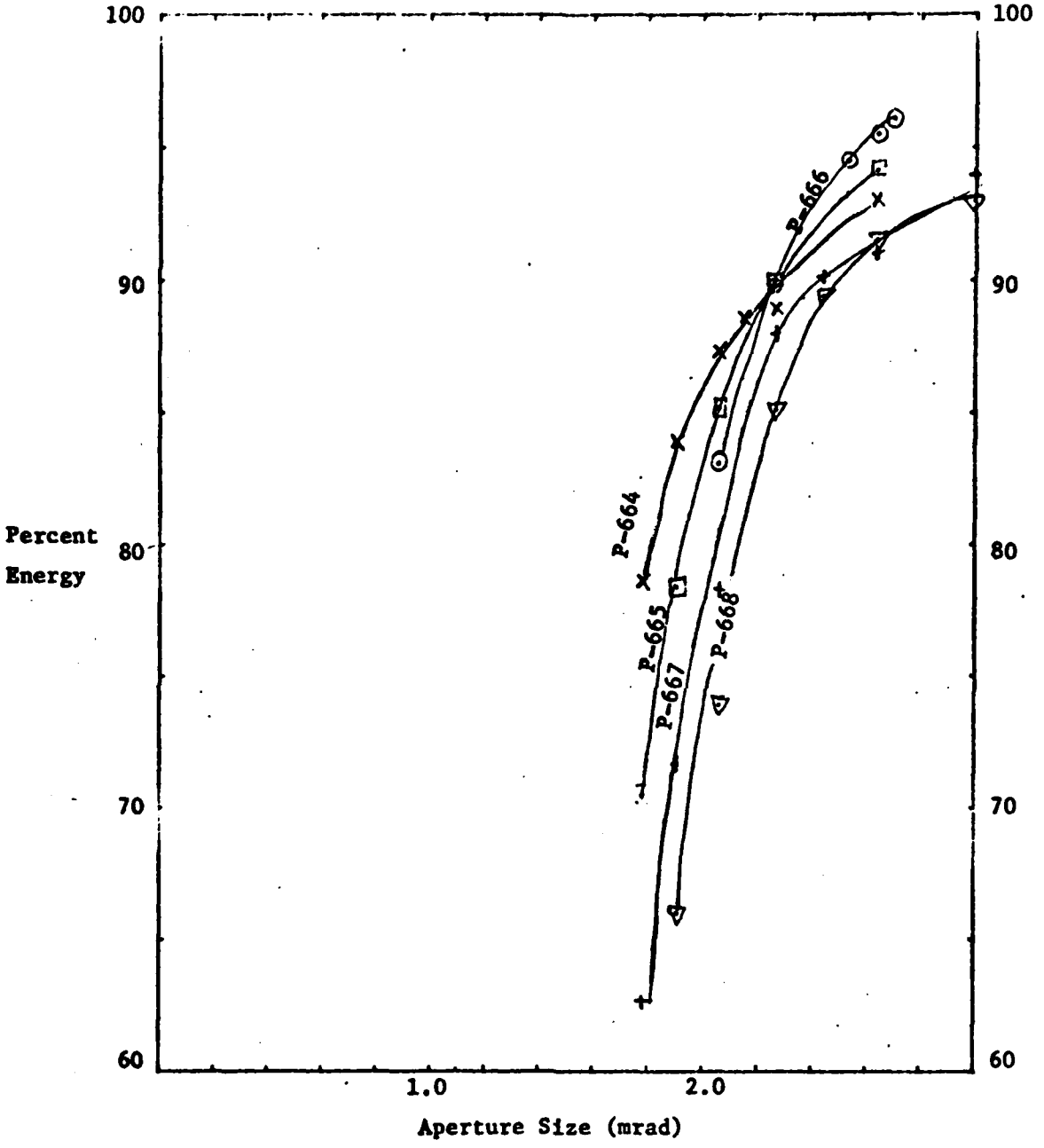

Figure 5. Comparison of divergence of five glass laser rods. 10 pps and 75% output mirror.

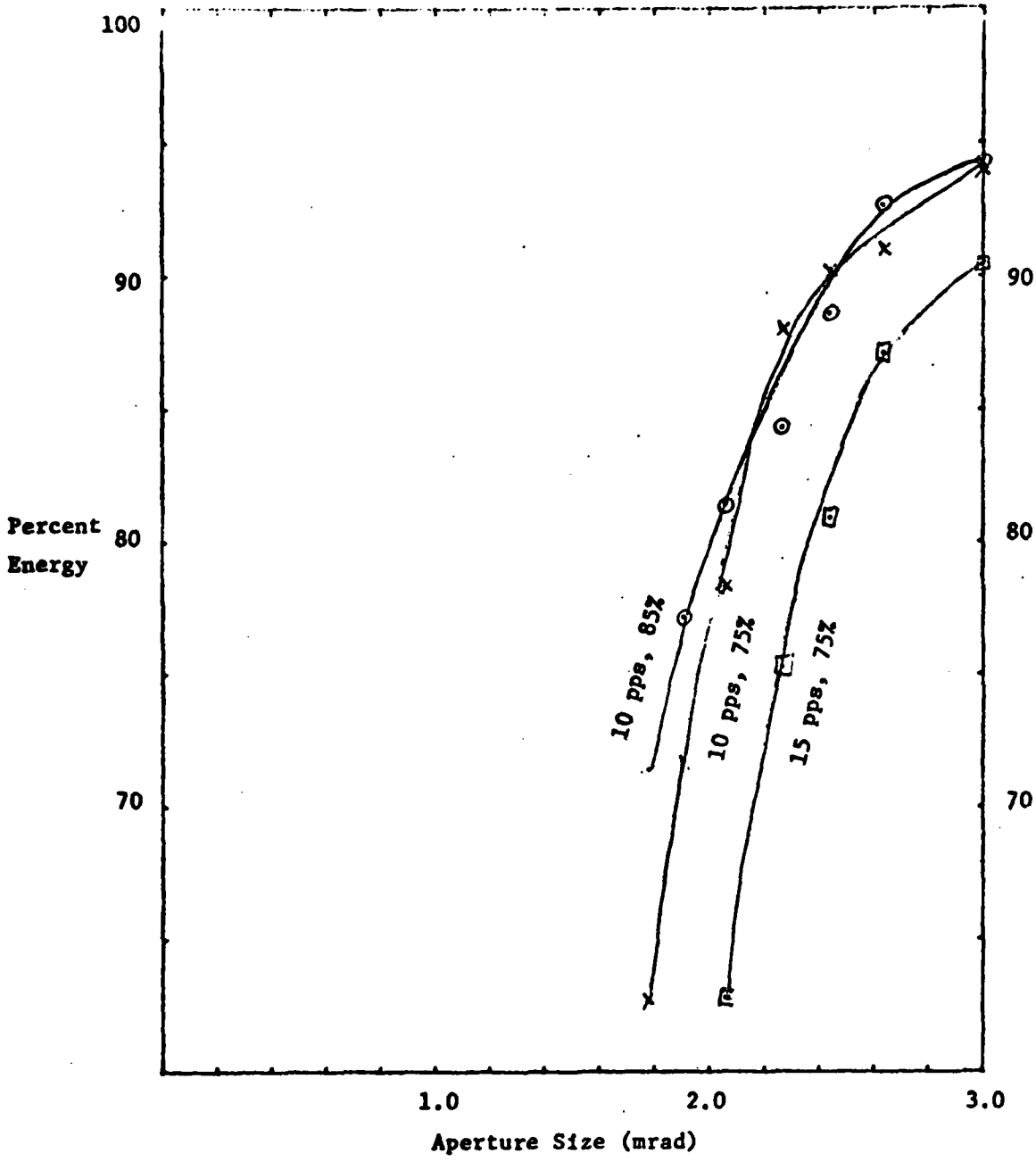

Figure 6. Divergence measurements of glass rod P-667 at 10 and 15 ~~20~~ pps and with a 75% and 85% output mirror.

TABLE 1

ROD	FOCUS	ASTIGMATISM	COMA	SPERICAL ABERRATION	P-V	RMS
P-664	.017	.024	.019	-.055	.152	.026
P-665	.048	.022	.038	-.083	.135	.025
P-666	-.011	-.02	.003	-.026	.156	.025
P-667	.066	.019	.056	-.066	.115	.024
P-668	0.10	-.038	.032	-.042	.125	.022
7750	-.103	-.227	.060	.073	.272	.065
4864	-.107	-.516	.183	.099	.676	.140

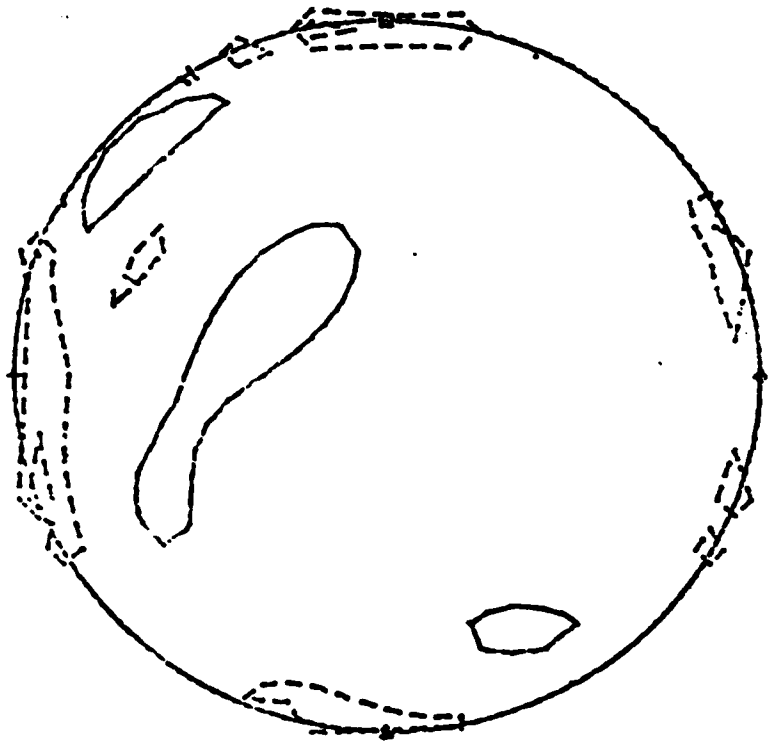

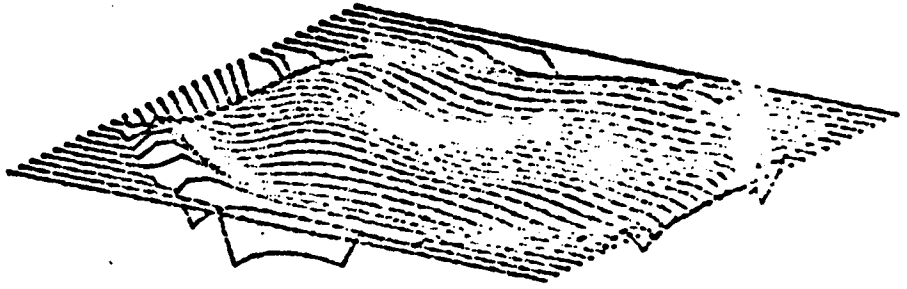

CONTOUR STEP 0.050
WAVEFRONT
ID NUMBER P-664 GLASS ROD
[illegible]-81 14:30:37 FILE: P664.DAT

Figure 7

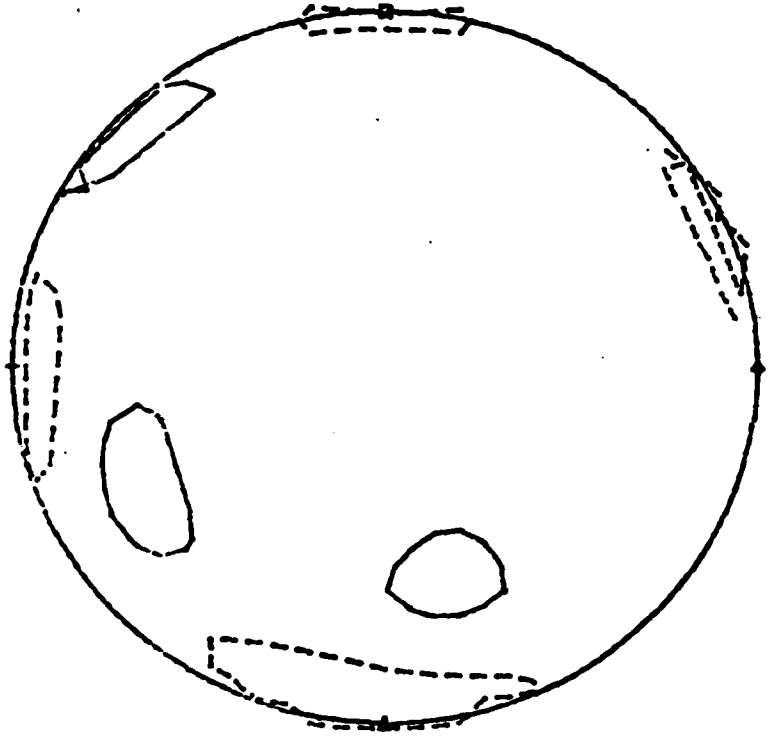

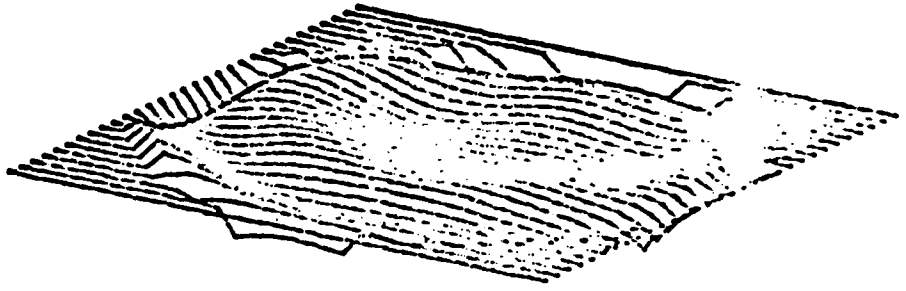

Figure 8

CONTOUR STEP 0.050
WAVEFRONT
ID NUMBER P-005 GLASS ROD
05-NOV-81 15:05:42 FILE: P665.DAT

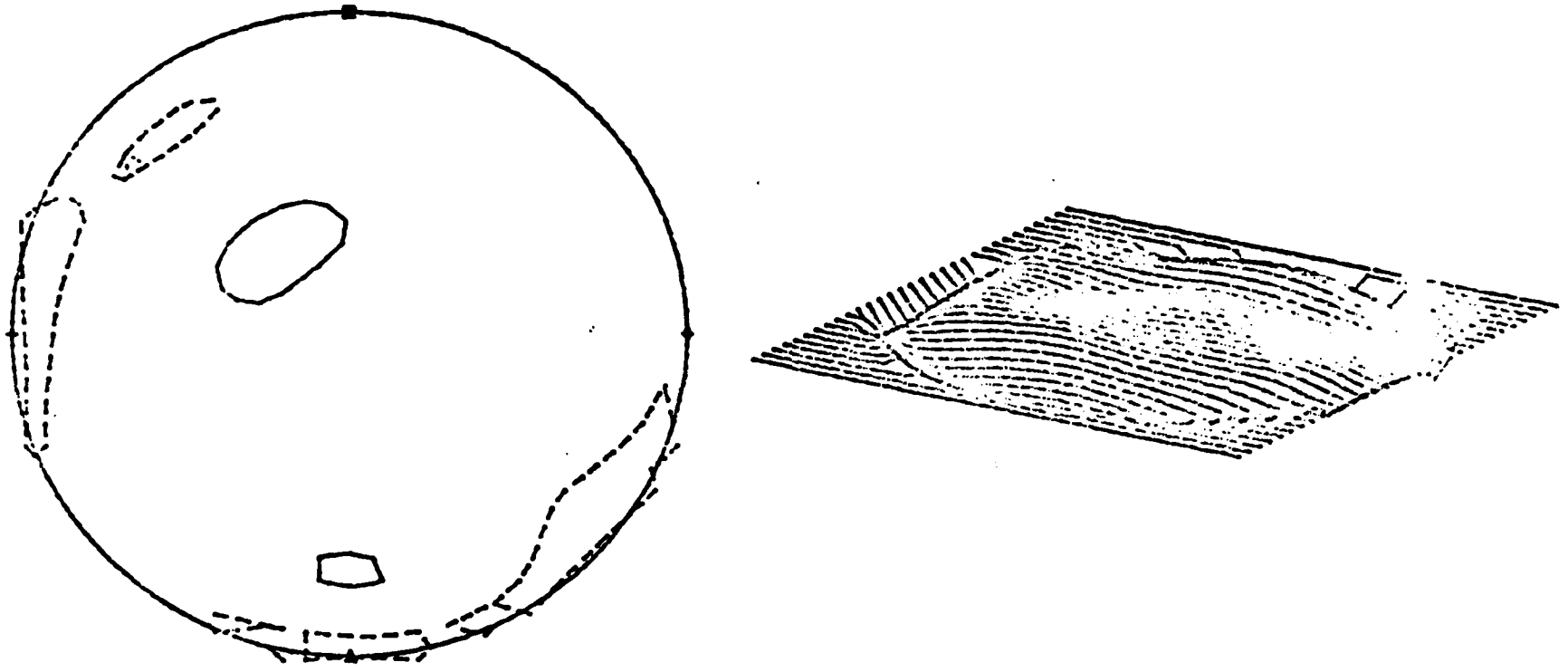

CONTOUR STEP 0.050
WAVEFRONT
ID NUMBER P-686 GLASS ROD
05-NOV-81 14:41:57 FILE: P686.DAT

Figure 9

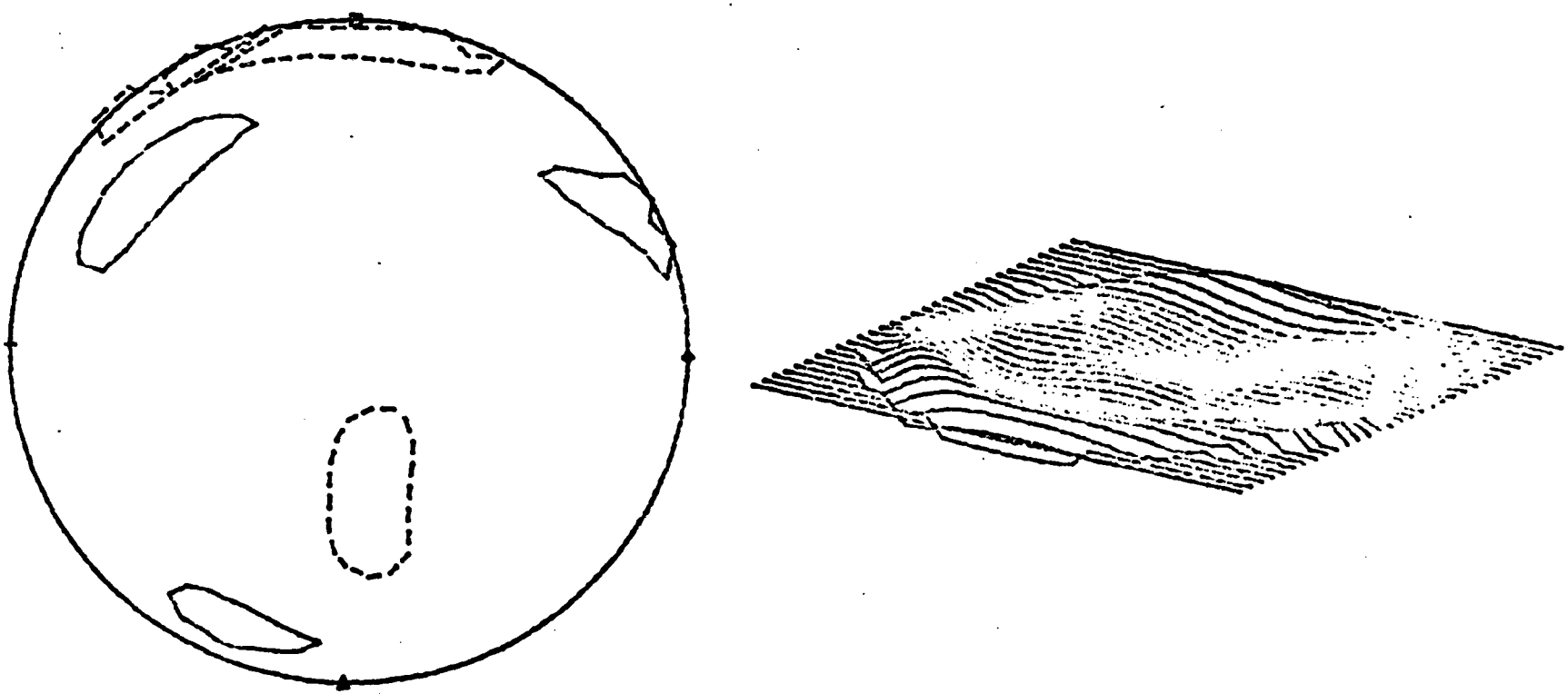

CONTOUR STEP 0.050
WAVEFRONT
ID NUMBER P-667, GLASS ROD DATE 5 NOV 1981
05-NOV-81 12:57:54 FILE: P667.DAT

Figure 10

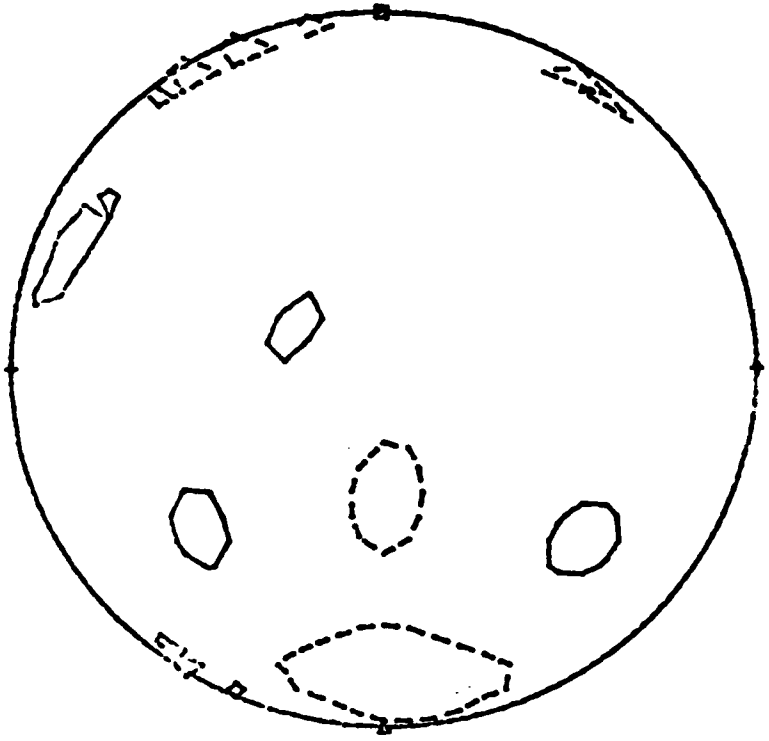

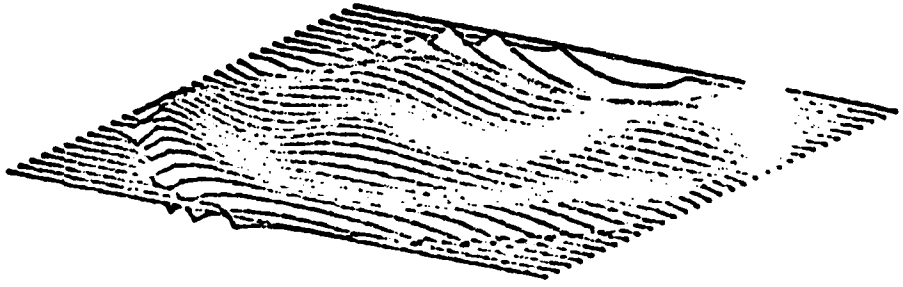

CONTOUR STEP 0.050
WAVEFRONT
ID NUMBER P-[illegible] GLASS ROD
05-[illegible]-81 10:[illegible]3:15 FILE: P668.DAT

Figure 11

TASK II

The Cladding of Q-100 Laser Glass

TASK II

The Cladding of Q-100 Laser Glass

Introduction and Summary

The cladding of Q-100 required not only developing the requisite cladding glass to match the Q-100 core, but also developing the apparatus necessary to prepare the preforms and actually accomplish the cladding/redraw operation.

Typically, in order to produce clad laser rods of a size applicable to most military applications, a preform, with a diameter approximately fifteen times the diameter of the final rod, must be fabricated. The preform in this case involved a three inch diameter cylinder of cladding glass with a two inch diameter core of Q-100. The fabrication of the cladding cylinder was accomplished on a special Sunnen hone/core-drill assembly especially modified for this purpose. The Q-100 core was machined on a conventional on-center grinder. The final parts, mated together, made up the preform.

Upon assembly, the preform is placed in the cladding/redraw apparatus. Heat is then applied to a narrow zone of the preform to bring that area up to the working range of the glass. Then, in a single operation, the preform is drawn into long rods and mated with the cladding.

After drawing, the resulting rods are strengthened and annealed in an annealing furnace. Following this operation, the strengthened and annealed rods are selected and fabricated into laser rods of various sizes.

Note:

Although Task IV is charged with strengthening laser rods, it was decided that it would be very desirable to develop a method whereby we could clad Q-100 with a silicate cladding glass. This accomplishment would permit us to utilize conventional ion-exchange procedures to strengthen the final laser rod. A substantial portion of the cladding development is devoted to this end.

The Development of Cladding Glass For Q-100 Laser Glass Rods

Phosphate laser glasses have been used widely due to their low nonlinear refractive index, high specific gain, and low thermo-optic distortion. Therefore, they compose the majority of glass types in Kigre's laser glass family. The disadvantages of phosphate glasses are their relatively high thermal expansion, low mechanical strength and consequently, the reduced thermal shock resistance. In terms of chemical durability, the recently developed Q-98 and Q-100 by Kigre has been proven to have high resistance to weathering. However, the high solubility of these glasses in salt baths restrict the possibility of ion exchange for improving their mechanical strength and thermal shock resistance.

Kigre, Inc. has been working toward a new cladding glass for phosphate glass laser rods. The primary target is a silicate glass which has a higher chemical durability than phosphate glasses, and is ion-exchangeable as well. For the purpose of being an acceptable cladding glass, the glass must:

1. match the thermal expansion of the core glass to avoid permanent residue stress up in the core glass. Generally speaking, the path-length change for a stressed cladded rod at room temperature can be expressed as:

$$\Delta P = \frac{E\Delta\alpha\Delta t\, B}{2(1-\mu)} \qquad (1)$$

Where: E - Young's modulus of the core glass;

μ - Poisson ratio of the core glass

$\Delta\alpha = \alpha_{cl.} - \alpha_{core}$, the difference in coefficients of thermal expansion between cladding and core glasses;

$t = t_{strain} - t_{room}$, the difference between the strain point of the core glass and room temperature;

B - Stress optical constant of the core glass. For Q-100 laser glass we have;

$E = 5.41 \times 10^5$ kg/cm^2

μ = 0.271

Δt = 376 -20 - 356^{o}C

B = -1.3 nm/cm/Kg/cm^{2}

Substituting to equation (1), we get

$$\Delta P = 1.72 \times 10^{8} \Delta\alpha \ ^{o}C \text{ nm/cm} \qquad (2)$$

Therefore, for a expansion difference of $\Delta\alpha = 1 \times 10^{-7}/^{o}C$ between two glasses, we can expect a path difference of 17 nm/cm in the glass or a 170 nm path difference in a 10 cm long laser rod. On the contrary, suppose we require a $\Delta P < \lambda/10$ at 1054 nm laser output, the difference of $\Delta\alpha$ must be within the range of:

$$\Delta \alpha < 0.6 \times 10^{-7}/^{o}C$$

In the practical case, we will be able to compensate the laser induced path difference by the mismatch in thermal expansion between the two glasses. This might become another advantage of a cladded rod. However, for the sake of ensuring the ΔP not extended beyond a certain limit, we must be able to control the thermal expansion coefficient of the cladding glass within a tolerance indicated by equation (2).

2. maintain a better chemical durability. The glass should be able to withstand weathering and hot water (as a coolant) corrosion. A silicate glass with thermal expansivity as high as Q-100 has to contain more alkali ions than normal, making it difficult to maintain the glass chemical durability.

3. be ion exchangeable for chemical strengthening. This is important for improving the threshold of a laser rod and prolonging the lifetime of the rod.

4. be optically adjustable and durable. The refractive index of the cladding glass must be higher than the core glass, and the doped ion be able to absorb the 1.054 μm wavelengths to minimize the parasitic oscillation of the laser beam. A definite amount of uv absorption and high resistance to solarization is also preferable for protecting the core glass from solarization.

5. be technologically matched to the core glass. In addition to the matching of thermal expansion as indicated before, the softening point of the cladding glass must be close to the core glass and no chemical reaction

or devitrification should occur in the sealing temperature range within the operation period of time. This has been the major point of consideration since the silicate based glass is chemically different from the phosphate core glass Q-100.

Experimental

Fifty to one hundred grams of glass are melted in 50 ml platinum crucible under the temperature of 2000-2100^{o}F. Each melt has been stirred twice using a platinum rod to ensure the homogeneity of the glass. After casting the glass block, usually 1 x 1½ x ½ in^{3} in size, it is annealed from 800 to 700^{o}F with a rate of 2-4^{o}F/min. Two different series of glass have been melted and the properties have been measured or tested for each melt.

1. Silico-borate glass series.

The chemical compositions of this series are shown in table 1.

Table 1. Chemical Compositions of the Silico-borate Glass Series

Number	SiO_2	Al_2O_3	B_2O_3	Na_2O	Li_2O	ZnO	PbO	BaO
				(In Mol%)				
SCP-4	18.0	5.0	36.0	27.4	-	11.3	2.3	-
SCP-4a	18.0	5.0	36.0	27.4	-	7.3	2.3	4.0
SCP-4b	18.0	5.0	36.0	27.4	-	3.3	2.3	8.0
SCP-4c	18.0	5.0	36.0	27.4	-	3.3	6.3	4.0
SCP-10	15.0	5.0	36.0	30.0	-	4.0	-	10.0
SCP-11	15.0	5.0	36.0	15.0	15.0	4.0	-	10.0
SCP-12	15.0	5.0	31.0	20.0	15.0	4.0	-	10.0
SCP-13	15.0	5.0	36.0	13.5	15.0	6.0	-	9.5
SCP-14	17.0	5.0	34.0	15.0	15.0	4.0	-	10.0
SCP-15	16.0	5.0	35.0	13.0	15.0	6.0	-	10.0
SCP-16	18.0	5.0	33.0	13.0	15.0	8.0	-	8.0
SCP-17	20.0	5.0	33.0	13.0	15.0	8.0	-	6.0
SCP-17s			SCP-17 + 2.5 wt% Sm_2O_3					
SCP-18	20.0	5.0	35.0	13.0	13.0	8.0	-	6.0
SCP-19	22.0	5.0	33.0	13.0	13.0	8.0	-	6.0

The properties of these glasses are listed in table 2.

Table 2. Some Properties of the Silico-borate Glass Series

Glass Number	$\Delta\alpha$(1)	ΔTf(2)	n_D	DPS(3)	Interface Observation
SCP-4	-3	$+100^o$	1.5524	No	Small Dots
SCP-4a	-3	$+70^o$	-	No	Small Dots
SCP-4b	-1	$+40^o$	1.5637	No	Small Dots
SCP-4c	-1	$+40^o$	1.5691	No	Small Dots
SCP-10	+3	-25^o	1.5535	No	Clear
SCP-11	+3	-50^o	1.5698	No	Clear
SCP-12	+4	-20^o	1.5700	No	Clear
SCP-13	+2	-20^o	1.5772	No	Clear
SCP-14	+2	-20^o	1.5761	Weak	Clear
SCP-15	+2	-20^o	1.5777	Weak	Clear
SCP-16	+2	-15^o	-	2 Phase	Clear
SCP-17	+1	$+10^o$	1.5741	2 Phase	Clear
SCP-17s	0	$+15^o$	-	2 Phase	Clear
SCP-18	-2	-	-	2 Phase	Clear
SCP-19	-3	-	-	2 Phase	Clear

Note: (1) $\Delta\alpha$ = Difference of thermal expansion related to Q-100's.

(2) ΔTf = Difference of softening temperature related to Q-100's.

(3) DPS = Degree of phase separation.

One kilogram of glass has been made with the composition SCP-17s. Ion exchange test with a sodium-potassium nitrate bath shows a positive result of surface strengthening. The Sm^{3+} doping also gives a satisfactory optical density at 1.054 μm.

The major problem with silico-borate glass is its poor chemical durability. They dissolve in hot water fairly quickly. Nevertheless, further improvement of the durability by means of increasing silica content in the glass is restricted by the phase separation.

The phase separation can be observed by light scattering. The silico-borate glasses show weak scattering in SCP-14 and SCP-15 and heavy scattering has been observed in SCP-16 to 19. In the case of phase separation crystal growth and bulk divitrification might occur during prolonged heat treatment, in the cladding and stretching process with these glasses. Therefore, if the glass from the silico-borate series would be used for cladding, the poor water durability could be unavoidable and a durable surface coating should be applied to prevent laser rod deterioration from water attack.

2. Silicate glass series:

Table 3. Compositions of the Silicate Glass Series

Number	SiO_2	LiO_2	Na_2O	BaO	ZnO	La_2O_3	MoO_3	Al_2O_3	PbO
				(in Mol%)					
SL-3	48.54	18.35	7.23	14.0	10.0	0.5	0.39	1.0	-
SL-4	47.54	18.35	8.23	14.0	10.0	0.5	0.39	1.0	-
SL-5	48.54	18.35	7.23	16	8	0.5	0.39	1.0	-
SL-6	48.54	18.35	7.23	18	6	0.5	0.39	1.0	-
SL-7	48.54	18.35	7.23	20	4	Sm_2O_3 0.54	0.34	1.0	-
SL-8	48.54	18.35	7.23	19.4	4.6	0.54	0.34	1.0	-
SL-9	47.54	18.35	8.23	9.3	4.7	0.54	0.34	1.0	10.0
SL-10	48.2	18.4	7.5	14.26	4.7	0.60	0.34	1.0	5.0
SL-11	48.2	18.4	7.5	12.4	6.6	0.60	0.3	1.0	5.0

The properties of glasses in the present series are shown in Table 4.

Table 4. Some Properties of the Silicate Glass Series

Glass Number	$\Delta\alpha$	ΔTf
SL-3	-10	+10
SL-4	-2	+60
SL-5	-6	+85
SL-6	-4	0
SL-7	+2	-
SL-8	+2	+50
SL-9	+10	+20
SL-10	+3	+10
SL-11	-2	+30

Experimental Procedures

The evaluation of the various cladding glass candidates required special experimental procedures. Some of these procedures are described as follows:

Evaluation of Thermal Properties

	Difference of Thermal Expansion Related to Q100 *	Difference of Softening Temperature Related to Q100 **	
		Start Softening	End Softening
SCP17S	+1	$+20^{o}F$	$0^{o}F$
SL8	+2	$\sim +35^{o}F$	$\sim +70^{o}F$
SL11	-2	$+10^{o}F$	$\sim +50^{o}F$

Note * Looking through a pair of sealed samples with a depth of 8mm and a thickness of 3mm, one unit difference of thermal expansion should induce a birefringence just strong enough to be identified under the polariscope. Plus sign means the thermal expansion of cladding glass is higher than Q100.

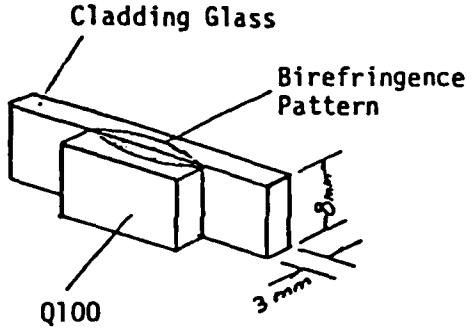

** Two identical glass stripes (approx. 1 x 0.25 x 0.07 in^3 in dimension) with ground surface are heated horizontally at a rate of $4^{o}F$/min. The differences between cladding and standard (Q100) in softening temperature are recorded when the bending occurs (start softening) and also when it reaches the final stage (end softening). Plus sign means that the softening temperature of cladding is higher than the Q100.

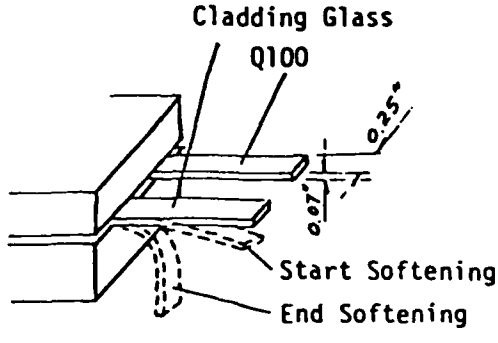

Evaluation of Chemical Durability

Chemical durability is measured as the weight loss in milligram of the sample per cm^2 exposed surface per hour treated in boiling water.

	Weight Loss in $mg/cm^2/hr$		
	Polished Rod	Fine Ground Rod	Polished Plate
SCP17S ion exchanged	2.3	3.4+	
unexchanged		2.7+	3.2
SL8		1.5+	0.19*
SL11		0.07	0.19
Q100		0.14+	0.16*
Q246			0.02

Note * With reddish and bluish metalic luster on the surface after treatment.
+ With microcrackes on the surface before and after treatment.

Some Descriptions on the Sealing and Related Properties of Cladding Glasses

The polished surfaces of Q100 and the silicate glass can be sealed together at 875^{o} x 1 hr. (The temperature scale is according to the Heavy Duty Oven reading temperature in the present description. Usually this scale is higher than normal temperature for approx.$50^{o}F$)

The surface of Q100 starts glaring at 920^{o}. Starting from 960^{o}, the sharp corner becomes round and it is very soft over $1020^{o}F$. At temperature higher than $1100^{o}F$, surface devitrification occurs, depending upon the atmosphere. Under the influence of lead and/or lithium vapor, intensive crystallization develops on the surface at $1100^{o}F$. Otherwise, it will remain clear at $1100^{o}F$ at least for 30 minutes.

The elongation rates of glass rods (1/4" in diameter) under a tension of 0.34 kg/cm^2 were tested in Heavy Duty Oven and the results are:

	Elongation Rate (mm/min) of Glass Rod at Temperature				
	$885^{o}F$	$900^{o}F$	$930^{o}F$	$950^{o}F$	$1000^{o}F$
SL8				0.04	0.27
SL11		0.1	0.3	1.0	
Q100	0.1		1.5-2.0		

The silicate cladding glasses SL-8 and SL-11 show significant surface change at temperature above softening point, probably due to the volatization of lithium (and also lead for SL-11). For example, a polished surface of SL-11 becomes wavy when heated up to 1100°F or higher.

Comments on the Cladding Glasses

The silica-borate glass SCP-17S is chemically soluable under the action of boiling water. (See Tab 4) Even it performs better under the attack of salt bath during ion exchange (according to Michael Myers) than the phosphate glass. I think it should be rejected because we have silicate glasses as better candidates.

The SL-8 and SL-11 are not sufficiently durable among silicate glasses because of their low silicate content. They can be desolved in boiling water by a rate order of micron per hour. Unlike SL-8, the SL-11 does not show observable surface deterioration after treated in boiling water for one hour. Further improvement in chemical durability of these glasses is restricted by their high expansion and low softening point.

The softening temperature of lead free silicate glass SL-8 is approximately 25°F higher than SL-11 in the beam bending test and 70°F higher in the rod elongation test. The fine ground surface of SL-8 glass shows to be easier crystallized than SL-11. The 5% PbO in SL-11 glass does not make significant change to the interface contamination. Therefore, the SL-11 is more preferable than SL-8 from my present experience.

Comparing the properties of P715Pα1 (Lanthanum substituted Q-100 glass) with SL-11 in cladding process, the following advantages and disadvantages are being expected.

1. The polished surface of SL-11 might have some invisible changes beyond 1015-1050°F due to volatization and crystallization, whereas the phosphate glass P715α1 remains clear down to approx. 1100°F. For a silicate cladding process, the sealing must be conducted between 950° and 1000°. This is available because the inner core of Q-100 is fairly soft in that temperature range.
2. The elongation rate of SL-11 is 1mm/min at 950° and approx. 10mm /min. at 1000°F, under a tension of 0.3 kg/cm^2. As it seals on Q-100, no reaction was observed on the interface at 1015°F for 20 min. between two glasses even the Q-100 was moderately soft. It is possible to get a clear inter-

face with high temperature stretching except the sealing surface of SL-11 was exposed at high temperature for a long time before sealing.

3. For a phosphate cladding P715Pα1, the short working temperature range will cause some difficulties in stretching process. However, it appears to be adequate in terms of surface (interface) deterioration.

Diagram Showing the Temperature Dependency of Glass Properties Related to Sealing and Stretching Process

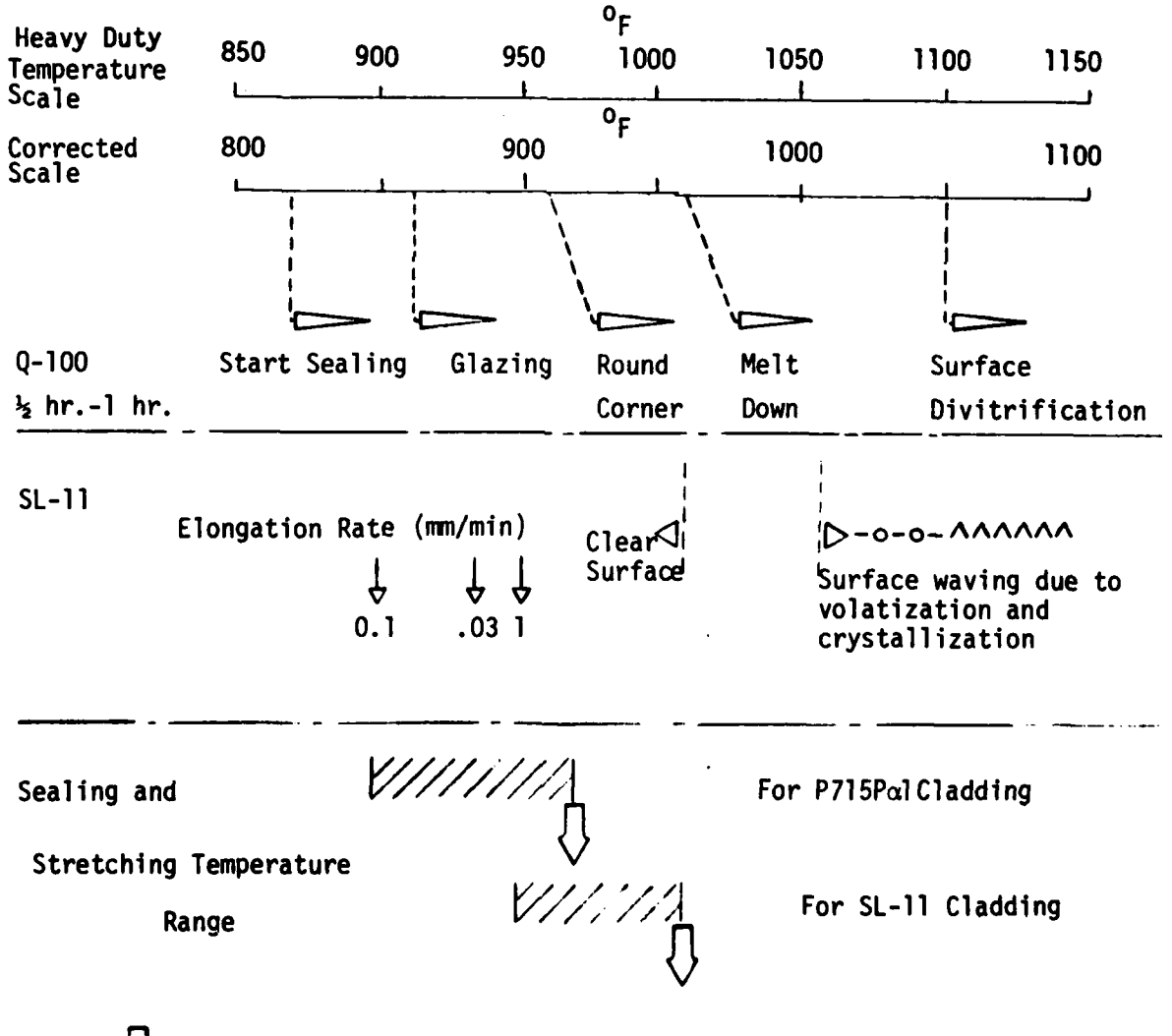

Conclusion

The cladding of Q-100 with Lanthanum phosphate cladding glass has been successfully accomplished. The resultant clad rods exhibited a 23% gain in efficiency, and a lasing threshold reduced by 35%. These results are due to the manner in which the cladding glass acts as a lens, focusing the light energy into the center of the laser rod. Once a silicate glass is properly matched to Q-100, the efficiency should be in the same range while the rupture strength should increase several fold with the use of a ion-exchange process. Performance graphs of clad Q-100 versus unclad Q-100 are given at the end of this section.

Two silicate glasses, SL-8 and SL-11, have been melted in a 1 Kg size. They have been tested for ion exchange, water durability, and spectrophotometric measurement. Each of these tests shows desired performance. The glasses are free of phase separation and give clear interfaces after their sealing with Q-100.

However, the softening temperatures of silicate glasses in this series are higher than Q-100. Moreover, the viscosity of glasses changes much more slowly with temperature than the phosphate glasses. In order to stretch these glasses in the cladding process, the temperature has to be raised up to the point at which the Q-100 core will be very fluid and be difficult to handle within the outer tube. Further reducing the softening point of the silicate glass by introduction of more glass modifiers or substitution of the silica by boric oxide might cause the glass surface to devitrify prior to the sealing point.

Further research in this area is necessary before a practical silicate cladding glass is a reality.

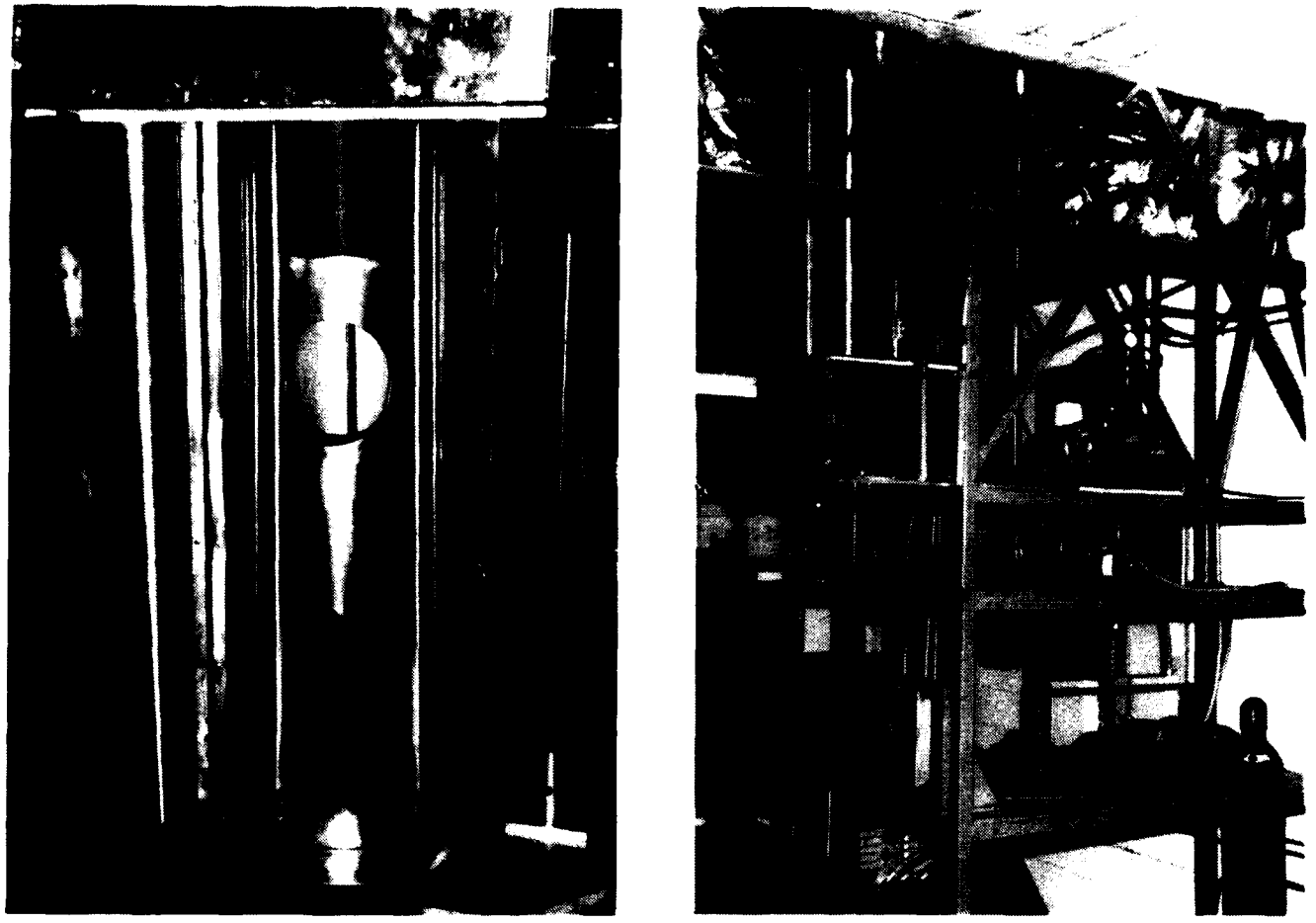

Redraw Apparatus

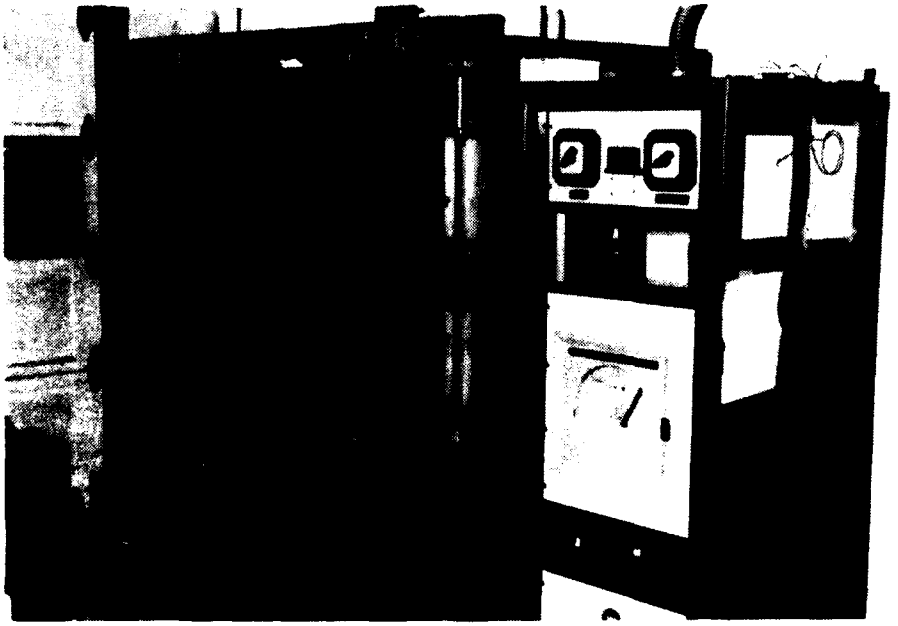

Annealer

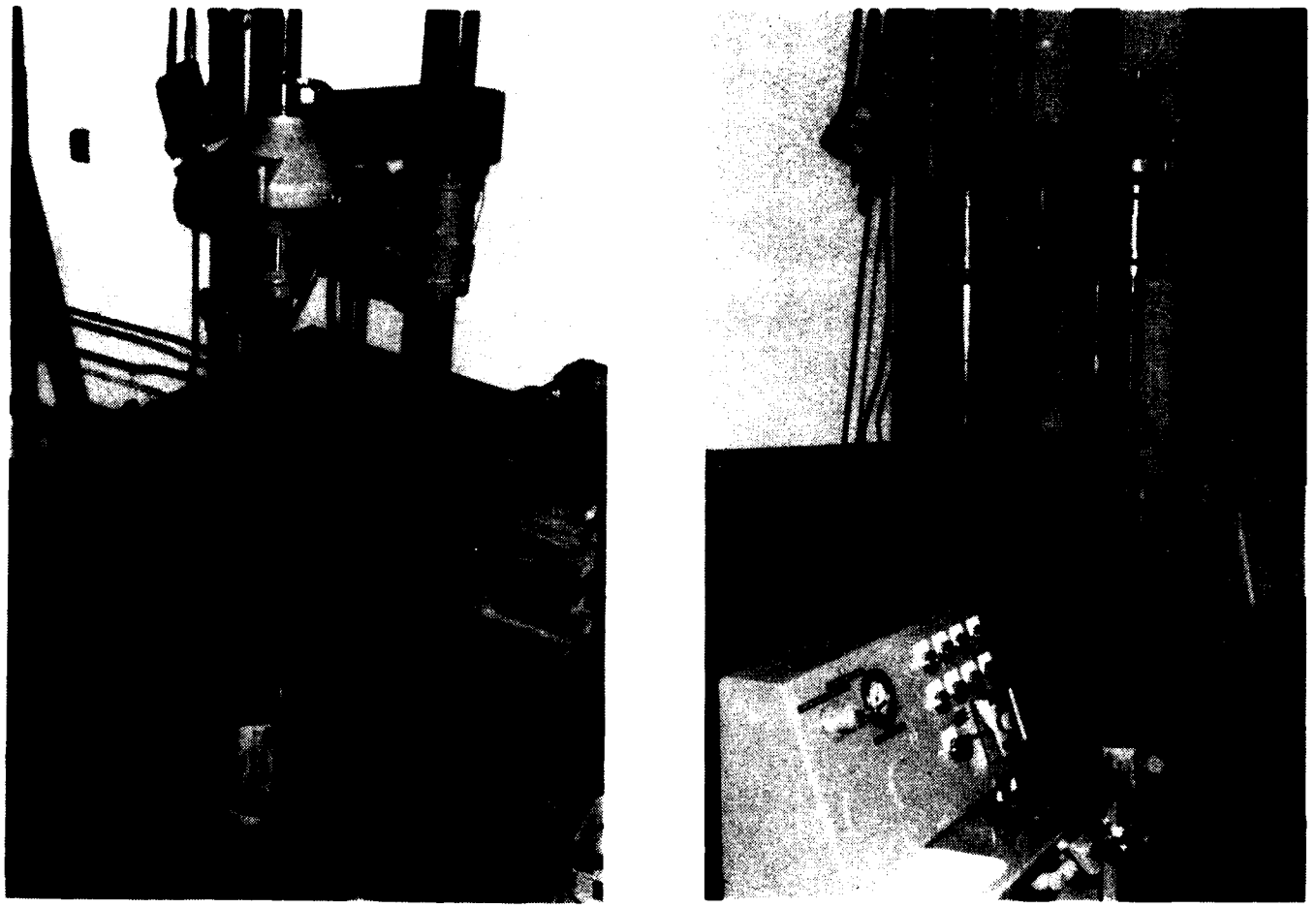

Oversized Drilling and Honing Machine

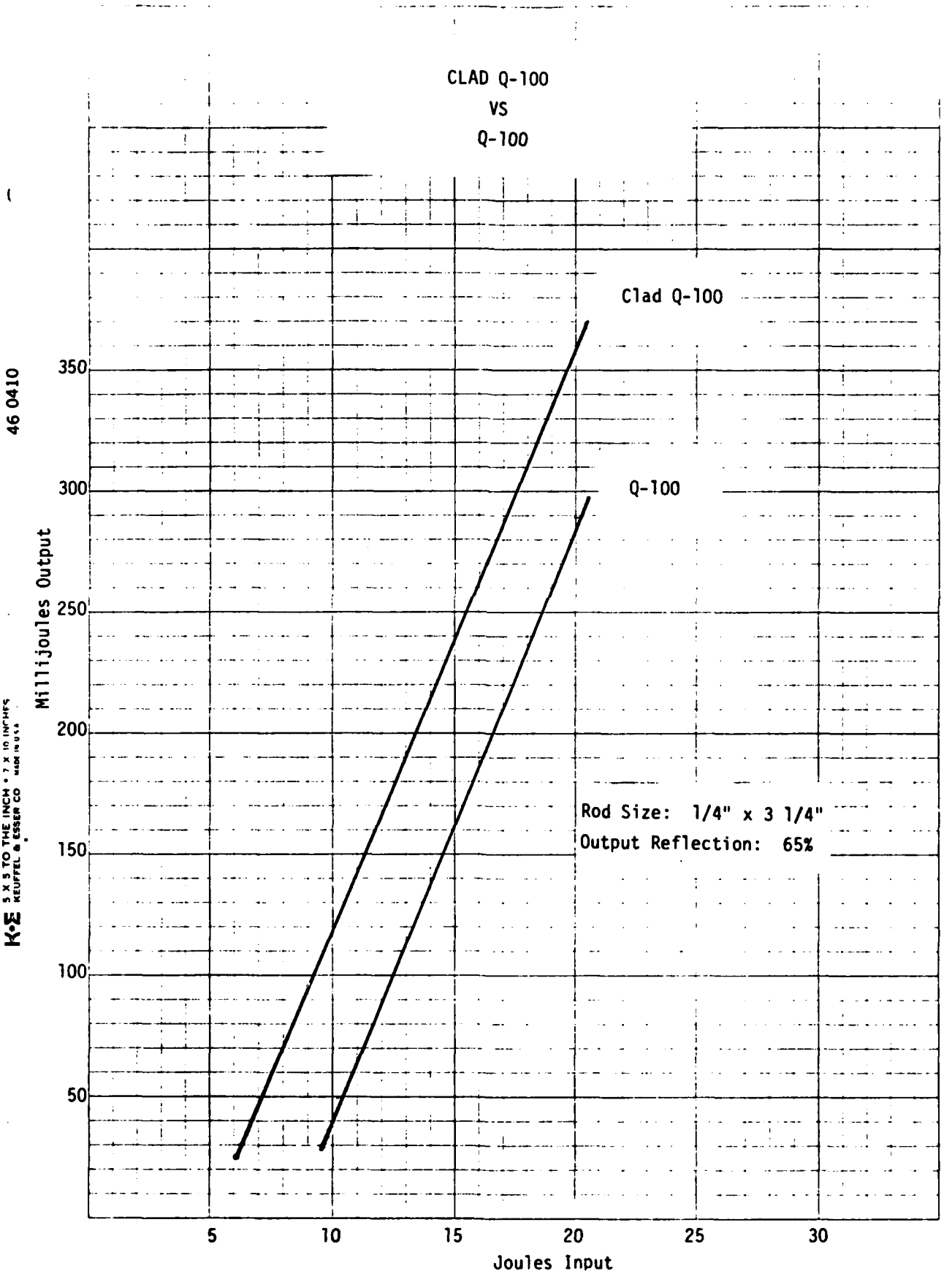
CLAD Q-100
VS
Q-100
Clad Q-100
Q-100
Rod Size: 1/4" x 3 1/4"
Output Reflection: 65%
Millijoules Output
350
300
250
200
150
100
50
5
10
15
20
25
30
Joules Input
46 0410
5 X 5 TO THE INCH • 7 X 10 INCHES
KEUFFEL & ESSER CO MADE IN U.S.A.

TASK III

Selective Filtering and/or Energy Transfer to Reduce Thermal Loading

TASK III

Selective Filtering and/or Energy Transfer to Reduce Thermal Loading

Introduction and Summary

Task III of the referenced contract was charged with investigating schemes for reducing the thermal loading of laser rods. This was to be accomplished by selectively filtering the flashlamp radiation to transmit the useful radiation corresponding to the neodymium pump bands, and exclude that radiation which would serve only to heat the laser rod, thereby degrading its performance. As a corollary, it was also deemed advisable to investigate means for possibly transferring a portion of the unusable flashlamp radiation, located in the U.V. portion of the spectrum, into the neodymium pump bands via fluorescence. With the development of a filter glass denoted L-386, essentially all of the objectives of this task have been realized. Although more testing must be accomplished to completely characterize the new filter, test results, at this time, clearly indicate significant improvements in the operation of neodymium doped laser rods resulting from the use of this filter material.

Background

The problem of increasing beam divergence and/or stress-birefringence effects which limit the brightness of neodymium lasers operated at high average powers is well known. Attempts to alleviate this problem have, for the most part, dealt with schemes to limit the heating of the laser rod by either modifying the flashlamp radiation or increasing the quantum efficiency of the laser rod. In this instance, we have sought to modify the flashlamp radiation by filtering out that portion which serves only to heat the laser rod rather than contribute to the laser rods performance. In addition, we have also attempted to improve the performance of neodymium laser rods by absorbing a portion of the unused ultra-violet flashlamp radiation, and re-emitting that energy by means of fluorescence into the neodymium pump bands.

Spectroscopic Studies

A rather extensive study of fluorescing ions in glasses can be found in Appendix A. This study established the candidate ions selected for evaluation in this development effort.

Because of the apparent prospects of Pr^{3+}, Dy^{3+} and UO_2^{2+} as candidates for fluorescent conversion, rather extensive spectroscopic studies were employed and evaluated. A description of this work along with results and discussion can be found in Appendix B.

In addition to the above mentioned candidate ions, it was decided to also investigate at some length the following ions:

Ce^{3+}
Eu^{3+}
Tb^{3+}
Sm^{3+}
Tm^{3+}
Yb^{3+}

While it is true that the fluorescent lifetime of these ions are rather long, (all but Ce^{3+} have fluorescent lifetimes of the order of milliseconds) it was felt that significant shortening of these lifetimes could be achieved through concentration quenching. Also, the fluorescence occurring at times shorter than the fluorescent lifetime that would be useful even in Q-switched lasers. In either case, these ions are prime candidates for use as absorbers in our "window" filter.

TESTING

Critical to the evaluation of this filter material is the mode of testing. We chose two test set-ups to evaluate the efficacy of the material.

The first such test included use of a cavity-test apparatus developed by Kigre, Inc. as a quality assurance instrument for use with the M-1 laser cavity assembly. (See Page No. 3) It is essentially an uncooled glass laser rod, mirrors, and flashlamp arrangement which facilitates the testing of the M-1 laser cavity assemblies prior to final assembly. In this test, we fabricated M-1 cavity assemblies using the various candidate filter glasses and compared their performance in this unit against that of a standard M-1 assembly. This test permitted us to determine the basic energy transfer of the filter material in relation to a well-known standard.

M-1 CAVITY TEST

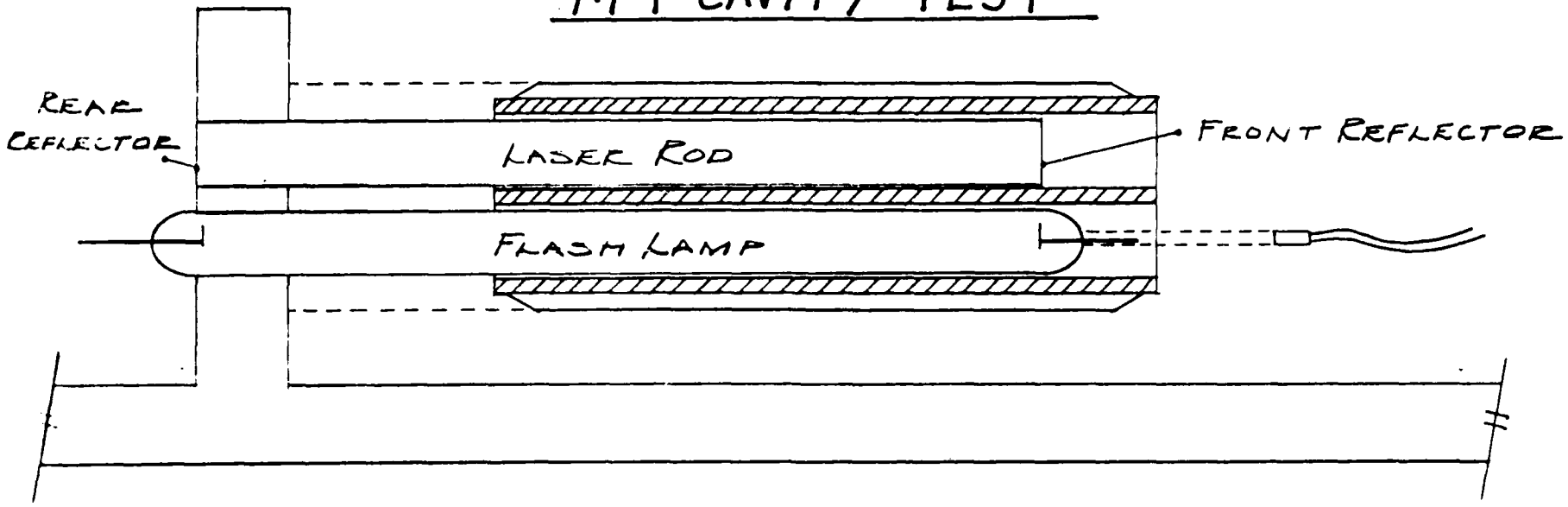

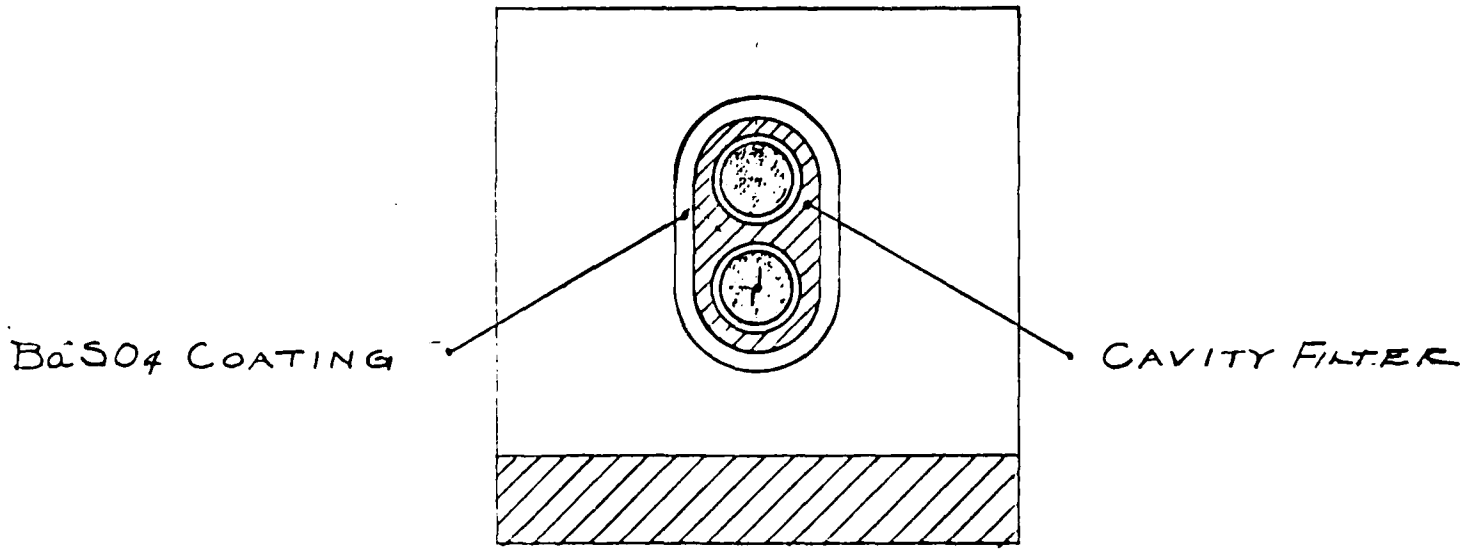

The second test, (see Page No.5) and the one we used most often, involved the testing of the filter in a "wet" system at various pulse repetition rates versus the same system with no filter. The laser is a simple flooded-cavity unit with silver plated reflectors. The various candidate filters were fabricated in simple slide form and situated between the flashlamp and the laser rod. In this manner we could vary the thickness of the filter slides and optimize the doping levels to fit practical systems.

FRESNEL REFLECTIONS

One problem anticipated in the development of a "fluorescent converter" filter was the fact that in a dry system the Fresnel reflection of the glass-air interface would tend to trap a majority of the fluorescent radiation within the filter. Although such trapping would not appreciably effect the operation of the filter in a "wet" system, dry and/or gas-cooled systems would be severely affected. For this reason, we also embarked upon a program to reduce the Fresnel reflections by developing an anti-reflection coating process which we could apply to our more common filter cavity configurations.

Using our "wet" cavity results as a guide, we determined that we need only approximate the reflectivity of an air-water interface. That is, if we could reduce the Fresnel reflections to approximately 1%, we permit the majority of the fluorescence to escape the confines of the filter. It appeared that this goal was gainable through chemical anti-reflection processes similar to that employed by the camera industry prior to World War II. This company-funded effort resulted in the dry-cavity comparative data as shown below.

	Input	
	650 Volts	750 Volts
Standard M-1 Cavity	68mj	107mj
AR Coated M-1 Cavity	80mj	124mj

PROCEDURE

The task of designing a filter to transmit only that radiation which corresponds to the neodymium pump bands would be relatively straight-forward except for the fact that we would like to permit energy transfer via fluorescence. Conventional absorbing agents used in heat-blocking and/or U.V. blocking filters do not fluoresce and, because of their strong absorption at the exciting wavelengths of fluorescing ions, would prevent any possibility of a fluorescent converter.

TEST LASER SET-UP

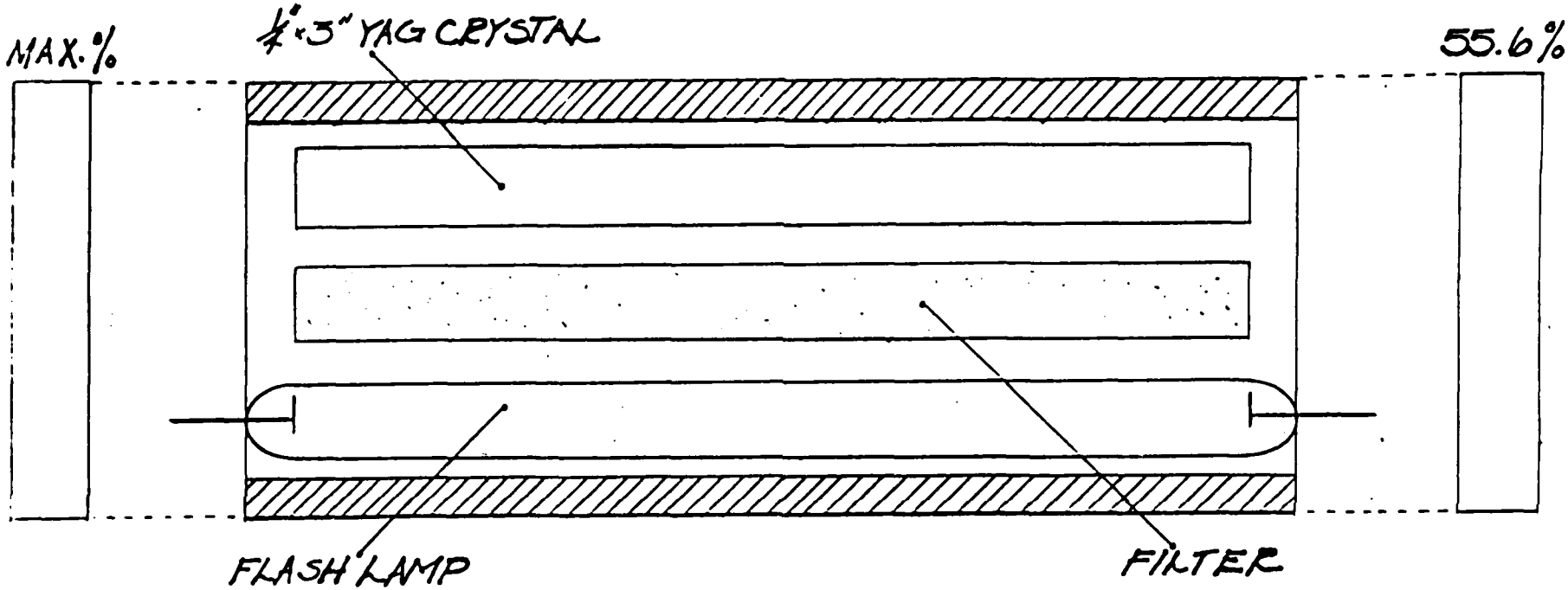

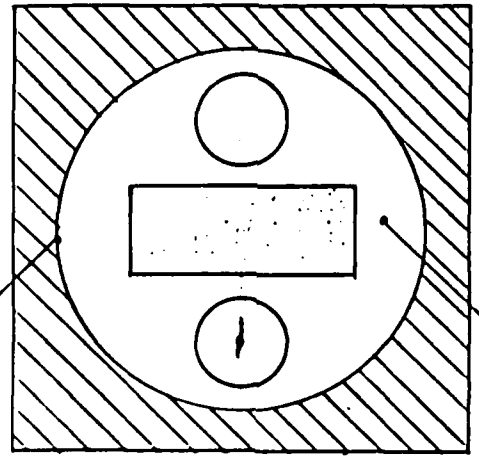

Because of this situation, the absorbing ions utilized in this filter must either fluoresce themselves at the proper wavelength, or be compatible with some ion that does fluoresce at the proper wavelength. Our procedure then, was dictated by the aforementioned constraints. The particular glass-base chosen as a host for the candidate fluorescing and absorbing ion candidates was chosen with the same constraints in mind plus the additional properties as follows:

1. Non-solarizing
2. High transmission across entire visable spectrum
3. High rupture strength

The glass-base chosen for this work was our commercial filter material designated KF-2. A careful check was made to assure that the anti-solarent used in this material did not in any way interfer with the neodymium pump bands. The task of designing a proper fluorescent converter mandates that we take into account the mechanisms involved. Here, the flashlamp energy must first be absorbed in the fluorescent material, which would then re-emit to fluorescently pump the Nd^{3+} laser rod. This fluorescent pumping could be beneficial in two ways; first, the short wavelength radiation which is not efficiently absorbed by the neodymium can be converted to wavelengths which are strongly absorbed; and second, the conversion of short wavelength pump light to longer wavelengths will minimize the amount of heat generated in the laser rod. However, if the fluorescent material is to efficiently pump the neodymium, and not simply absorb and waste the short wavelength radiation from the flashlamp, it must display several characteristics. These characteristics would be:

1. An efficient absorption at "short" wavelengths;
2. An emission at a strong Nd^{3+} absorption band;
3. A high quantum efficiency for fluorescence;
4. A short fluorescent decay time ($\tau < \tau nd$);
5. A low refractive index host.

The importance of the first three characteristics is obvious. While the fourth characteristic is only important in Q-switch applications, it will be included here since Q-switched applications are of immediate concern. (However, it is important

in any application that the fluorescent decay time of the "active filter" be less than the flashlamp pump pulse). The fiftn characteristic is included to minimize any trapping of fluorescence in the host. However, the importance of this is dependent on many factors which especially includes the index of refraction of any cooling liquid between the "active filter" and the laser rod.

"WINDOW" FILTER DEVELOPMENT

As is mentioned previously, the design of a filter to absorb certain wavelengths and transmit others is a relatively straight-forward endeavor. One essentially selects dopants which absorb in the desired portion of the spectrum and add them to the glass metrix until one achieves the desired level of absorption. Since we were interested essentially in fluorescent energy transfer, we selected our absorbing ions mainly from the list of prospective fluorescent converter candidate ions. The development process went through the following stages:

1. Solarization Evaluation...Since we were considering the use of rare-earth ions as absorbing agents in our window filter, we were interested in determining their anti-solarent properties,...if any. The most logical ions for our initial investigation were Europium and Terbium. Glass sample doped with these ions were tested in a laser system for visual signs of solarization. The results are noted below.

Melt No.	Doping	No. of Shots	Solarization
L-317	5% Eu_2O_3	12,000	Very light
L-318	5% Tb_2O_3	8,000	Heavy
L-319	10% Tb_2O_3	7,000	Very heavy

Based upon these melts, we chose our commercial filter glass composition as our glass-host. The commercial composition gives us is well tested base material whose properties are well known. This base-glass has been in use as a filter material in YAG laser cavities for about 10 years.

2. Absorption Considerations...In order that we might maximize our options for introducing beneficial energy transfer while developing the window filter, our initial candidates for our absorbing ions is chosen from

the trivalent rare-earth ions listed in the section dealing with fluorescing ions in glasses, (Appendix A) spectroscopic samples containing the following ions were prepared. Their transmission spectras were then run on a Beckman DK-2A spectrograph.

Melt No.	Dopants & Wt.%
L-317	5% Eu_2O_3
L-318	5% Tb_2O_3
L-319	10% Tb_2O_3
L-366	2.5% Eu_2O_3
L-356	5% Dy_2O_3
KSF-5	5% Sm_2O_3
P-926	3.5% Tu_2O_3
L-331	1% CeO_2
L-338	1.4% Dy_2O_3
L-340	0.7% Pr_2O_3
L-355	2% Dy_2O_3
L-357	2% Pr_2O_3
L-351	0.1% UO_2

From the spectra of the various melts listed above, the following ions appeared to absorb at wavelengths which would not interfere with the neodymium pump-bands.

Melt No.	Rare-Earth Oxides
L-317 and L-336	Eu_2O_3
L-318 and L-319	Tb_2O_3
KSF-5	Sm_2O_3
L-331	CeO_2

It was decided that a reasonable window filter might be constructed using the cumulative absorptions of each of these rare-earth oxides. Following that rationale, a number of melts were made at various dopant levels to ascertain the appropriate balance between the presence and quantity of each constituent. The following melts

were then prepared:

	Melt No. Wt.%						
Dopant	L-340	L-341	L-369	L-320	L-371	L-372	L-378
Eu_2O_3	8.0	8.0	8.0	8.0	8.0	8.0	8.0
Tb_2O_3	6.0	6.0	6.0	6.0	6.0	6.0	6.0
CeO	-	0.15	0.3	0.15	0.15	-	0.5
Sm_2O_3	1.15	1.15	1.15	1.15	2.3	2.3	1.15

From these melts, M-1 test cavities were fabricated and tested versus a standard M-1 cavity in the M-1 cavity test apparatus. The results are listed below.

Melt No.	(650V) A (Mj)	(750V) B (Mj)
Standard M-1	68	104
L-331 (1% CeO_2)	79	117
L-341	78	115
KSF-5 (5% Sm_2O_3)	77	113
L-355 (2% Dy_2O_3)	72	110
L-351 (0.1% UO_2)	55	83
L-356 (5% Dy_2O_3)	54	88
L-357 (2% Pr_2O_3)	63	99

From the above table, one can observe that Dy_2O_3, Pr_2O_3, and UO_2 all degrade performance significantly on a single-shot basis. All of the other rare-earth ions appear to be useful in terms of their transmission of the neodymium pump-bands.

ANALYSIS OF WINDOW FILTER DATA

From the transmission spectra plus the actual lasing data gained from the M-1 cavity test apparatus, it appears that the L-341 combination would serve as an acceptable window filter. Comparing the performance figures using the L-341 material and the L-331 clear (1% CeO_2), it would also appear that L-341 does permit some energy transfer via fluorescence. L-341 does block a small portion of the neodymium pump bands, yet, its performance is equivalent to a material which has much less blocking. (See Page No. 15 for transmission spectra of L-341.)

FLUORESCENT CONVERTER ACTIVITY

Based upon the disappointing results of the Dy_2O_3, Pr_2O_3, and UO_2 doped cavities, it was decided that even with sensitizing, the improvements to be gained would be minimal. Also, recognizing that the "window filter" did apparently display some fluorescent conversion, we decided to isolate the working constituent and optimize the doping levels for maximum fluorescent conversion efficiency. To this end, an open-ended series of melts were made and tested. Table No.1 lists these melts.

Table No. 1
Melt No. & Wt.%

Dopant	L-379	L-380	L-381	L-382	L-383	L-384	L-388	L-386
Eu_2O_3	14	17	20	20	20	23	17	17
Tb_2O_3	-	-	-	-	-	-	-	-
CeO	-	-	-	-	-	-	-	.15
Sm_2O_3	-	2.3	2.3	-	4.6	2.3	4.6	4.6

	L-368	L-367	L-366	L-365	L-369	L-300
Eu_2O_3	-	4	2.5	-	8	8
Tb_2O_3	14	10	-	2.5	6	6
CeO	.15	.15	-	-	.3	.15
Sm_2O_3	1.15	1.15	-	-	1.15	1.15

At least two slides approximately .070" thick were fabricated from each of the melts listed. These slides were then tested in the liquid cooled laser test cavity illustrated on Page No. 5. Typical results of these tests are listed in Table No. 2

Table No. 2

Input Joules/Pulse	Millijoules Output/Pulse						
	Without Filter	L-383	L-384	L-381	L-380	L-379	L-382
10.1	132	105	120	115	119	120	132
12.5	182	153	162	165	182	171	180
15.1	232	204	220	229	231	220	236
18.0	285	255	282	279	295	271	306
21.1	332	323	339	350	363	349	349
24.5	369	384	404	412	420	404	409
28.1	447	452	479	502	516	495	501
32.0	498	525	551	578	590	570	578
36.1	545	588	610	642	651	633	658
40.5	567	665	683	711	718	711	716
45.1	619	730	771	791	813	721	767
50.0	649	792	830	852	848	838	862

The data was acquired at a pulse repetition rate of 3 HZ, resulting in an maximum average power input to the YAG laser rod of about 150 watts. An additional test using the same laser test head was instituted using a 30 HZ repetition rate and an average power of about 360 watts. Typical results are shown below.

Melt No.	None	L-371	L-378	L-380	L-386
Output/Pulse	147mj	128mj	206mj	190mj	202mj

Taking into consideration the importance of absorptions at one micron plus other considerations, melt L-386 was judged to provide the best overall performance. A final test using the liquid cooled test laser comparing performance with and without the L-386 filter is shown on Page No. 13. (See transmission spectra of L-386 on Page No. 14.)

RESULTS

Careful slope-efficiency measurements using the laser test apparatus shown on page number 5 result in the graph shown on page 13. As the graph illustrates, imposition of a filter slide of L-386 into the test apparatus versus the same test run with no filter in place results in a significant improvement in performance. As one would expect, the extent of the improvement improves markedly as the energy-per-pulse increases due to the increased "bluing" of the flashlamp. That is, the flashlamp is generating a greater portion of its emission in the UV part of the spectrum as its color-temperature increases. This shifting in color temperature of the flashlamp is being absorbed by the filter and coverted via fluorescent-emission into the neodymium absorption bands. In the case of no filter, this energy is simply absorbed by the laser and surroundings as heat.

Another factor must be taken into account. The filter slides used in this test were .070 inches thick. The separation between the flashlamp and laser rod is about .160 inches. Because of the index of refraction of the glass (approximately 1.55), the apparent rod-lamp distance is reduced from .150 inches distance (with no filter), to about .127 inches...resulting in some inherent improvement in performance associated only with the improvement in "cavity filling factor". This improvement is illustrated by the performance curve of the cavity wherein the L-386 filter was replaced by an identical KF-2 "clear" filter.

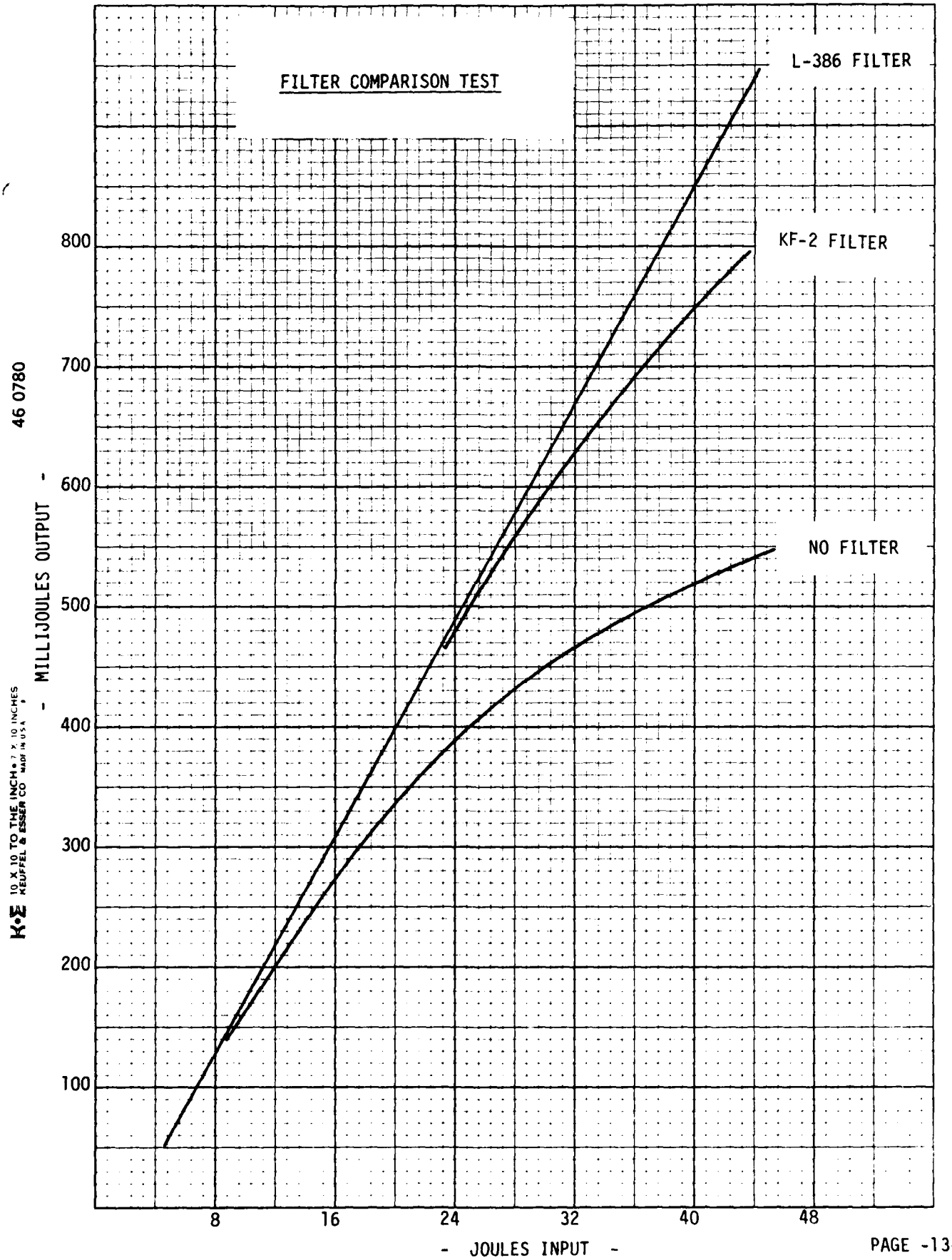
FILTER COMPARISON TEST
L-386 FILTER
KF-2 FILTER
NO FILTER
800
700
600
500
400
300
200
100
8
16
24
32
40
48
- MILLIJOULES OUTPUT -
- JOULES INPUT -
46 0780
K•E 10 X 10 TO THE INCH • 7 X 10 INCHES
KEUFFEL & ESSER CO MADE IN U.S.A.

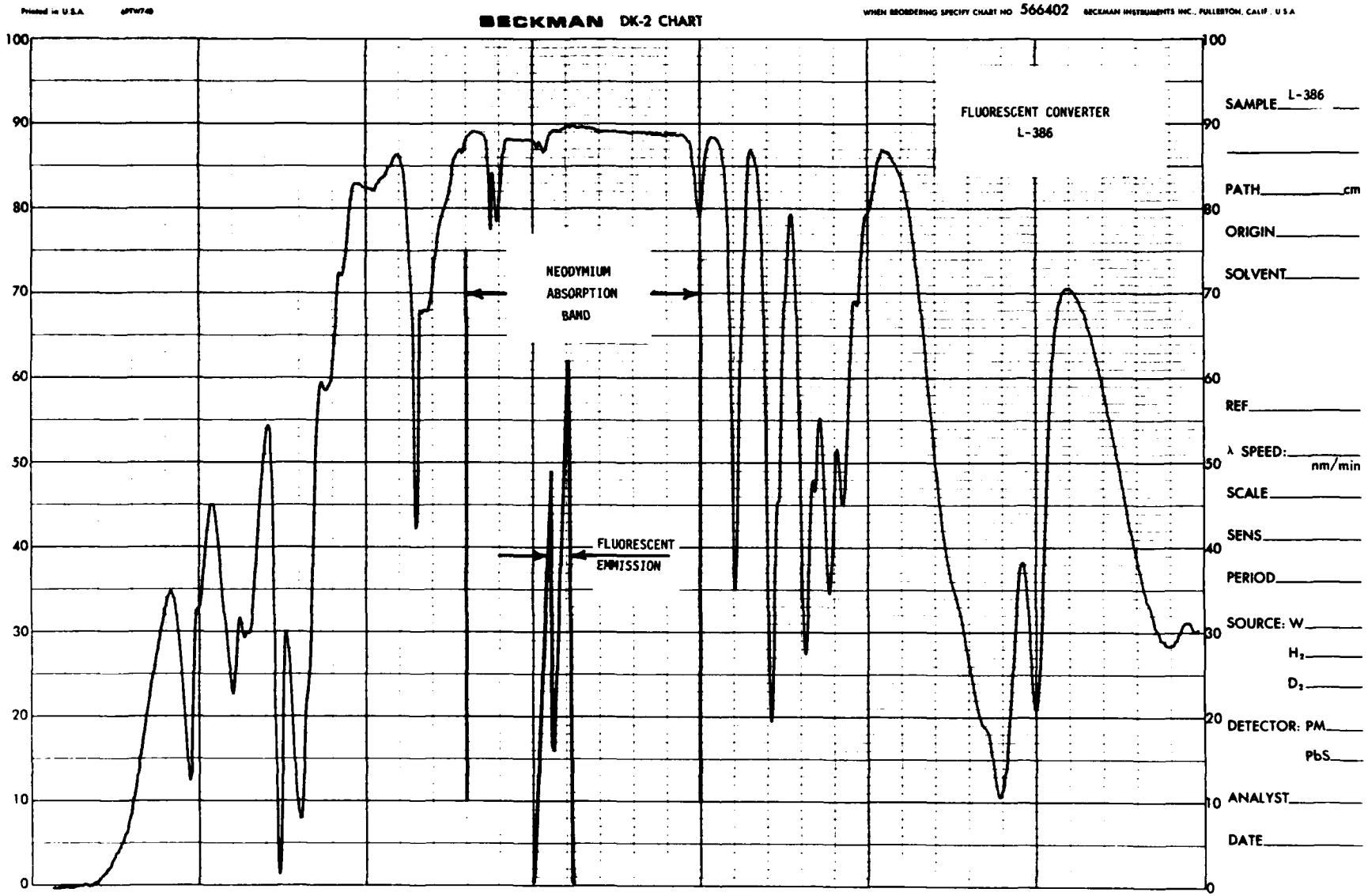
Printed in U.S.A.
BECKMAN DK-2 CHART
WHEN REORDERING SPECIFY CHART NO 566402
BECKMAN INSTRUMENTS INC., FULLERTON, CALIF., U.S.A.
FLUORESCENT CONVERTER
L-386
NEODYMIUM
ABSORPTION
BAND
FLUORESCENT
EMMISSION
SAMPLE L-386
PATH cm
ORIGIN
SOLVENT
REF
λ SPEED: nm/min
SCALE
SENS
PERIOD
SOURCE: W
H₂
D₂
DETECTOR: PM
PbS
ANALYST
DATE
100
90
80
70
60
50
40
30
20
10
0

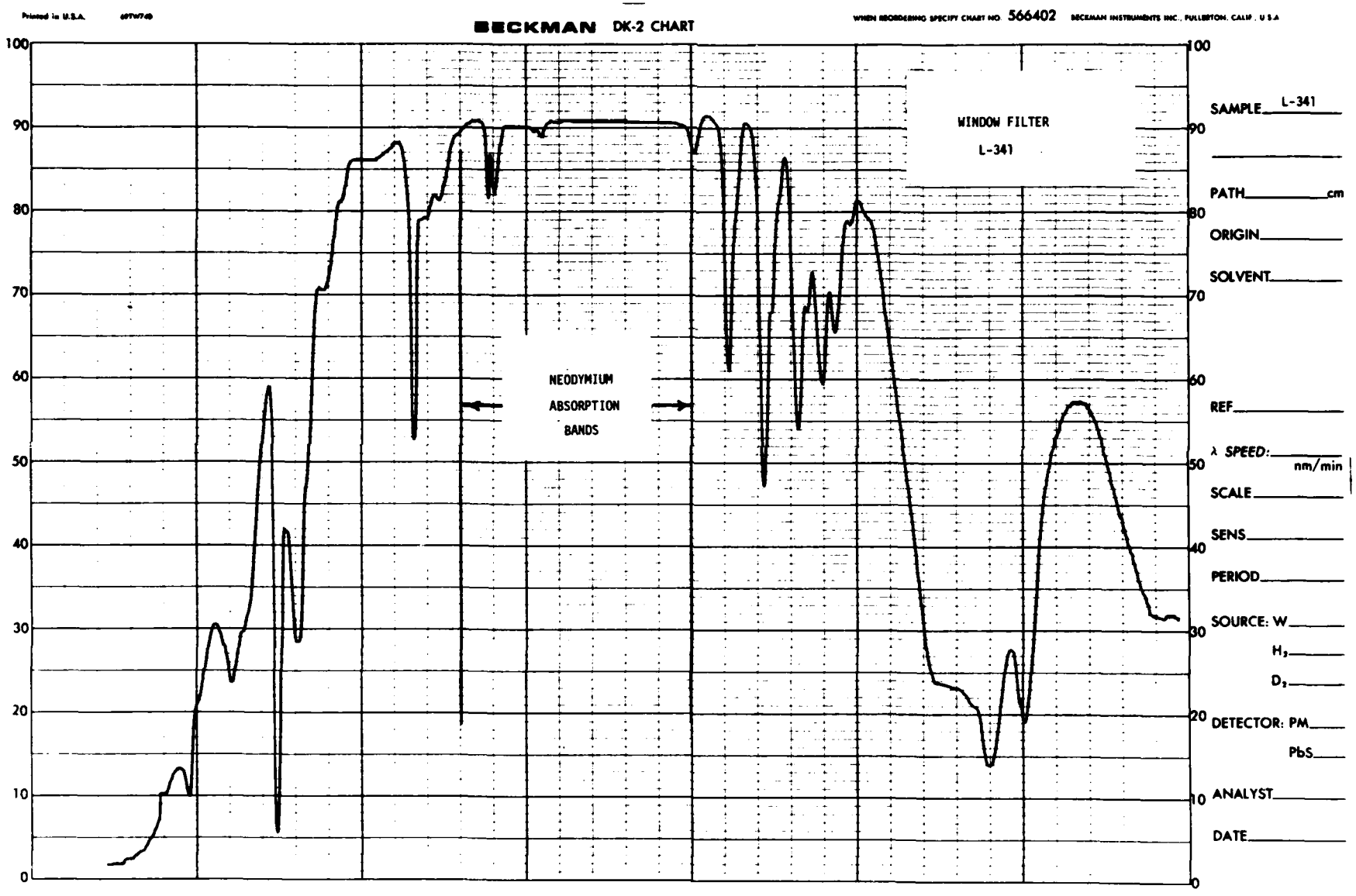
BECKMAN DK-2 CHART
WHEN REORDERING SPECIFY CHART NO. 566402
WINDOW FILTER
L-341
NEODYMIUM
ABSORPTION
BANDS
SAMPLE L-341
PATH cm
ORIGIN
SOLVENT
REF
λ SPEED: nm/min
SCALE
SENS
PERIOD
SOURCE: W
H₂
D₂
DETECTOR: PM
PbS
ANALYST
DATE
100
90
80
70
60
50
40
30
20
10
0

Addendum to Task III

Subsequent to depletion of funds from this contract, Kigre, Inc. undertook an in-house research program into the development of fluorescent conversion by meands of a fluorescent envelope surrounding the flashlamp and laser rod. Final testing of FC-4 fluorescent converter in a standard M-1 configuration with a Q-88 laser rod demonstrated a 17.89% increase in efficiency over the standard M-1 $BaSO_4$ cavity (Graph A 3.1). FC-4 is now commercially available from Kigre, Inc. at a price comparable to that of $BaSO_4$.

Graph A 3.1

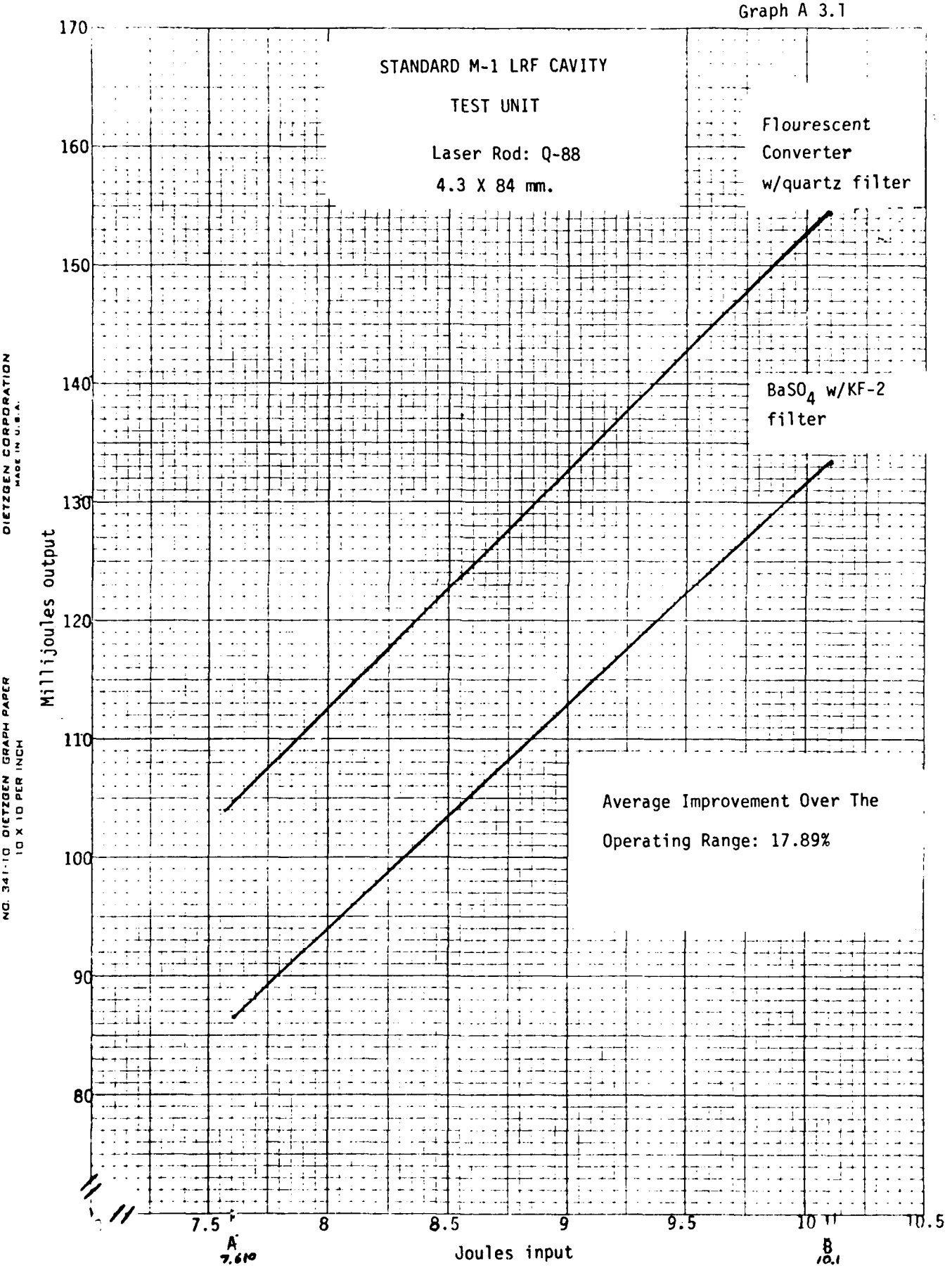

DIETZGEN CORPORATION
MADE IN U.S.A.

NO. 341-10 DIETZGEN GRAPH PAPER
10 X 10 PER INCH

APPENDIX A

By:

C. F. Rapp

Appendix A

Fluorescent Glasses For Use In Fluorescently Pumping Nd^{3+} Doped Laser Glass

1. Introduction

In certain cases it may be desirable to fluorescently pump a neodymium doped laser glass rather than directly excite the laser glass with the light from a flashlamp. That is, the flashlamp energy is first absorbed in a fluorescent material which then re-emits to fluorescently pump the Nd^{3+} laser glass. This fluorescent pumping could be beneficial in two ways; first, the short wavelength radiation which is not efficiently absorbed by the neodymium can be converted to wavelengths which are strongly absorbed; and, second, the conversion of short wavelength pump light to longer wavelengths will minimize the amount of heat generated in the laser rod. However, if the fluorescent material is to efficiently pump the neodymium, and not simply absorb and waste the short wavelength radiation from the flashlamp, it must display several characteristics. These characteristics would be:

1. An efficient absorption at "short" wavelengths;
2. An emission at a strong Nd^{3+} absorption band;
3. A high quantum efficiency for fluorescence;
4. A short fluorescent decay time ($\tau < \tau nd$);
5. A low refractive index host.

The importance of the first three characteristics is obvious. While the fourth characteristic is only important in Q-switch applications, it will be included here since Q-switched applications are of immediate concern. (However, it is important in any application that the fluorescent decay time of the "active filter" be less than the flash lamp pump pulse). The fifth characteristic is included to minimize any trapping of fluorescence in the host. However, the importance of this is dependent on many factors which especially includes the index of refraction of any cooling liquid between the "active filter" and the laser rod.

2. FLUORESCENT GLASSES

Ions which fluoresce in glass can generally be divided into five groups. These would include:

1. The fluorescent transition metal ions;
2. The filled shell fluorescent ions;
3. The trivalent rare earths;
4. The divalent rare earths;
5. The actinides.

(Actually the trivalent rare earths, the divalent rare earths and the actinides could be considered as a single group so that there would then only be three different groups). Within these five groups there are approximately 30 ions which are known to fluoresce in glass. These ions are outlined in the attached Table 1. The most promising candidates for fluorescently pumping neodymium in glass can easily be selected from the ions listed in Table 1 by examining their known absorption and emission properties.

The Transition Metal Ions - the Mo^{3+} and Mn^{2+} ions can have reasonable quantum yields for their fluorescence. However, both ions have fluorescent decay times which are greater than one millisecond. Since this is about 3 times the decay time of the neodymium ion in a phosphate or a "high gain" silicate glass, these ions would not be suitable for fluorescently pumping a Q-switched neodymium laser. Also, the Cr^{3+}, Fe^{2+}, Co^{2+}, Ni^{2+} and V^{5+} ions apparently fluoresce with very low quantum yields. Therefore, none of the transition metal ions appear suitable for fluorescently pumping neodymium doped glass.

The Filled Shell Fluorescent Ions, Ce^{3+} and Eu^{2+} - These eight ions are considered together since they have a number of common characteristics. These would include: 1) all eight ions have intense allowed absorption bands in the UV region of the spectrum; 2) all except copper have allowed emissions with short decay times. (Copper has a forbidden d → s transition but still has a decay time of only 1/3 that of neodymium); 3) all have high quantum efficiencies; 4) all have broad emission bands which can be shifted significantly in different hosts. Therefore, these ions do show some promise for fluorescently pumping neodymium. However, their ability to enhance the neodymium laser efficiency would probably be limited by the fact that they primarily absorb in the UV and by their broad emission bands. These ions may in general be more useful as sensitizers.

The Trivalent Rare Earths and Uranium - Of these various ions, only the Pr^{3+}, Dy^{3+} and UO_2^{2+} ions display fluorescent decay times which are reasonable for fluorescently pumping neodymium. (Sm^{3+}, Eu^{3+} and Tb^{3+} might be considered if the system were not Q-switched. Ho^{3+}, Tm^{3+} and Yb^{3+} fluoresce at wavelengths which are too long for pumping neodymium) In addition to having reasonable decay times, the Pr^{3+}, Dy^{3+} and UO_2^{2+} ions also emit at wavelengths where the neodymium ion absorbs strongly. (For example, see the attached Figure 1 for the UO_2^{2+} emission - Nd^{3+} absorption overlap; and Figure 2 for the Dy^{3+} emission - Nd^{3+} absorption overlap.) Therefore, it would appear that Pr^{3+}, Dy^{3+} and UO_2^{2+} doped glasses are the most promising candidates for fluorescently pumping neodymium doped laser glass. Unknown factors are the quantum yields of the visible fluorescent bands of the Pr^{3+} and Dy^{3+} ions. (The UO_2^{2+} ion does have a high quantum yield.) Also, since the Pr^{3+} and Dy^{3+} ions do not absorb strongly at short wavelengths, sensitization by one or more of the filled shell fluorescent ions, Ce^{3+} or Eu^{2+} may be desirable.

Schott fluorescent uranium filters: GG17, GG21

	GG-17	GG-21
ρ	2.49	2.48
Tg (10^{13} poice)	618 ^{o}C	622 ^{o}C
α	$79X10^{->}/^{o}C$	$81X10^{->}/^{o}C$
η_D	1.514	1.514
ν_D	65.0	66.0

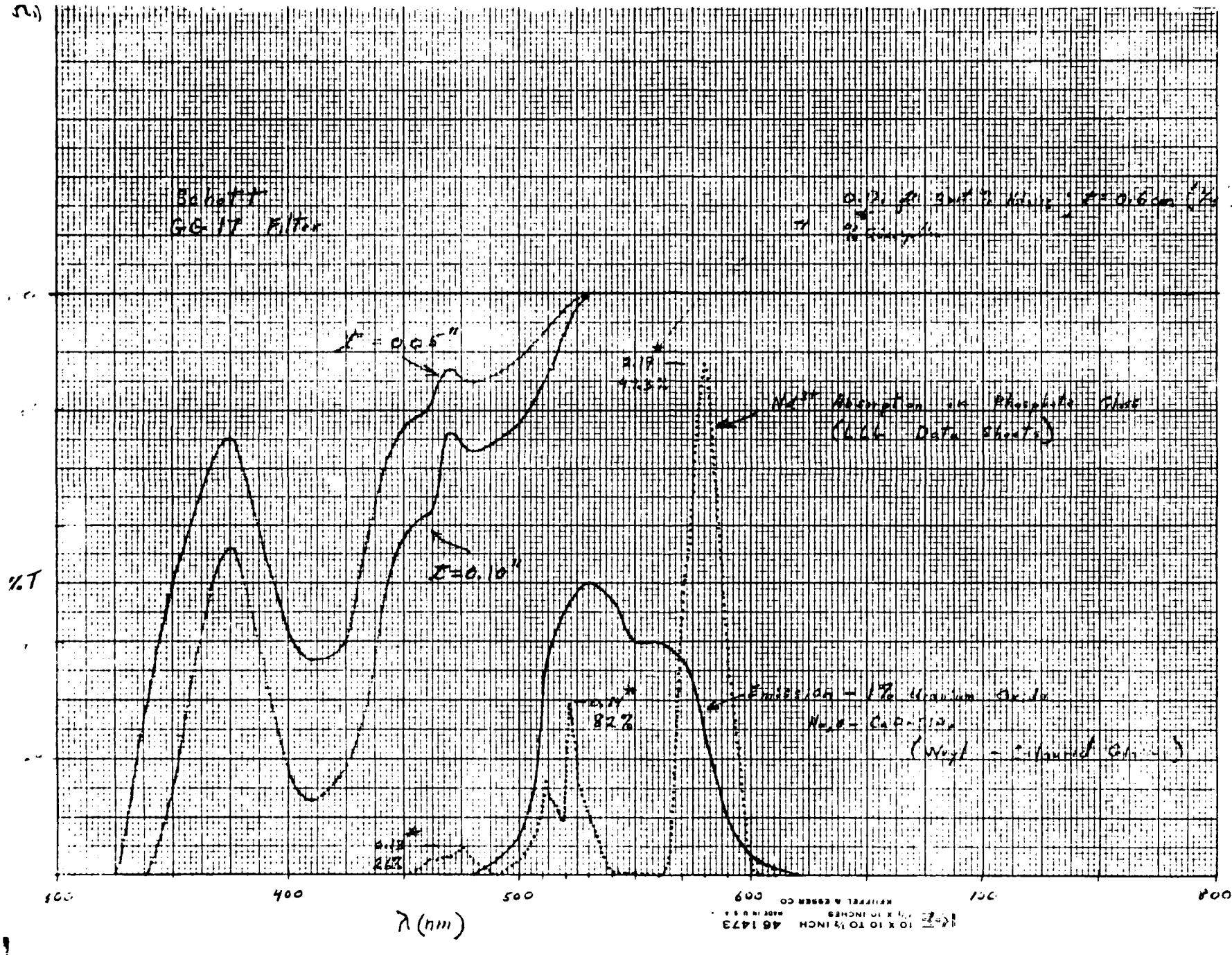
Schott
GG-17 Filter
T = 0.05"
T = 0.10"
%T
λ (nm)
400
500
600
800

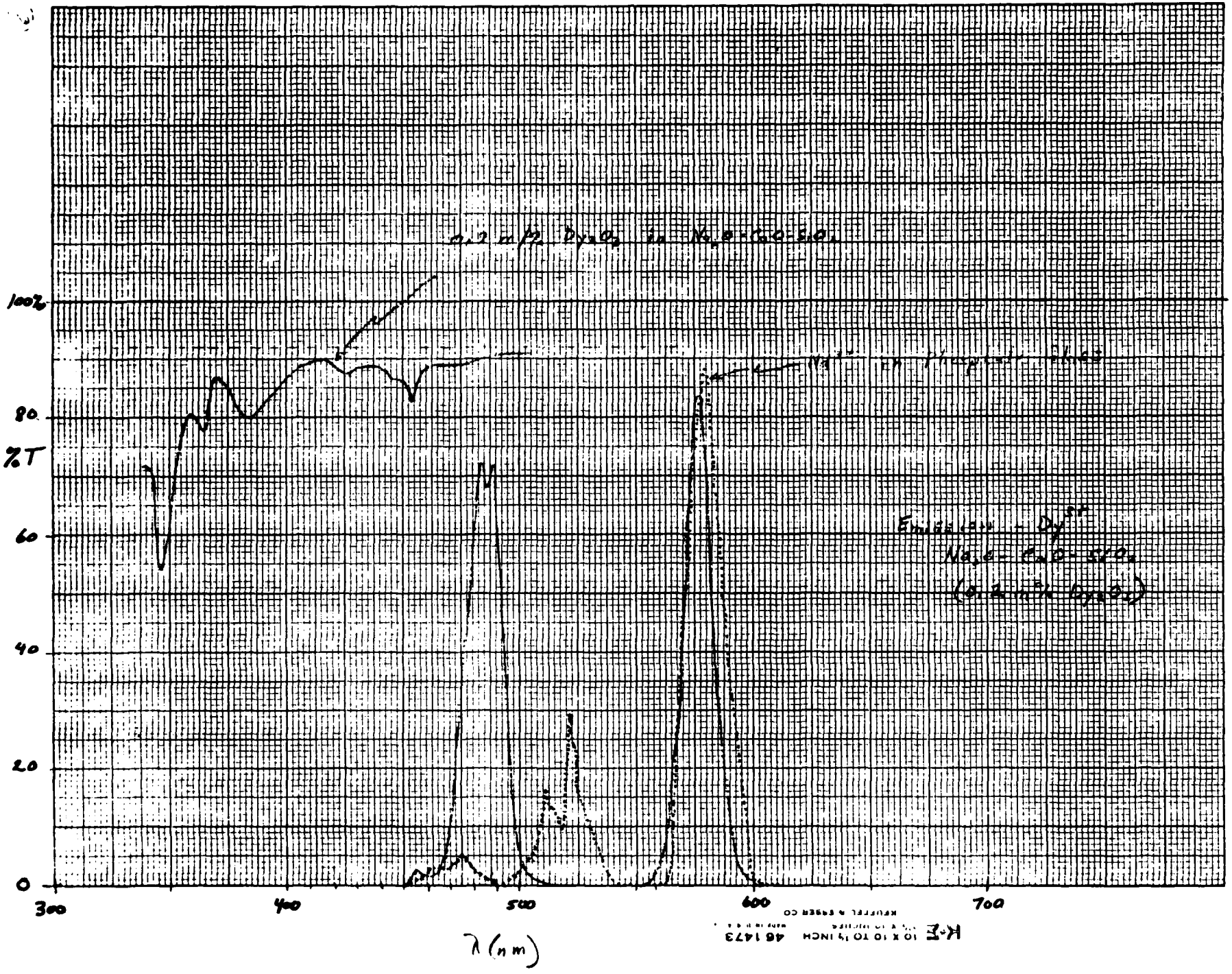
0.12 m mol Dy_2O_3 in Na_2O-CaO-SiO_2
100%
80
%T
60
40
20
0
300
400
500
600
700
λ (nm)
Emission (sharp) - Dy^{3+}
Na_2O - CaO - SiO_2
(or a mixture of Dy_2O_3)

Table 1. Ions Which Fluoresce in Glass

Transition Metal Ions

	Reference
Mo^{3+}	1
Mn^{2+}	3
Cr^{3+}	
Fe^{2+}	12
Co^{2+}	12
Ni^{2+}	12
V^{5+}	14

Filled Shell Fluorescent Ions

	Reference
Cu^{+}	11
Ag^{+}	14
Sn^{2+}	13
Pb^{2+}	15
Sb^{3+}	13
Bi^{3+}	15
Tl^{+}	15

Trivalent Rare Earths

Ce^{3+}	Tb^{3+}
Pr^{3+}	Dy^{3+}
Nd^{3+}	Ho^{3+}
Sm^{3+}	Er^{3+}
Eu^{3+}	Tm^{3+}
Gd^{3+}	Yb^{3+}

Divalent Rare Earths

	Reference
Eu^{2+}	16
Yb^{2+}	16
Sm^{2+}	16

Actinide

UO_2^{2+}

Table 2. Fluorescent Decay Times of Filled Shell, Rare Earth, and Actinide Ions in Glass

	τ (Millisec)	Reference
* Ce^{3+}	0.0001	
* Pr^{3+}	0.2	9
Nd^{3+}	0.3-0.8	10
Sm^{3+}	1.0	7
Eu^{3+}	2.5	4
Gd^{3+}	4.2	5
Tb^{3+}	2.5	5,7
* Dy^{3+}	0.5	7
Ho^{3+}	1.0 (at 2μ)	8
Er^{3+}	10.0 (at 1.5μ)	6
Tm^{3+}	0.5 (at 1.8μ)	6
Yb^{3+}	1.0	6,8
---		
* Eu^{2+}	0.002	
Yb^{2+}	?	
Sm^{2+}	?	

	τ (Millisec)	Reference
* Tl^{+}	0.003	15
* Pb^{2+}	0.003	15
* Sn^{2+}	0.008	13
* Sb^{3+}	0.005	13
* Bi^{3+}	0.003	15
* Cu^{+}	0.10	11
---		
* UO_2^{2+}	0.20	2,14

Table 3. Possible Low Index Glasses for Use in Fluorescent Pumping Applications

SiO_2	74.91	61.94	46.30
B_2O_3	12.45	25.82	42.33
Na_2O	11.26	11.19	10.44
CaO	0.10	0.14	0.08
Al_2O_3	0.89	0.84	0.80
N_d	1.495	1.489	1.485

1,2 - Ethonediol)
Ethylene glycol) $N_d = 1.4314^{20}$
Glycol)

Water $N_d = 1.333$

FLUORESCENT DECAY TIMES IN GLASS

T (millisec)

* *	Ce^{3+}	0.0001
* *	Pr^{3+}	0.2 (low ϕ ??)
	Nd^{3+}	0.3-0.5
	Sm^{3+}	1.0
	Eu^{3+}	2.5
	Gd^{3+}	4.2
	Tb^{3+}	2.5
*	Dy^{3+}	0.5
	Ho^{3+}	1.0
	Er^{3+}	10.0
	Tm^{3+}	(0.5) at 1.85μ
	Yb^{3+}	1.0

* *	Eu^{2+}	0.004
	Yb^{2+}	
	Sm^{2+}	

* *	$T\ell^{+}$	0.003
* *	Pb^{2+}	0.003
* *	Sn^{2+}	0.008
* *	Sb^{3+}	0.005
* *	Bi^{3+}	0.003
* *	Cu^{+}	0.10
* *	UO_2^{2+}	0.20

Mo^{++2} fluoresces at 1.025μ

1/2 width is ~ 80nm wide

	RE^{3+} Ionic Radius (Å)	Mole %	Immisibility Limit Mole % B_2O_3
La_2O_3	1.15		
Ce_2O_3	1.11		
Pr_2O_3	1.09		
Nd_2O_3	1.08		76.0
Pm_2O_3	1.06		
Sm_2O_3	1.04		73.5
Eu_2O_3			73.3
Gd_2O_3	1.02		72.7
Tb_2O_3	1.00		
Dy_2O_3	0.99		71.0
Ho_2O_3	0.97		70.1
Er_2O_3	0.96		69.7
Tm_2O_3	0.95		69.5
Yb_2O_3	0.94		69.0
Lu_2O_3	0.93		
Y_2O_3	0.93		70.0
Cs_2O		↑	
K_2O		Complete	
Na_2O		↓	
Li_2O			
BaO	1.35	16	84
PbO	1.21	19	81
SrO	1.13	21	79
CaO	0.99	27	73
CdO	0.97	47	53
ZnO	0.74	49	51
MgO	0.65	47	53
Al_2O_3	0.50	?	

REFERENCES

1. S. Parke and A. J. Watson, Phys and Chem of Glass, 10, (2), 37-42 (1969).
2. J. C. Joshi, N. C. Pandey, B. C. Joshi and Janordan Joshi, Journal of Luminescence 16, 435-440 (1978).
3. W. H. Turner and J. Eastman, J. Am. Cer. Soc. 53, 329-335 (1970).
4. P. K. Gallagher, C. R. Kurkjian and P. M. Bridenbough, Phys and Chem of Glass, 6, (3), 95-103 (1965).
5. A. D. Pearson, G. E. Peterson and W. R. Northover, J. of Appl. Physics, 37, (2), 729-734 (1966).
6. W. H. Gandy, R. J. Ginther and J. F. Weller J. Appl. Physics 38, 3030-31 (1967).
7. Yu V. Denisou, B. V. Dghurinskii and V. A. Kizel, Inorg. Materials, 3, (5), 757-61 (1967).
8. H. W. Gandy, R. J. Ginther and J. F. Weller, Appl. Phys. Letters, 6, (12), 237-39 (1965).
9. G. A. Moheeva, S. P. Lun'lein and P. P. Feofilov, J. Appl. Spectrosc. 4, (3), 175-79 (1966).
10. E. Snitzer, Phys. Rev. Letters, 7, 444-46 (1961); and others
11. L. Parke and R. S. Webb, Phys and Chem of Glasses, 13, (6), 157-160 (1972).
12. C. Hirayama and F. E. Camp, J. Electrochem Soc., 115, (12), 1275-1279 (1968).
13. S. Parke and R. S. Webb, J. Phys. D: Appl. Phys., Vol. 4, 825-828 (1971).
14. W. A. Weyl, Colored Glasses, reprinted by Dawson's of Pall-Mall, London (1959).
15. S. Parke and R. S. Webb, J. Phys. Chem. Solids, 34, 85-95 (1973).
16. A. Wachtel, J. Electrochem. Soc., 117, (5), 708-711 (1970).

AD A147 471 THE DEVELOPMENT OF A HIGH AVERAGE POWER GLASS LASER SOURCE(U) KIGRE INC TOLEDO OH J D MYERS 31 MAY 84 N00014 81-C 2376

2/2

UNCLASSIFIED F/G 20/5 NL

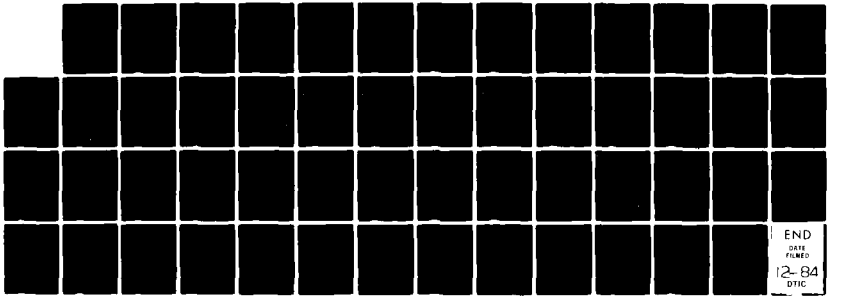

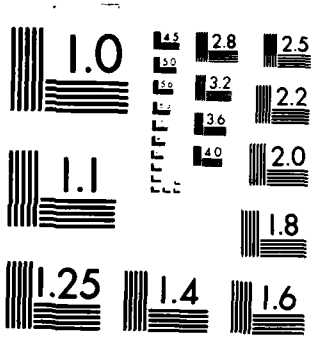

MICROCOPY RESOLUTION TEST CHART
NATIONAL BUREAU OF STANDARDS-1963-A

APPENDIX B

By:

C. F. Rapp

Spectroscopic Data By:

J. Chrysochoos

Appendix B

Spectroscopic Evaluation of Dy^{3+}, Pr^{3+} and UO_2^{2+} Doped Glasses For Use in Fluorescently Pumping Nd^{3+} Doped Laser Glass.

Introduction

The use of an "active" or fluorescent filter between the flash lamp and neodymium doped laser glass can improve a laser's performance in two ways. First, the short wavelength radiation which is not efficiently absorbed by the neodymium can be converted to wavelengths which are strongly absorbed; and, second, the conversion of short wavelength pump light to longer wavelengths will minimize the amount of heat generated in the laser rod.

In order to identify potential candidates for the fluorescent filter, a survey of fluorescent materials was done previously. In this survey several criteria were used to select candidates which might improve the efficiency of the neodymium laser. These criteria were that the fluorescent material should have:

1. An efficient absorption at "short" wavelengths;
2. An emission at a strong Nd^{3+} absorption band;
3. A high quantum efficiency for fluorescence;
4. A short fluorescent decay time ($\tau < \tau$ Nd);
5. A low refractive index host.

Materials which seemed most likely to meet these criteria were:

Dy^{3+} doped glass
Pr^{3+} doped glass and
UO_2^{2+} doped glass

In order to determine which materials should be tested as "active filters", several melts of these glasses were prepared and evaluated spectroscopically.

Summary and Conclusions

1. The Dy^{3+} doped glass is a promising candidate for an "active filter". The overlap between the Dy^{3+} emission and the Nd^{3+} absorption is excellent. Also, the Dy^{3+} quantum efficiency is good. However, the Dy^{3+} absorption at short wavelengths is somewhat weak. Therefore,

an additional sensitizer for the Dy^{3+} in the filter may be desirable (for example, Ce^{3+} or Eu^{2+}).

2. The UO_2^{2+} doped glass is a reasonable candidate for the "active filter". The UO_2^{2+} emission and Nd^{3+} absorption bands overlap reasonably well. Also, the UO_2^{2+} absorbs very efficiently at short wavelengths. However, the quantum efficiency of the sample tested was only "fair". Also, there is a significant possibility of interference by the UO_2^{2+} excited state absorption.

3. The Pr^{3+} doped glass appears less promising for use as an "active filter". This is based on the low quantum yield measured for the Pr^{3+} fluorescence. However, the Pr^{3+} emission band at 8600 Å was not detected by the instrument used. If this band were an order of magnitude more intense than the 6,000 Å band, the total quantum efficiency for the Pr^{3+} ion could be reasonable.

Recommendations would include:

1. Testing a Dy^{3+} doped glass filter in an active laser. (Probably about 0.5 mole % Dy_2O_3).

2. Testing a Ce^{3+} - Dy^{3+} doped glass filter in an active laser. (Probably about 0.5 mole % Dy_2O_3 + 0.02 mole % CeO_2. This should give an optical density for the Ce^{3+} of at least 2 to 3 /cm in the U.V.)

3. Testing a UO_2^{2+} doped glass filter in an active laser. (Probably about 0.35 wt % UO_2^{2+} to give an optical density of about 1/cm at 4,000 Å. If a "thin" filter is used, 1 wt % UO_2^{2+} may be needed.)

(Active laser testing should include an index matching liquid between the filter and laser rod to eliminate trapping of the fluorescence in the filter.)

Results and Discussion

1. Absorption Spectra

The absorption spectra from about 3,000 to 11,000 Å are given in Figure 1 through 5 for the five doped glasses.

As can be seen, the strongest Pr^{3+} absorption bands fall in a region where only very weak Nd^{3+} absorption bands exist ($\simeq$ 4,000-5,000 Å). Therefore, these bands fall in an ideal region. This is not true of

the Pr^{3+} band at about 5,900 Å which falls directly on one of the strongest Nd^{3+} bands. This weaker band could interfere with the direct pumping of the Nd^{3+}.

The 0.5 mole % Dy_2O_3 sample (L346) has the characteristic Dy^{3+} absorption spectrum. The pump bands for the Dy^{3+} fluorescence are those between about 3,400 Å and 4,700 Å. This again is an ideal region for an "active filter" to absorb. However, these bands are somewhat weak. Several bands are also seen between 7,000 and 10,000 Å. These bands do not contribute to the Dy^{3+} visible fluorescence. Unfortunately the bands at 7900 Å and 8900 Å can interfere with the direct pumping of the Nd^{3+}. Therefore, it may be desirable to keep the Dy^{3+} concentration somewhat low (< 0.5 mole %) and include a sensitizer such as Ce^{3+} to absorb the UV from the pump lamp. (Keeping the Dy^{3+} concentration low would also minimize any self quenching of the Dy^{3+} fluorescence - although the importance of this effect has not yet been determined.)

The long wavelength absorption spectrum (< 6000 Å) of the L345 sample is also characteristic of the Dy^{3+} ion. However, at wavelengths shorter than 6,000 Å the Dy^{3+} bands are hidden by some impurity. From the shape of the impurity absorption (with a peak at about 4400 Å) and from the location of the impurity emission band (see Figure 8), it would appear that the impurity is UO_2^{2+}. Since this impurity absorbs so strongly at short wavelengths the quantum efficiency measurements made on this sample are probably much lower than would be expected for an uncontaminated sample. It is also interesting to note that the impurity does not sensitize the Dy^{3+} fluorescence (see Figures 19 and 20).

The short wavelength absorption spectrum of the L351 sample is characteristic of UO_2^{2+}. However, the presence of a number of bands between 10,000 Å and 17,000 Å may suggest the presence of a reduced uranium species. Since the intensity of the UO_2^{2+} band at 4200 Å is only about 0.3/cm, a concentration of about 0.5 wt % UO_2^{2+} may be more desirable for an "active filter". This higher concentration would more effectively absorb the pump light between 3600 Å and 5,000 Å.

2. Emission Spectra

The emission spectra for the Pr^{3+}, Dy^{3+} and UO_2^{2+} samples are shown in Figures 6 through 10, and Figures 11 through 15. (Figures 11 through 15 were corrected for the instrument spectral response and were used for the quantum efficiency calculations.)

If Figures 6 and 7 are compared to Figure 24 it can be seen that a fair amount of overlap exists between the Pr^{3+} emission bands and the Nd^{3+} absorption bands. This is also true for the UO_2^{2+} emission band (Figure 10) and the Nd^{3+} absorption bands. However, the best spectral match occurs between the Dy^{3+} emission spectrum and the Nd^{3+} absorption spectrum. This is particularly true at 5800 Å where a perfect spectral match occurs. For comparison, the Dy^{3+} emission band locations are shown in Figure 24.

3. Excitation Spectra

The excitation spectra for the five samples are shown in Figures 16 through 23. As can be seen, the excitation spectra for the L346 Dy^{3+} sample match the absorption spectra quite well. Also, the shape of the excitation spectra are the same for the 4850 Å and 5750 Å bands. (This would be expected if both bands originated from the same energy level - as is the case here.)

The excitation spectra for the L345 Dy^{3+} sample are quite similar to those for the L346 sample. However, the effect of the impurity can be seen in that the short wavelength excitation bands become progressively less efficient in the contaminated sample. No indication can be seen that the contaminant is sensitizing the Dy^{3+} fluorescence.

The Pr^{3+} excitation spectra are also quite similar to the absorption spectra. However, it is interesting to note that the excitation spectra change when monitoring the 4900 Å band and the 6,000 Å band. This would suggest that the two emission bands originate from different energy levels and is one basis for the band assignments given in Table 1.

4. Relative Fluorescence Quantum Yield of Glasses

The fluorescence quantum yield, ϕ_{fl}, is given by $\phi_{fl} \propto \int_{\text{entire band}} I_F(\bar{\nu})\, d\bar{\nu} / I_o (1-10^{-ECL})$

Where $I_F(\bar{\nu})$ is the corrected fluorescence spectrum plotted on a wavenumber scale, I_o the intensity of the excitation light at λexc. In the presence of self-absorption of the fluorescence,

$$\phi_{fl} \propto \frac{\int I_F(\bar{\nu}) \times 10^{-ECL}\, d\bar{\nu} / I_0(1-10^{-ECL})}{(1-\int I_F(\bar{\nu})\,(1-10^{-ECL})\, d\bar{\nu})}$$

Self-absorption was ignored in the calculation below. If the unknown sample and a known reference are excited under identical geometrical conditions, including slits etc then:

$$\frac{(\phi_{fl})\ \text{sample}}{(\phi_{fl})\ \text{Ref}} = \frac{\int I_F(\bar{\nu})\, d\bar{\nu} / I_0(1-10^{-ECL}) \quad \text{Sample}}{\int I_F(\bar{\nu})\, d\bar{\nu} / I_0(1-10^{-ECL}) \quad \text{Ref.}}$$

The integrated areas are as follows:

L-343 (0.2 mole Pr_2O_3)	:	$(\int I_F(\bar{\nu})\, d\bar{\nu})$ Total = $9.6\times10^4 cm^{-1}$
$^3Po \rightarrow {}^3H6$	:	$(\int I_F(\bar{\nu})\, d\bar{\nu})$ band 1 = $5.5\times10^4 cm^{-1}$
$^3Po \rightarrow {}^3H4$	:	$(\int I_F(\bar{\nu})\, d\bar{\nu})$ band 2 = $3.5\times10^4 cm^{-1}$
L-344 (0.5 mole Pr_2O_3)	:	$(\int I_F(\bar{\nu})\, d\bar{\nu})$ Total = $6.86\times10^4 cm^{-1}$
$^3Po \rightarrow {}^3H6$	:	$(\int I_F(\bar{\nu})\, d\bar{\nu})$ band 1 = $2.1\times10^4 cm^{-1}$
$^3Po \rightarrow {}^3H4$	:	$(\int I_F(\bar{\nu})\, d\bar{\nu})$ band 2 = $3.7\times10^4 cm^{-1}$
L-345 (0.2 mole Dy_2O_3)	:	$(\int I_F(\bar{\nu})\, d\bar{\nu})$ Total = $6.2\times10^5 cm^{-1}$
$^4F9/2 \rightarrow {}^6H13/2$	:	$(\int I_F(\bar{\nu})\, d\bar{\nu})$ band 1 = $3.8\times10^5 cm^{-1}$
$^4F9/2 \rightarrow {}^6H15/2$	:	$(\int I_F(\bar{\nu})\, d\bar{\nu})$ band 2 = $1.5\times10^5 cm^{-1}$
L-346 (0.5 mole Dy_2O_3)	:	$(\int I_F(\bar{\nu})\, d\bar{\nu})$ Total = $20.5\times10^5 cm^{-1}$
$^4F_{9/2} \rightarrow {}^6H13/2$	:	$(\int I_F(\bar{\nu})\, d\bar{\nu})$ band 1 = $12.5\times10^5 cm^{-1}$
$^4F9/2 \rightarrow {}^6H15/2$	:	$(\int I_F(\bar{\nu})\, d\bar{\nu})$ band 2 = $7.2\times10^5 cm^{-1}$
L-351 (0.1 mole UO_2)	:	$(\int I_F(\bar{\nu})\, d\bar{\nu})$ Total = $38.6\times10^4 cm^{-1}$
Rhodamine GG in EtoH (Ref):		$(\int I_F(\bar{\nu})\, d\bar{\nu})$ Total = $31.7\times10^5 cm^{-1}$

Sample	λexc	ECL	10^{-ECL}	$(1-10^{-ECL})$	$\frac{I_o(1-10^{-ECL})}{\text{(Arbitr.Units)}}$	$\frac{\int I_F(\bar{\nu})d\bar{\nu}}{I_o(1-10^{-ECL})}$
L-343:	444	0.40	0.398	0.602	39.13	$2.45\times10^{3}cm^{-1}$ (Total
band (1)	444	0.40	0.398	0.602	39.13	$1.41\times10^{3}cm^{-1}$
band (2)	444	0.40	0.398	0.602	39.13	$0.895\times10^{3}cm^{-1}$
L-344:	438	~0.85*	0.141	0.859	86.76	$0.79\times10^{3}cm^{-1}$ (Total)
band (1)	438	~0.85*	0.141	0.859	86.76	$0.24\times10^{3}cm^{-1}$
band (2)	438	~0.85*	0.141	0.859	86.76	$0.43\times10^{3}cm^{-1}$
L-345:	364	~0.10*	0.794	0.206	31.52	$1.96\times10^{4}cm^{-1}$ (Total)
band (1)	364	~0.10*	0.794	0.206	31.52	$1.21\times10^{4}cm^{-1}$
band (2)	364	~0.10*	0.794	0.206	31.52	$0.476\times10^{4}cm^{-1}$
L-346:	364	0.22	0.603	0.391	59.82	$3.43\times10^{4}cm^{-1}$ (Total)
band (1)	364	0.22	0.603	0.391	59.82	$2.09\times10^{4}cm^{-1}$
band (2)	364	0.22	0.603	0.391	59.82	$1.20\times10^{4}cm^{-1}$
L-351	436	0.15	0.708	0.292	36.79	$1.05\times10^{4}cm^{-1}$ (Total)
Reference	499	0.33	0.468	0.532	38.84	$8.16\times10^{4}cm^{-1}$ (Total)

* Optical densities labelled with an asterisk were not measured directly because the appropriate absorption bands were off-scale. They were estimated from the appropriate density of the less concentrated sample and the ratio of the measurable (O.D.)'s at another wavelength:

$$\frac{(O.D.)'\ \lambda_1}{(O.D.)''\ \lambda 1} = \frac{(O.D.)'\ \lambda_2}{(O.D.)''\ \lambda 2}$$

or

$$(O.D.)'\ \lambda 1 = (O.D.)''\lambda 1 \times \frac{(O.D.)'\ \lambda 2}{(O.D.)''\ \lambda 2}$$

Values of (ϕfl) sample / (ϕfl) Ref and (ϕfl sample

Sample			(ϕfl) sample / (ϕfl) Reg	(ϕfl) samp *
L-343	:	Total	3.0×10^{-2}	0.026
	:	Band (1)	1.73×10^{-2}	0.016
	:	Band (2)	1.1×10^{-2}	0.0094
L-344	:	Total	0.97×10^{-2}	0.008
	:	Band (1)	0.24×10^{-2}	0.002
	:	Band (2)	0.53×10^{-2}	0.004
L-345	:	Total	0.24	0.20 to 0.23
	:	Band (1)	0.15	0.13 to 0.14
	:	Band (2)	5.8×10^{-2}	0.05
L-346	:	Total	0.42	0.38 to 0.40
	:	Band (1)	0.26	0.22 to 0.25
	:	Band (2)	0.18	0.15 to 0.17
L-351	:	Total	0.13	0.11 to 0.12

Values of (ϕfl) sample are based upon values of (ϕfl) Ref = 0.85-0.95 in EtoH.

The emission spectra recorded are portions of the overall emission. In the case of Pr^{3+} emission bands are likely beyond 700nm attributed to $^3P_0 \rightarrow {}^3F_{3,4}$, $^3P_0 \rightarrow {}^1G_4$ and $^1D_2 \rightarrow ({}^3H_J, {}^3F_j)$. The latter ones may be very weak. In spite of that, the low values recorded may imply strong self-quenching. Some self-quenching is apparent between samples L-343 and L-344 (0.5 mole Pr_2O_3).

The relatively low value obtained for the low concentration Dy^{3+} sample (L-345) is due to the presence of impuritis . The absorption spectrum also indicates such a contamination.

These quantum efficiencies are also summarized in Table 1. From these data it could probably be concluded that the Pr^{3+} quantum efficiency is too low to be effective in fluorescent pumping. (Unless the 8600 Å band is an order of magnitude more efficient than the 6,000 Å band). The quantum efficiency of the UO_2^{2+} sample is somewhat higher and may be reasonable for fluorescent pumping.

However, the Dy^{3+} quantum efficiency is quite reasonable. In fact, if the 4750 Å excitation band were used to calculate the quantum efficiency of the 0.2 mole % Dy_2O_3 sample, rather than the 3680 Å band where considerable impurity interference is present, a quantum efficiency of over 80% is obtained. Therefore, the Dy^{3+} is a promising ion for fluorescently pumping the Nd^{3+} ion.

5. Sensitization

The major drawback of the Dy^{3+} ion for use as an "active filter" for Nd^{3+} is its relatively few absorption bands at short wavelengths. This, however, might be improved through the use of a sensitizer.

If the various trivalent rare earths are considered as sensitizers, the only ions which appear likely to sensitize the Dy^{3+} are Tm^{3+} and Ce^{3+} (see Figure 25). The use of Tm^{3+} to sensitize the Dy^{3+} fluorescence was attempted by Dean and Drobnick. However, they observed a net decrease in the Dy^{3+} fluorescent intensity when the Tm^{3+} was added (see Figure 26). Apparently the Tm^{3+} quenches the Dy^{3+} to a greater degree than it sensitizers.

Therefore, the most promising candidate for sensitizing the Dy^{3+} ion would be Ce^{3+} (and possibly Eu^{2+} in some hosts). The Ce^{3+} absorption would cover most of the spectral region below about 3500 Å (see Fig. 27).

Table 1. Fluorescence Quantum Efficiencies of Pr_2O_3, Dy_2O_3 and UO_2 Doped Glasses

				ϕ
L343	0.2 mole % Pr_2O_3	6,000 Å	$^1D_2 \rightarrow {}^3H_4$	1.6%
		4,900 Å	$^3Po \rightarrow {}^3H_4$	0.94%
			Total =	2.6%
L344	0.5 mole % Pr_2O_3	6,000 Å	$^1D_2 \rightarrow {}^3H_4$	0.2%
		4,900 Å	$^3Po \rightarrow {}^3H4$	0.4%
			Total =	0.8%
L345	0.2 mole % Dy_2O_3	5,750 Å	$^4F9/_2 \rightarrow {}^6H13/_2$	14%
		4,850 Å	$^4F9/_2 \rightarrow {}^6H15/_2$	5%
			Total =	21%
L346	0.5 mole % Dy_2O_3	5,750 Å	$^4F9/_2 \rightarrow {}^6H13/_2$	23%
		4,850 Å	$^4F9/_2 \rightarrow {}^6H15/_2$	16%
			Total =	39%
L351	0.1 wt % UO_2		Total =	12%

Table 2. Relative Fluorescence Intensities At:

	Excitation λ	L345 (0.2 mole % Dy_2O_3)	L346 (0.5 mole % Dy_2O_3)
	4750 Å	9.5	4
	4550 Å	18	9.5
	3900 Å	28.5	19
*	3680 Å	60	75
	3550 Å	8	2?

* Used for quantum efficiency measurement.

If 4750 or 4550 Å excitation were used rather than 3680 Å, the L345 fluorescence intensity would be twice as great as L346. Since less light would be absorbed by the Dy_2O_3 in L345, the quantum efficiency of L345 must be more than twice that of L346; or at least 80%.

Figure 1. Absorbance Spectrum For L348.
(0.2 Mole % Pr_2O_3)

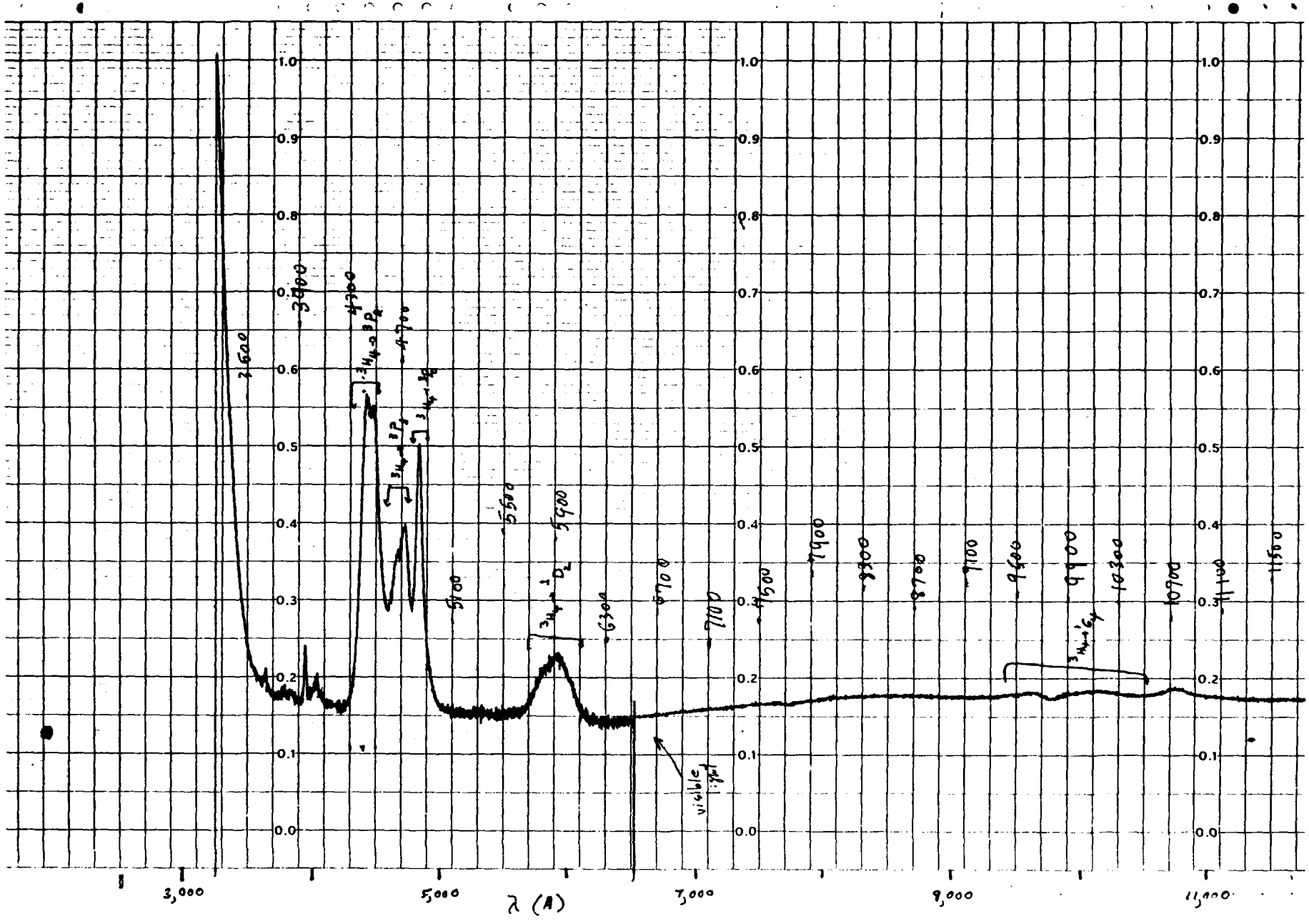

Figure 2. Absorbance Spectrum For L 344.
(0.5 Mole % Pr_2O_3)

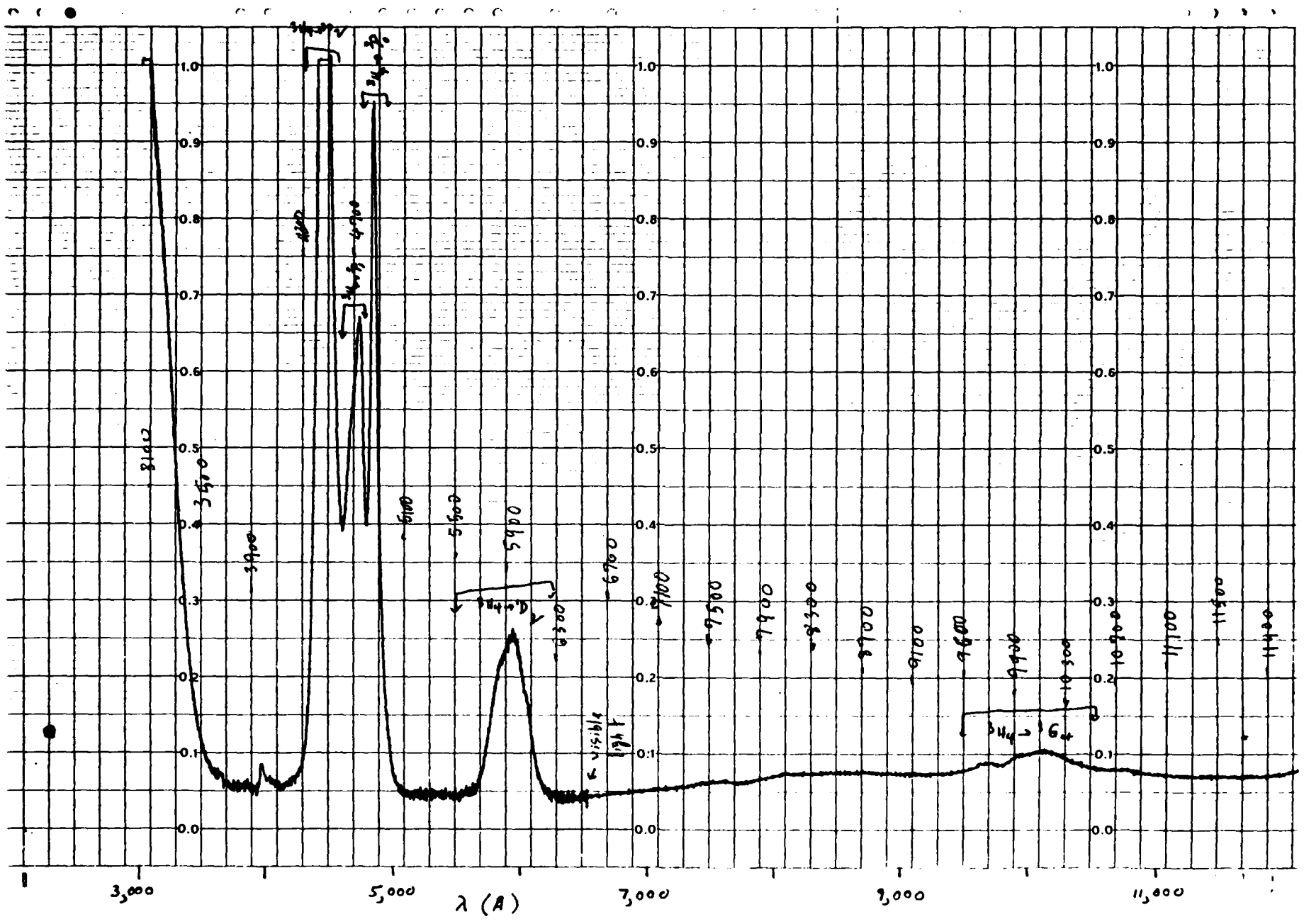

Figure 3 . Absorbance Spectrum For L345.
(0.2 Mole % Dy_2O_3)

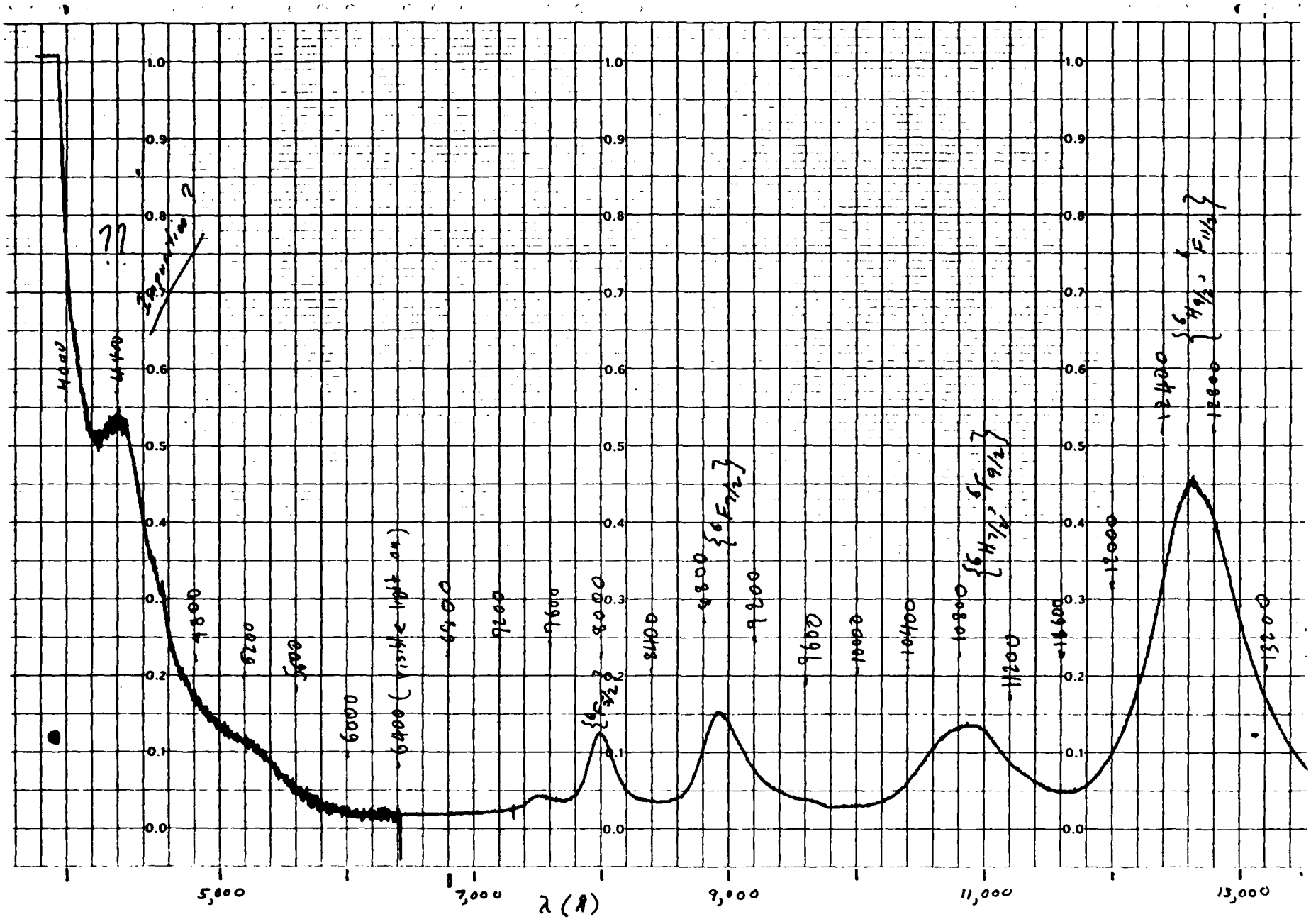

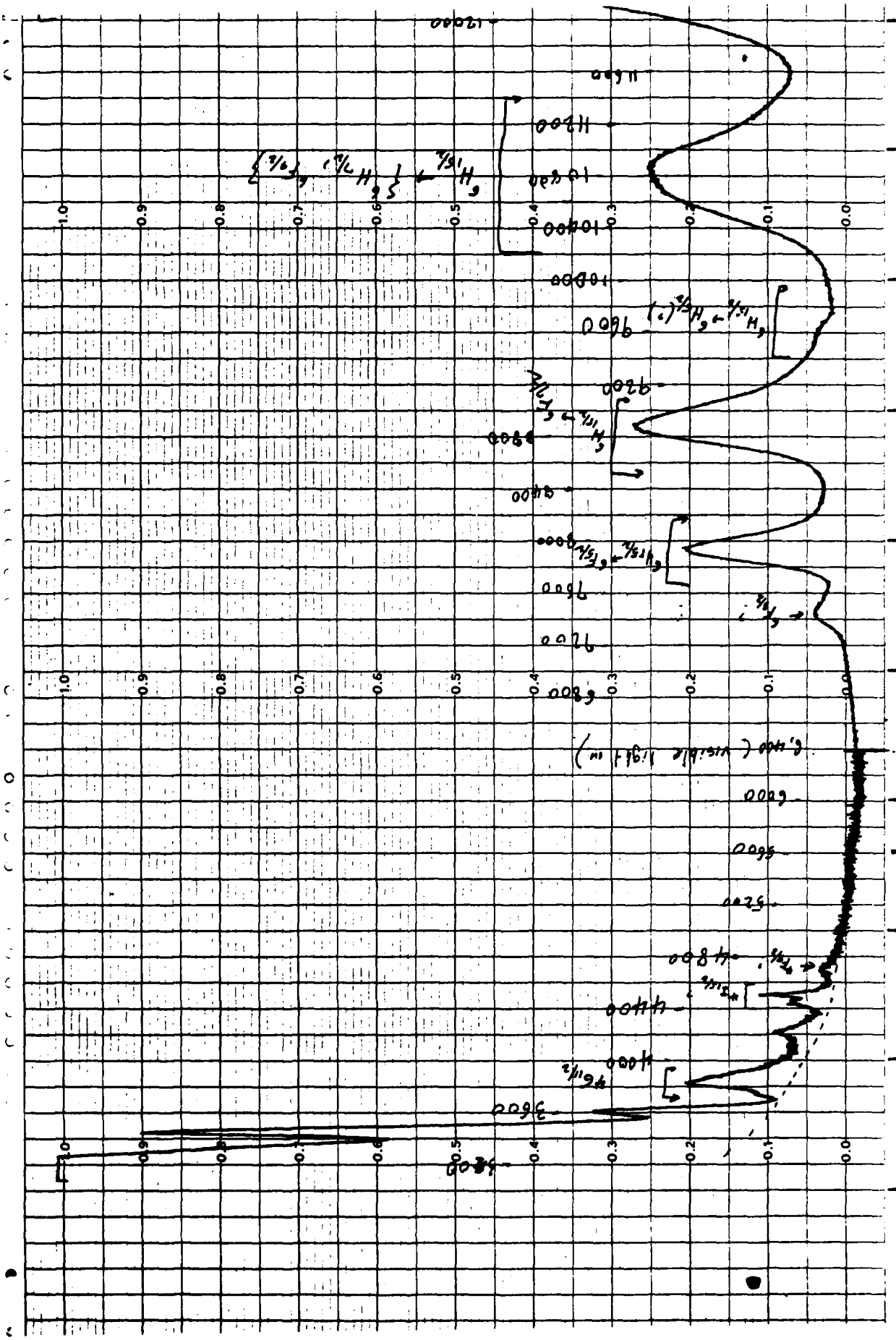

Figure 4. Absorbance Spectrum For L345.
(0.5 Mole % Dy_2O_3)

Figure 5. Absorbance Spectrum For L 951.
(0.1 Wt % UO_2)

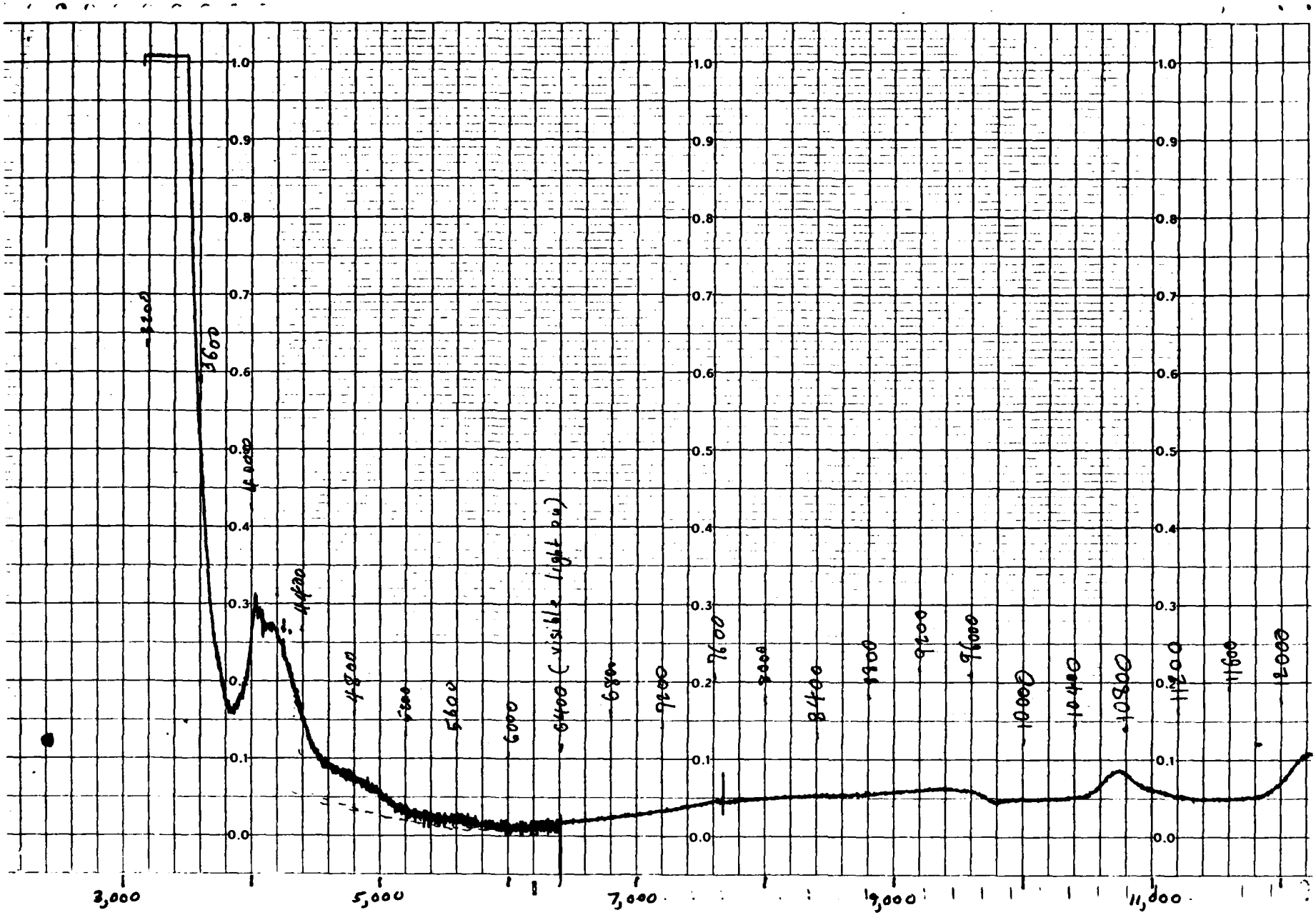

Figure 6. Emission Spectrum For L343. - Uncorrected.

(0.2 mole % Pr_2O_3)

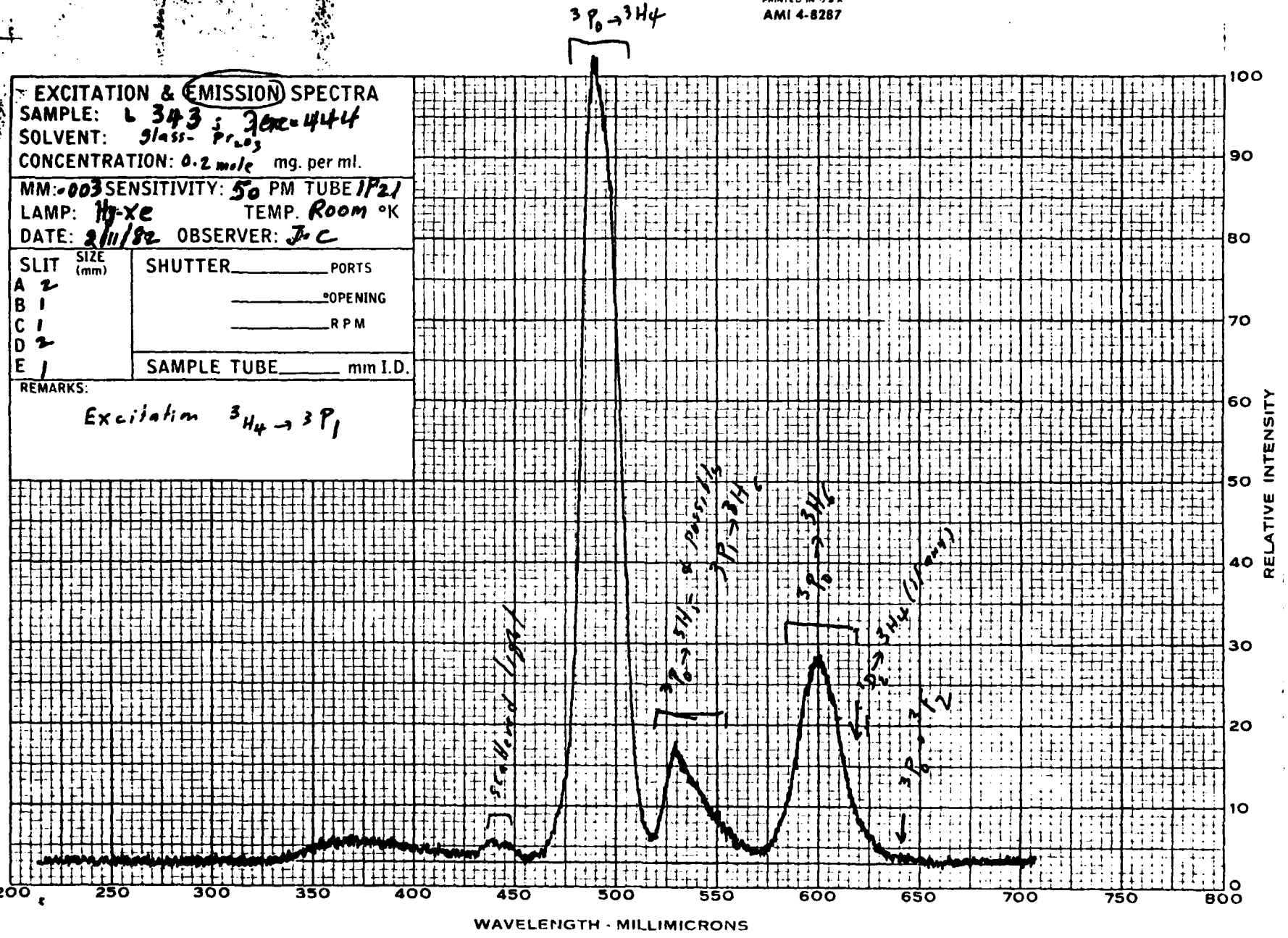

Figure 7. Emission Spectrum For L344. - Uncorrected.

(0.5 mole % Pr_2O_3)

EXCITATION & EMISSION SPECTRA
SAMPLE: L344 ; λ_{exc} = 438 nm
SOLVENT: glass
CONCENTRATION: 0.5 mole Pr_2O_3 mg. per ml.

MM: .003 SENSITIVITY: 50 PM TUBE: 1P21
LAMP: Hg-Xe TEMP. Room °K
DATE: 2/11/82 OBSERVER: J.C

SLIT	SIZE (mm)
A	2
B	1
C	1
D	2
E	.5

SHUTTER _____ PORTS
_____ °OPENING
_____ R P M
SAMPLE TUBE _____ mm I.D.

REMARKS:
Excitation: $^3H_4 \rightarrow {}^3P_1$

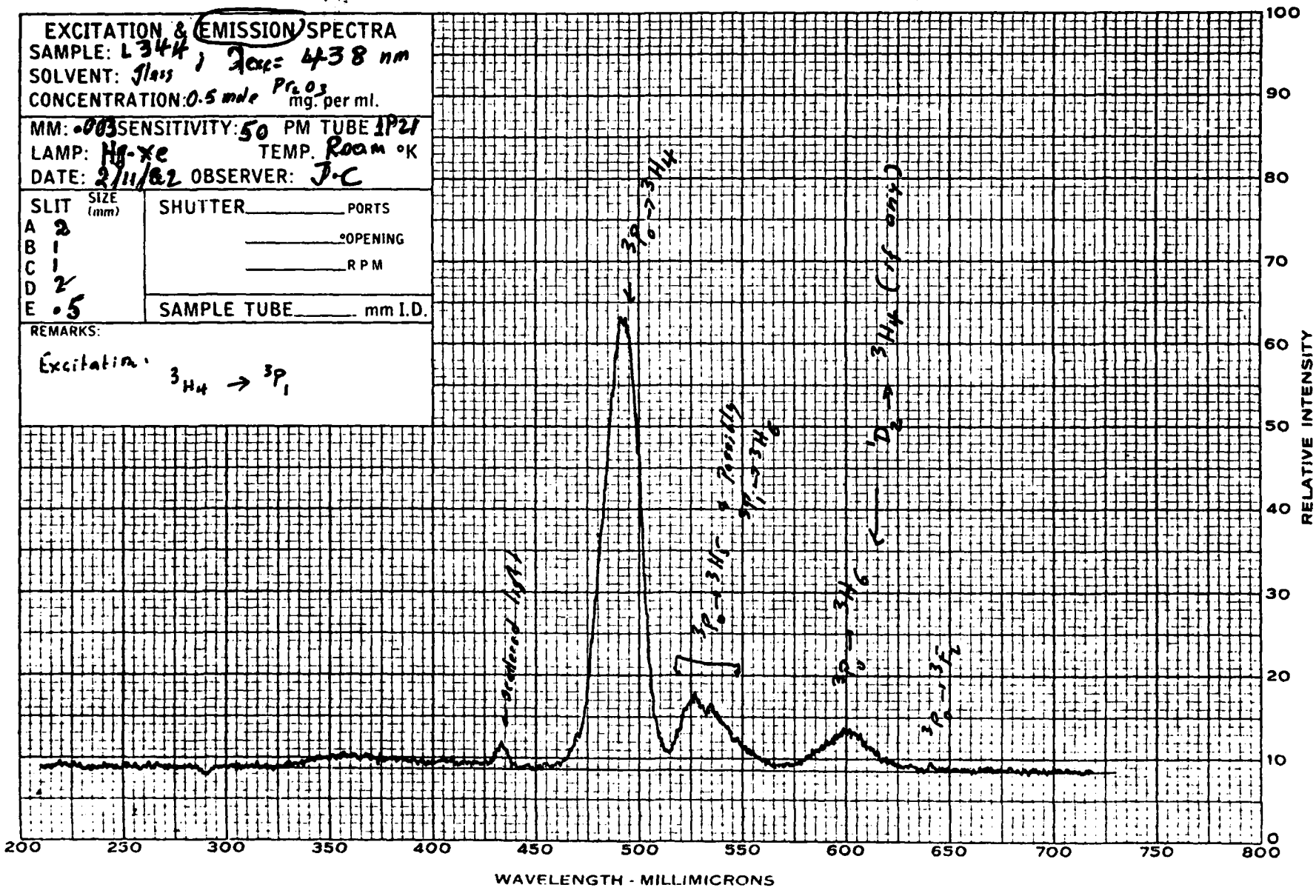

Figure 8. Emission Spectrum For L345 - Uncorrected

(0.2 Mole % Dy_2O_3)

RECORDING CHARTS
GRAPHIC CONTROLS CORPORATION
BUFFALO, NEW YORK
PRINTED IN U.S.A.
AMI 4-8287

EXCITATION & EMISSION SPECTRA
SAMPLE: L345; λ_{exc} = 364 nm
SOLVENT: Glass - Dy_2O_3
CONCENTRATION: 0.2 mole mg. per ml.

MM: .01 SENSITIVITY: 50 PM TUBE 1P21
LAMP: Hg-Xe TEMP. Room °K
DATE: 2/11/82 OBSERVER: J.C

SLIT	SIZE (mm)
A	2
B	1
C	1
D	2
E	.5

SHUTTER _____ PORTS
_____ °OPENING
_____ R P M

SAMPLE TUBE _____ mm I.D.

REMARKS:

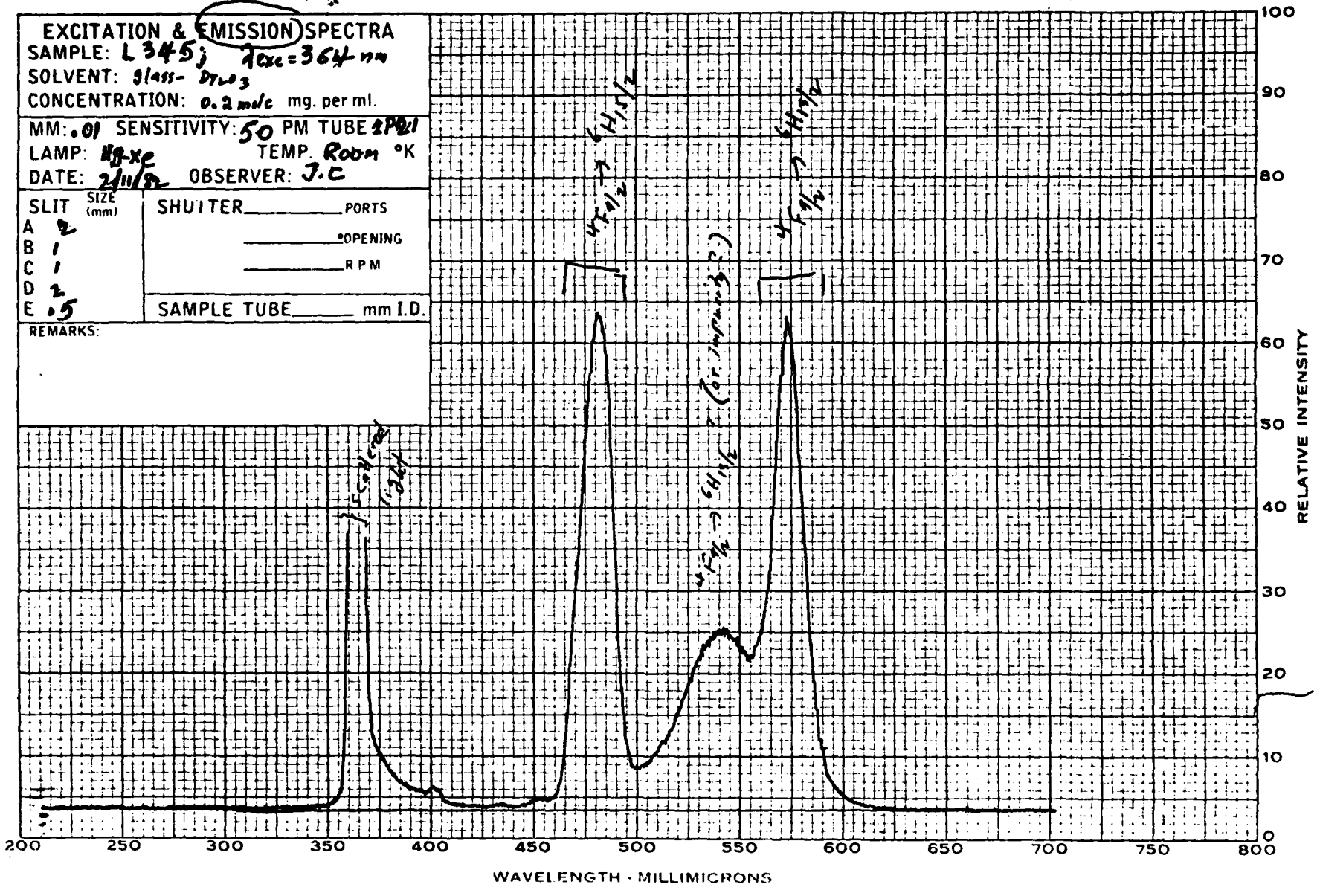

Figure 9: Emission Spectrum For L346 - Uncorrected.
(0.5 Mole % Dy_2O_3)

EXCITATION & EMISSION SPECTRA
SAMPLE: L346.: Zone: 364 nm
SOLVENT: Dy_2O_3 in glass
CONCENTRATION: 0.5 mole mg. per ml.

MM: .03 SENSITIVITY: 50 PM TUBE 1P21
LAMP: Hg-Xe TEMP. Room °K
DATE: 2/11/82 OBSERVER: J.E

SLIT	SIZE (mm)
A	2
B	1
C	1
D	2
E	0.5

SHUTTER _____ PORTS
_____ °OPENING
_____ R P M
SAMPLE TUBE _____ mm I.D.

REMARKS:

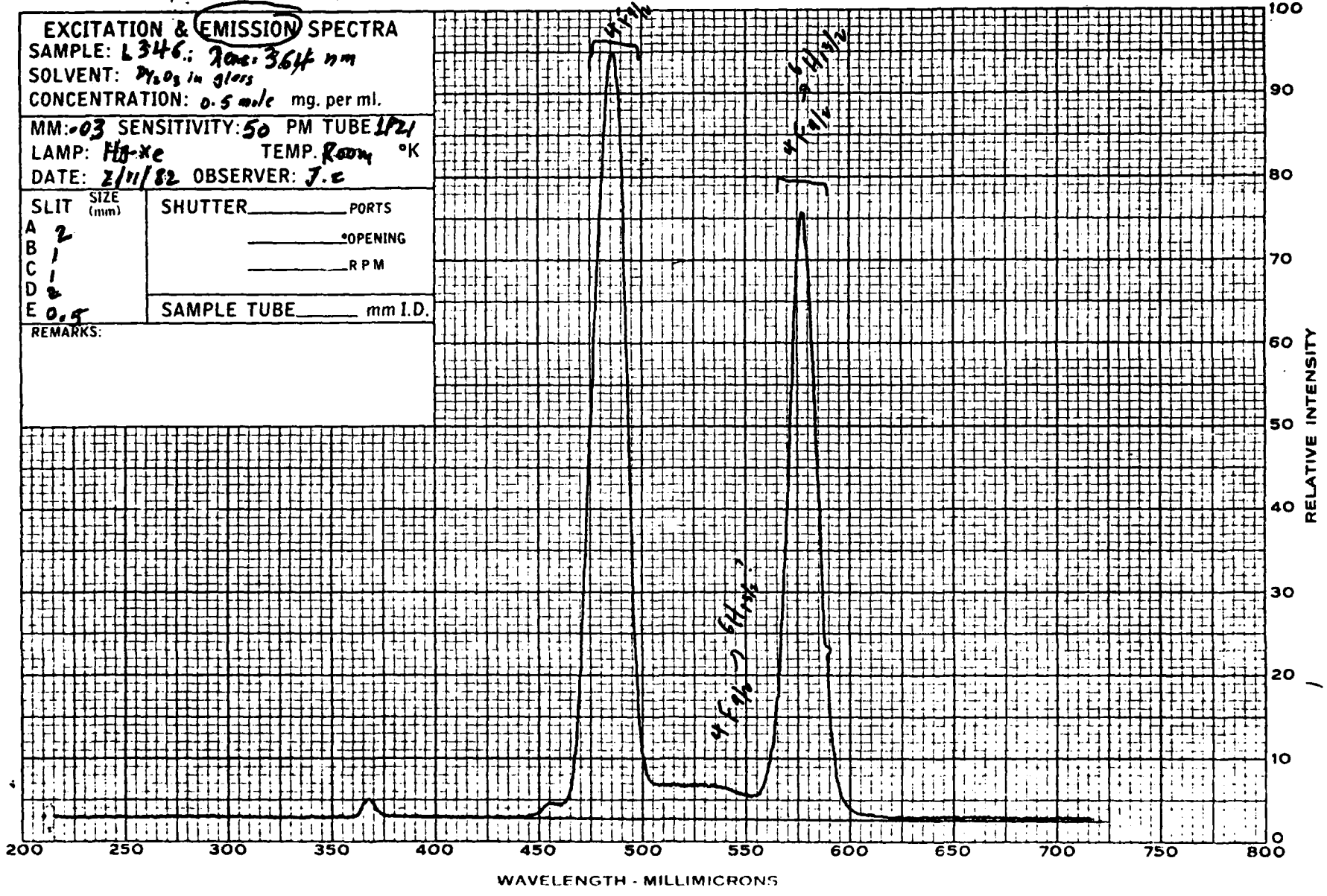

Figure 10. Emission Spectrum for L351 - Uncorrected

(0.1 wt% UO_2)

RECORDING CHARTS
GRAPHIC CONTROLS CORPORATION
BUFFALO, NEW YORK
PRINTED IN U.S.A.
AMI 4-8287

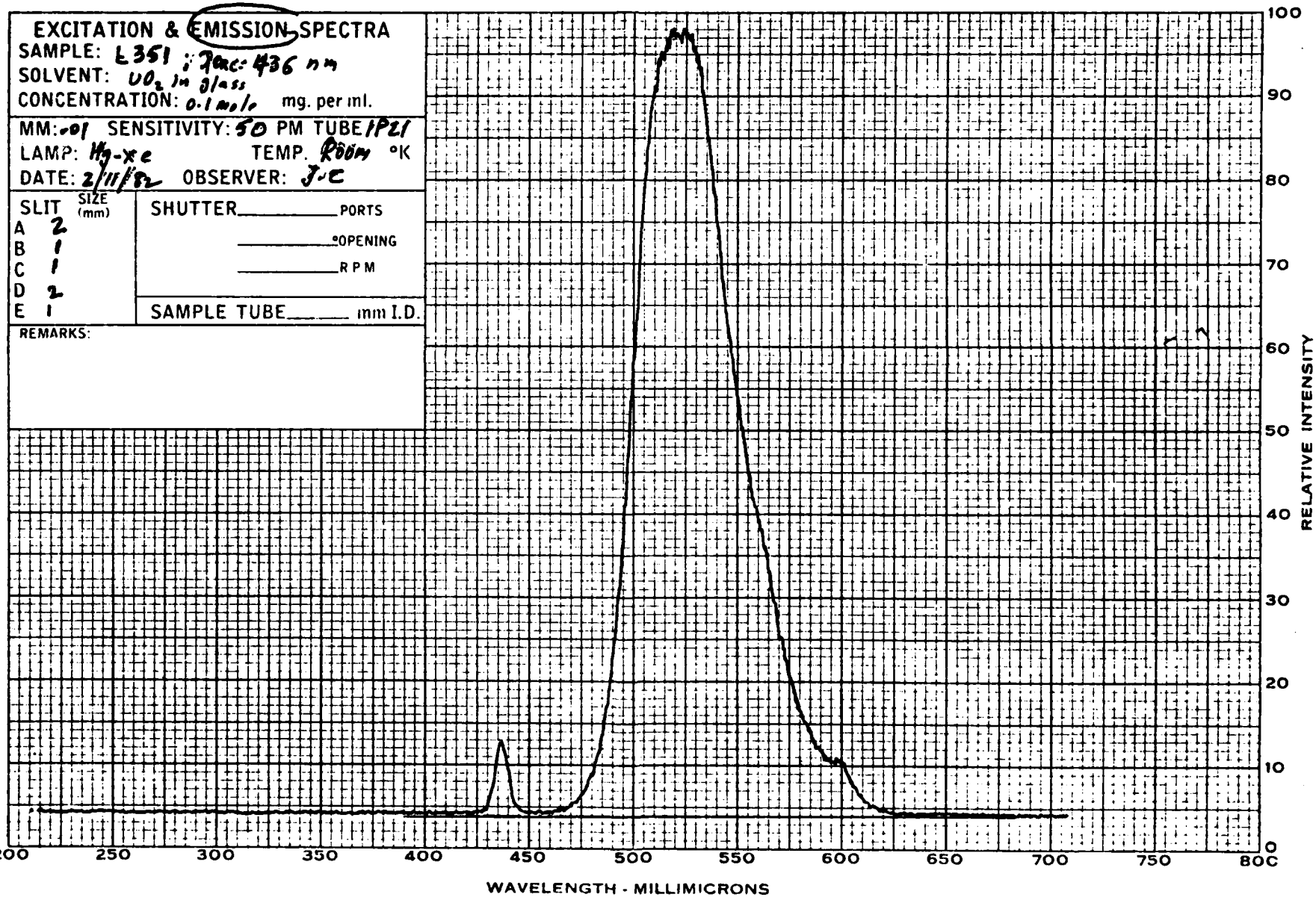

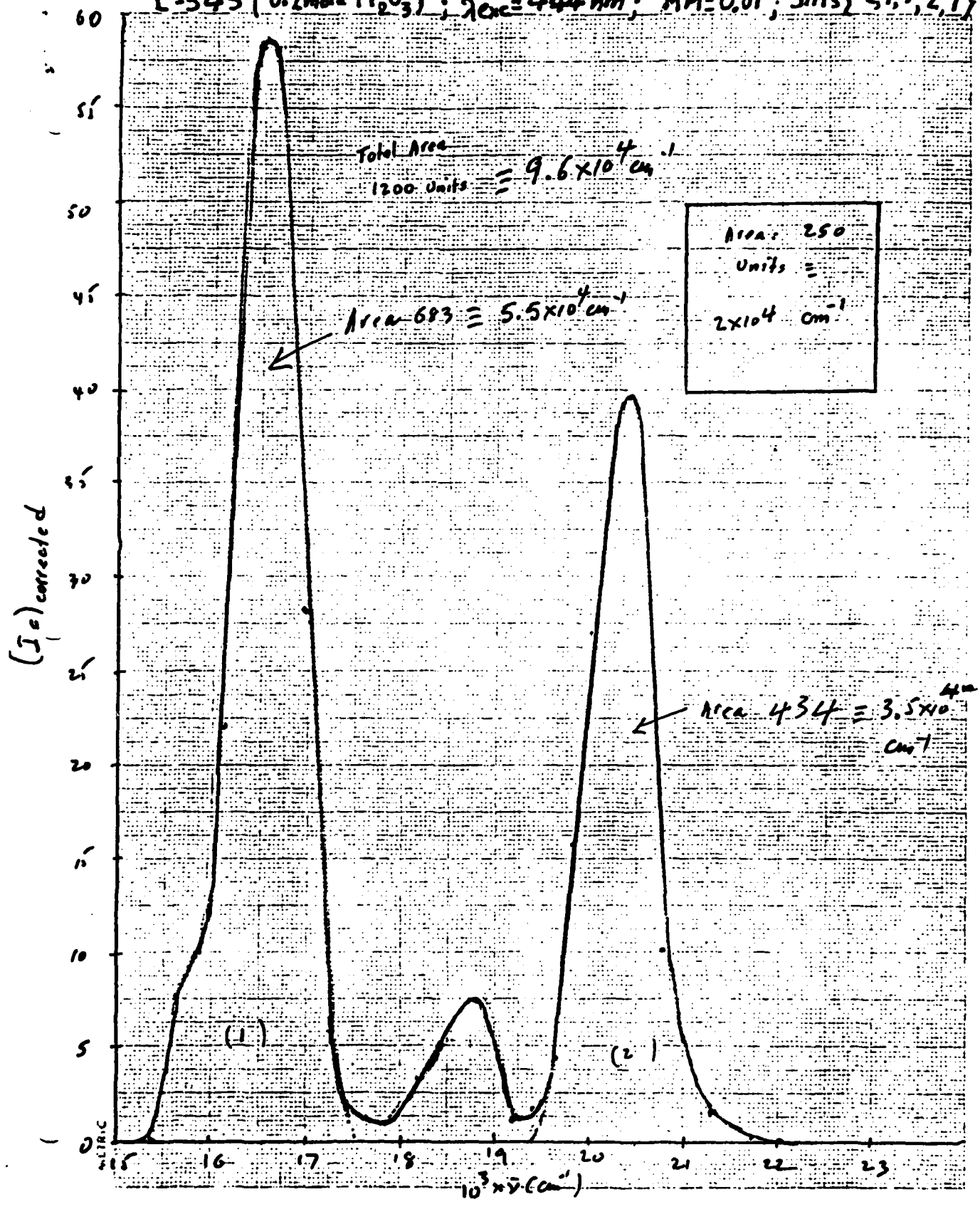

Figure 11. Corrected Emission Spectrum For L 343 (0.2 mole % Pr_2O_3).

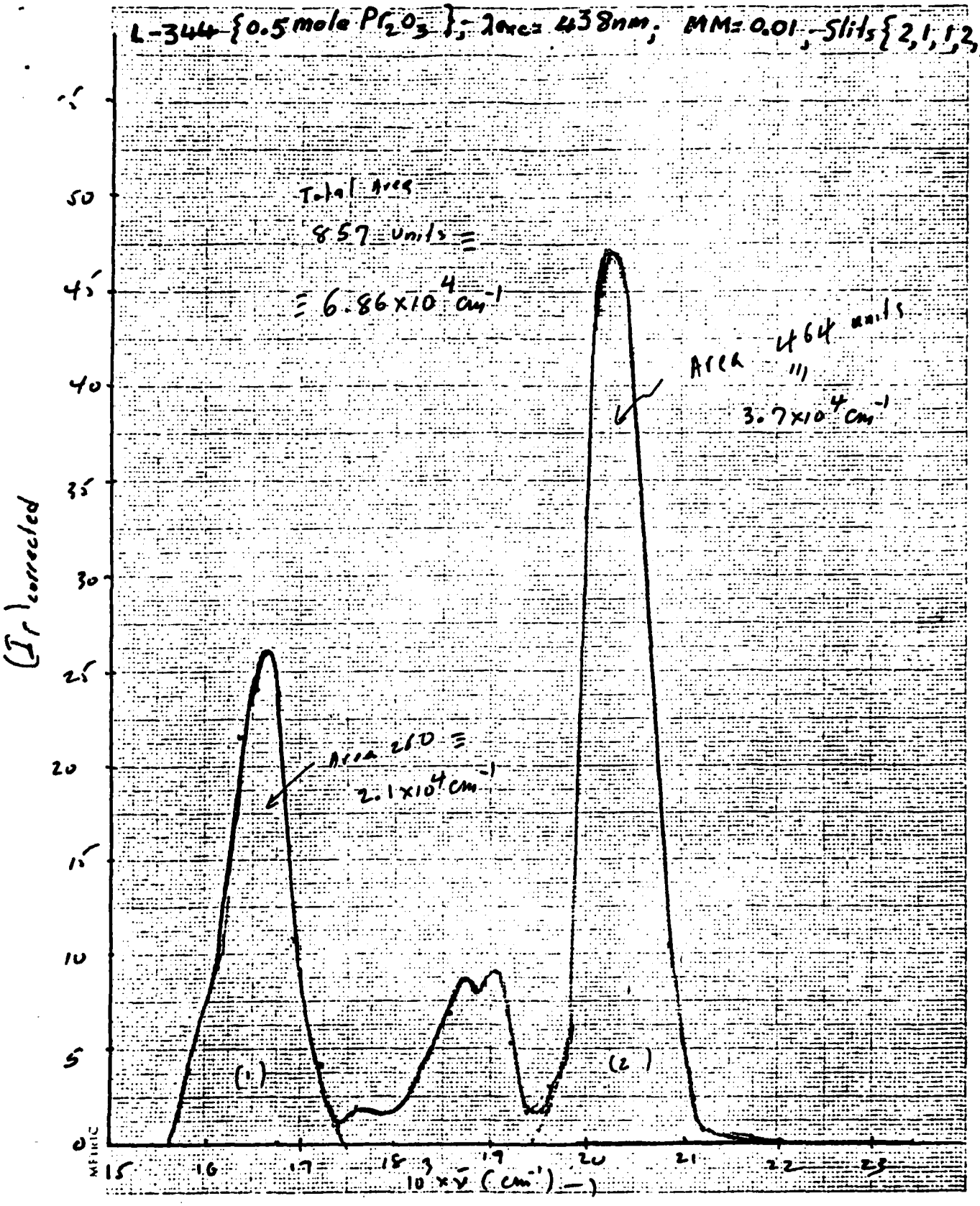

Figure 12. Corrected Emission Spectrum For L 344 (0.5 mole % Pr_2O_3).

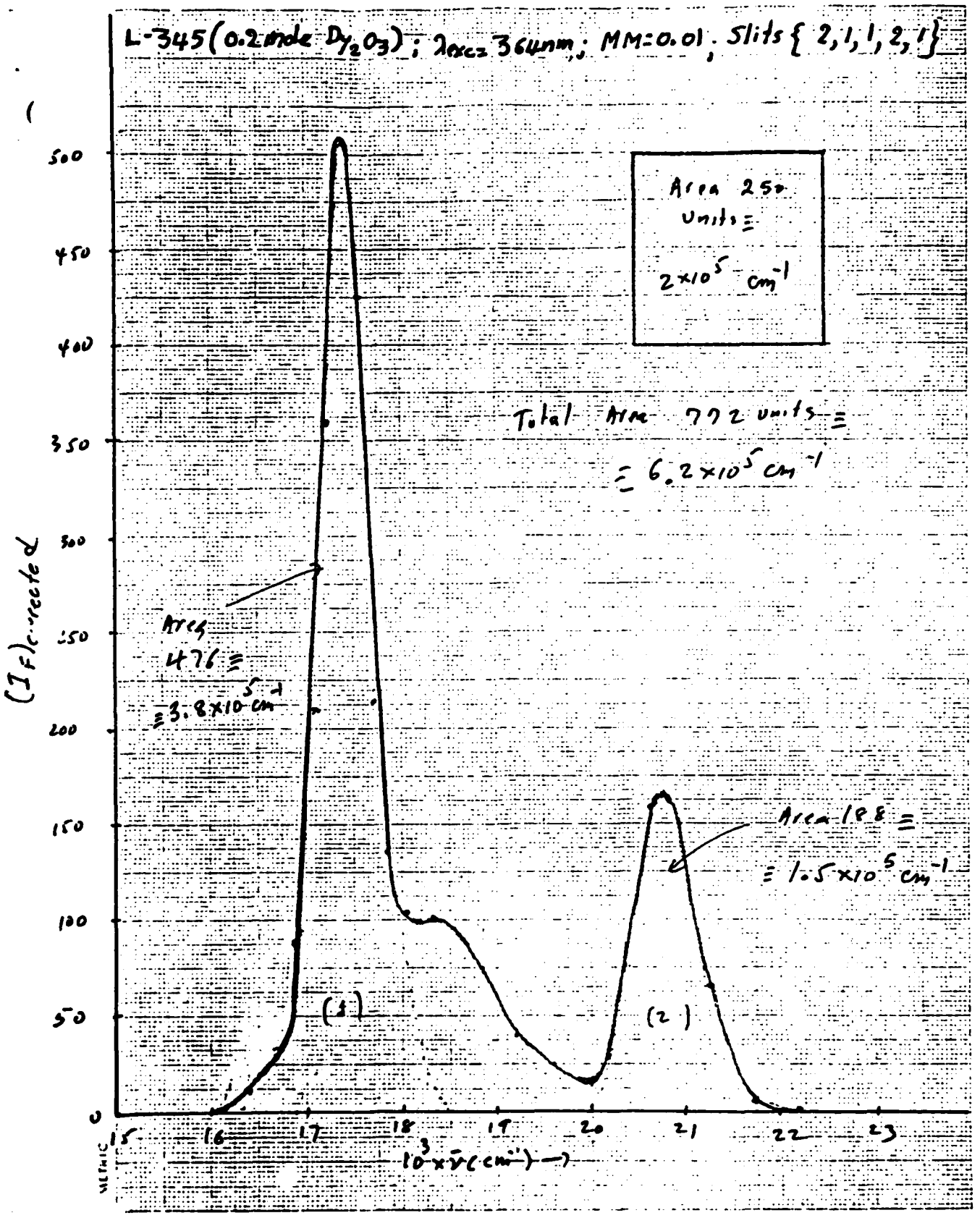

Figure 13. Corrected Emission Spectrum For L 345 (0.2 mole% Dy_2O_3).

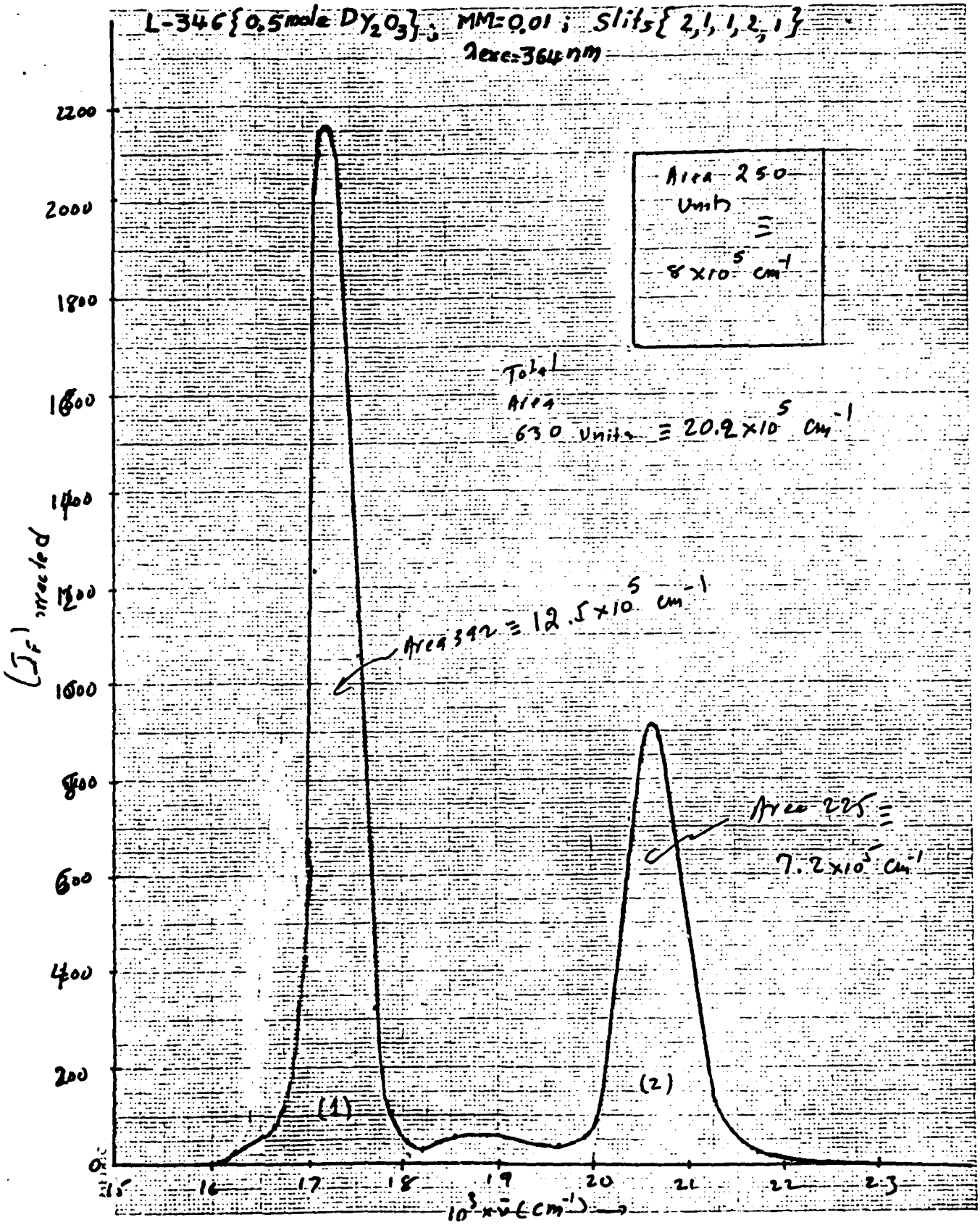

Figure 14. Corrected Emission Spectrum For L346 (0.5 mole% Dy_2O_3).

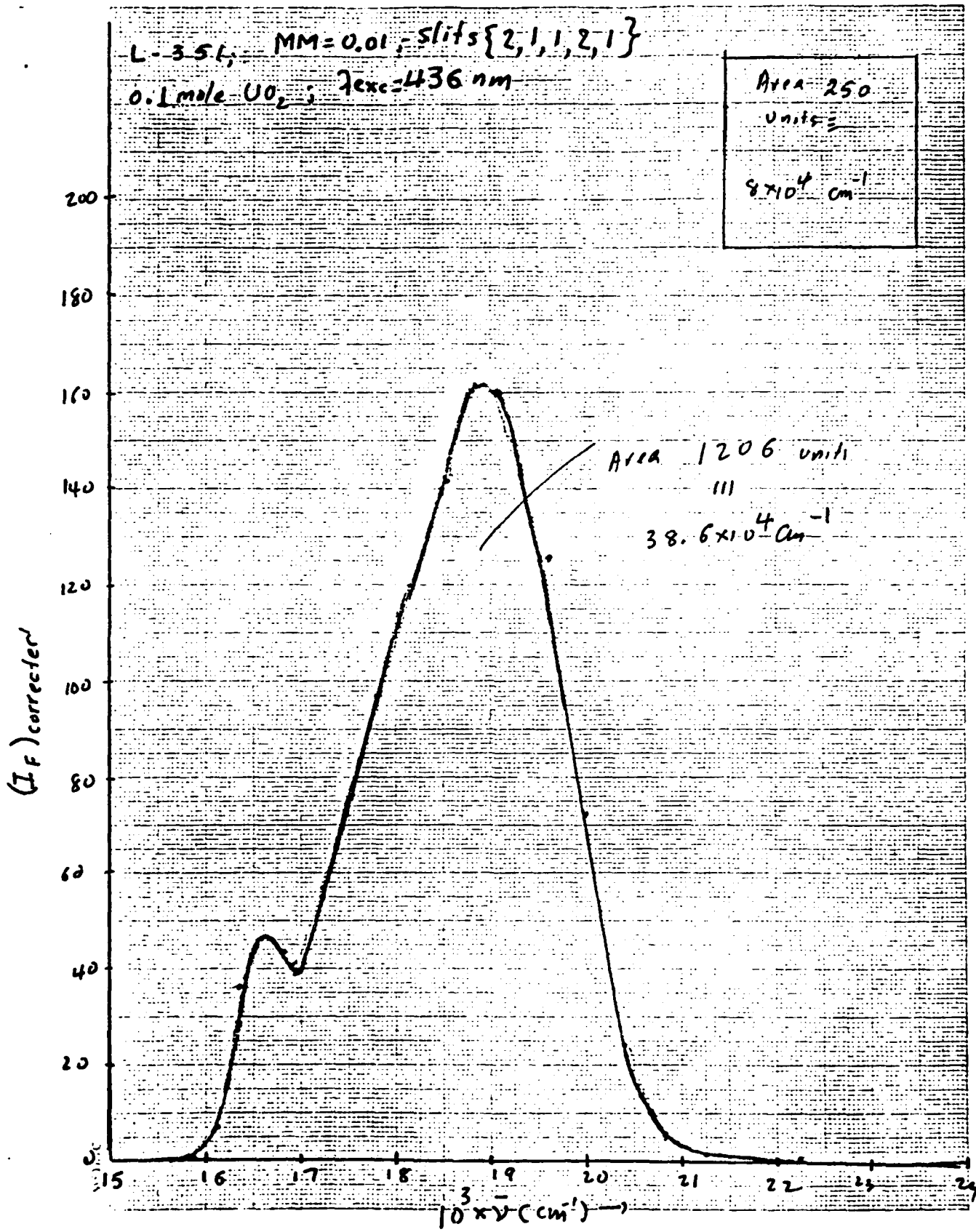

Figure 15. Corrected Emission Spectrum For L 351 (0.1 wt% UO_2).

Figure 16. Excitation Spectrum For L 343 (0.2 mole % Pr_2O_3)
λ_{el} = 490 nm.

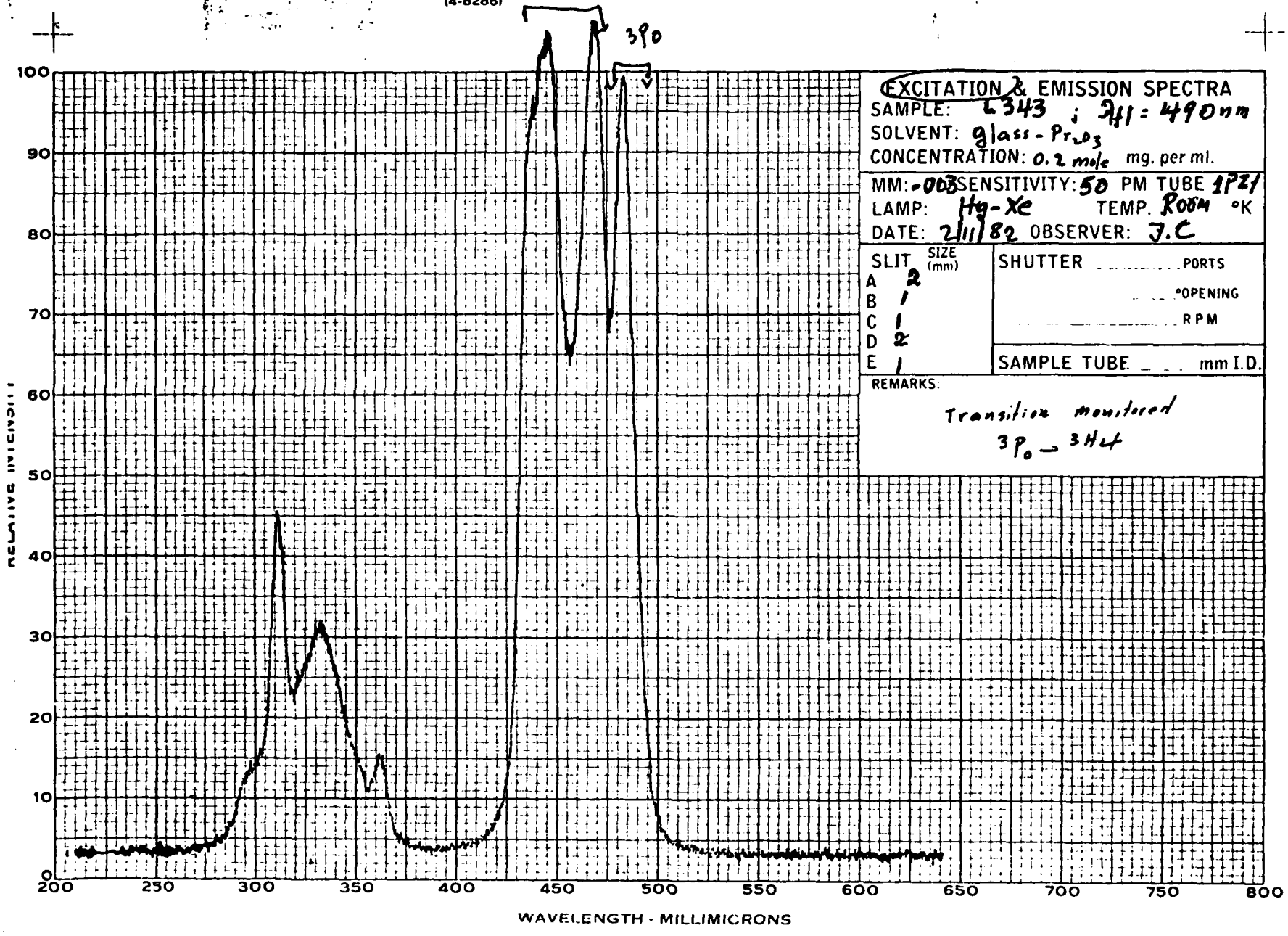

RECORDING CHARTS
GRAPHIC CONTROLS CORPORATION
BUFFALO, NEW YORK
PRINTED IN U.S.A.
No. AMI 1000
(4-8286)

Figure 17. Excitation Spectrum For L343 (0.2 mole% Pr_2O_3). λ_{fl} = 600 nm.

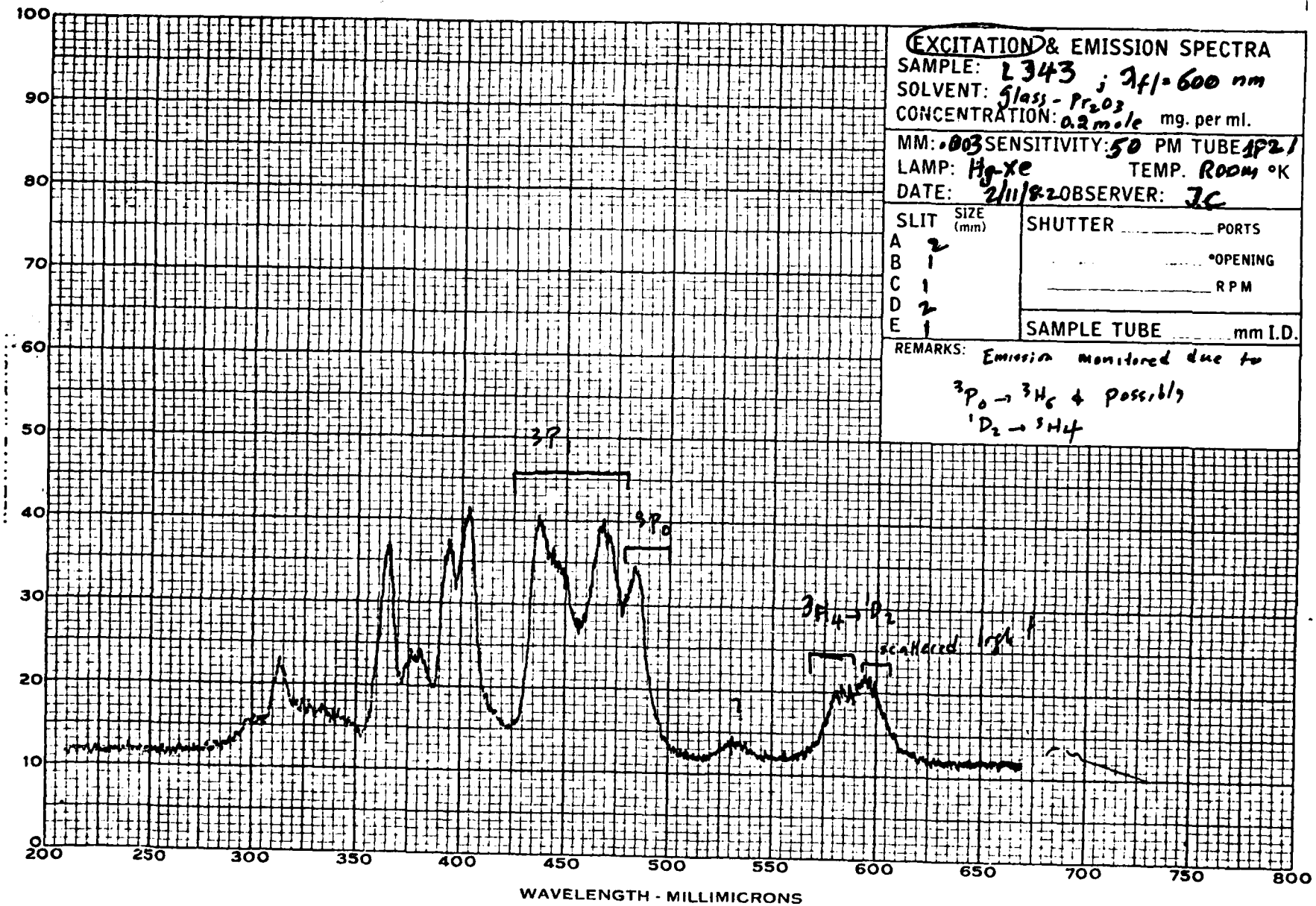

RECORDING CHARTS
GRAPHIC CONTROLS CORPORATION
BUFFALO, NEW YORK
PRINTED IN U.S.A.
No. AMI 1000
(4-8286)

Figure 18. Excitation Spectrum For L344 (0.5 mole% Pr_2O_3). λ_{fl} = 490 nm.

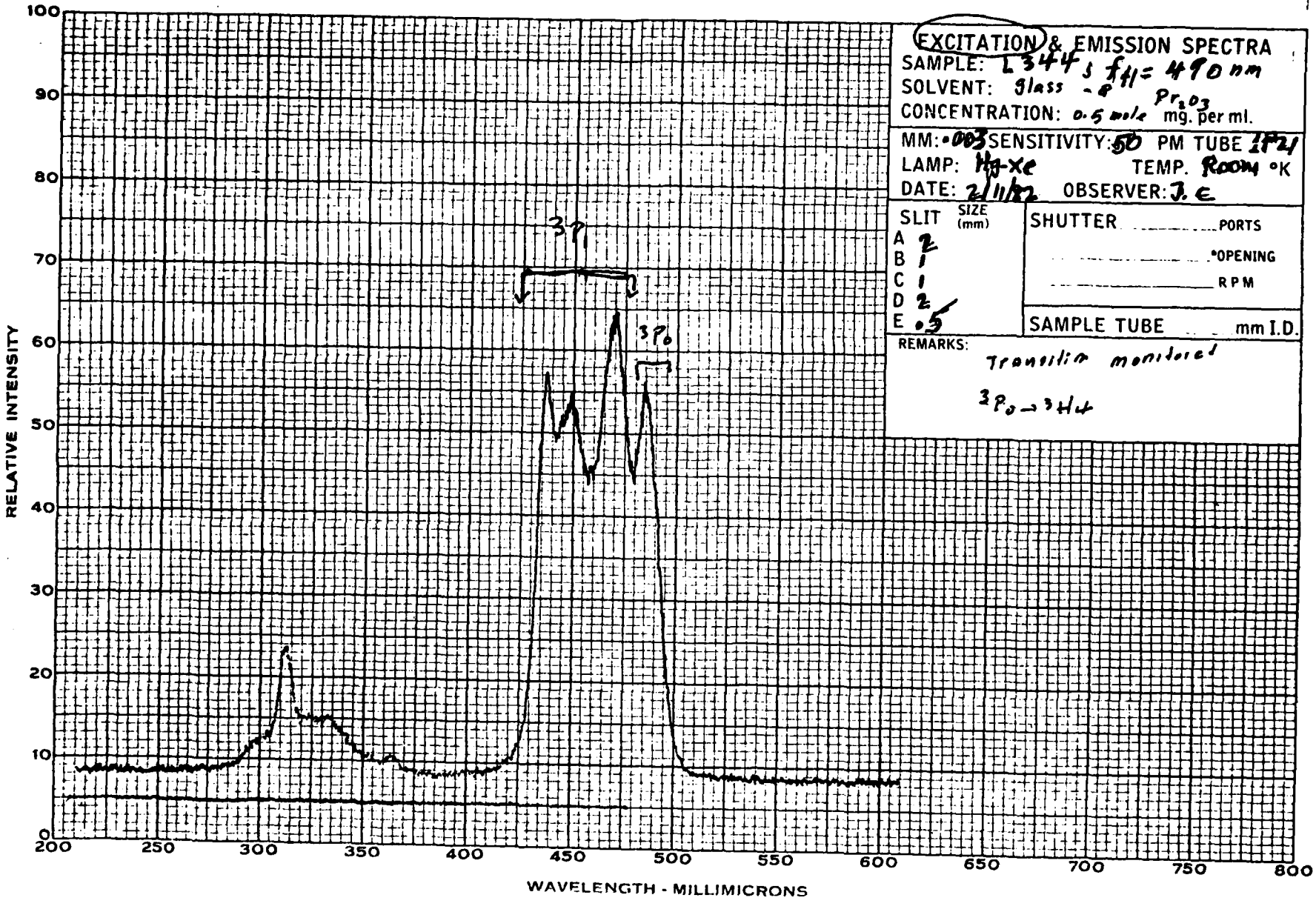

RECORDING CHARTS
GRAPHIC CONTROLS CORPORATION
BUFFALO, NEW YORK
PRINTED IN U.S.A.
No. AMI 1000
(4-8286)

Figure 19. Excitation Spectrum For L345 (0.2 mole % Dy_2O_3)
λ_{EI} = 575 nm

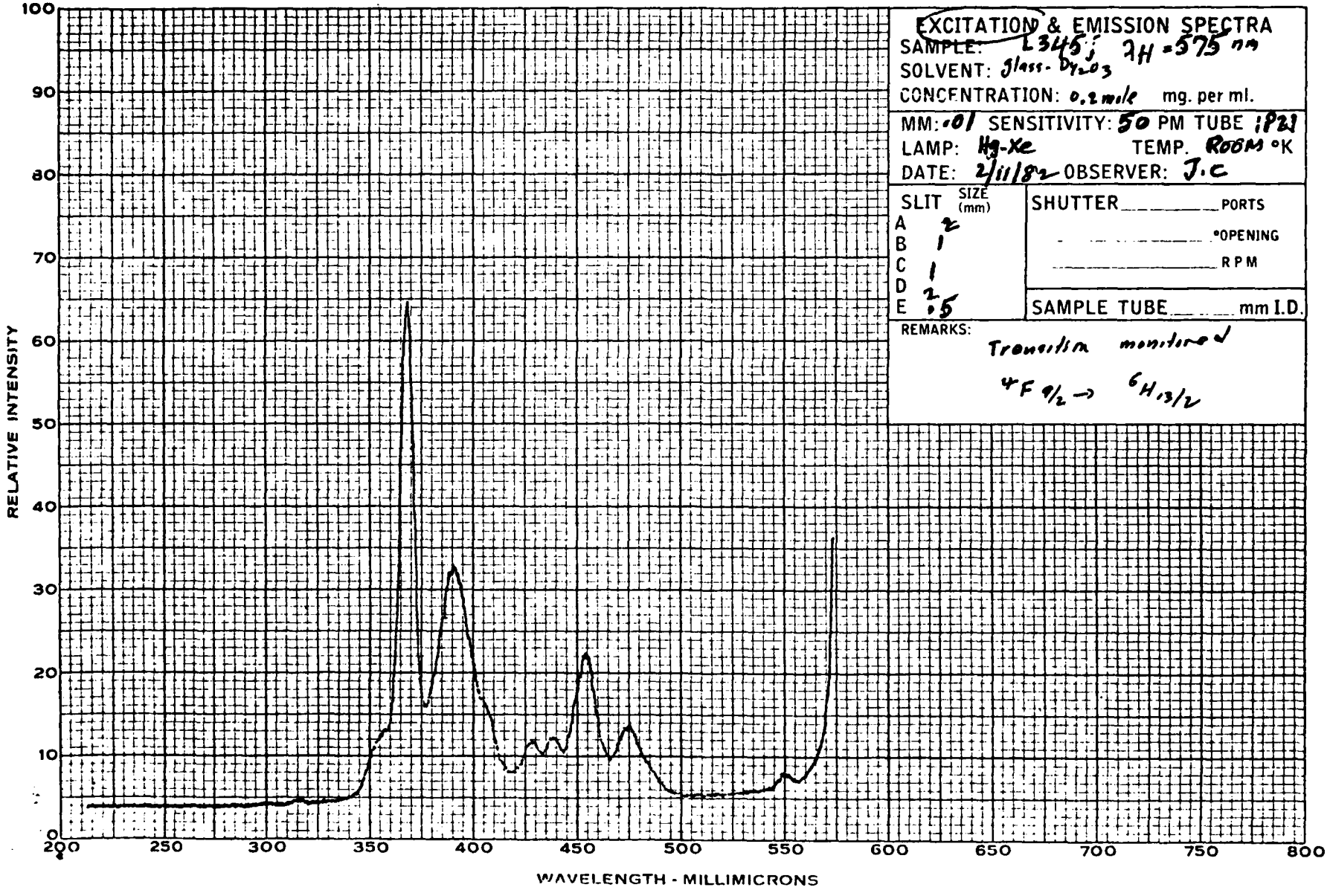

RECORDING CHARTS
GRAPHIC CONTROLS CORPORATION
BUFFALO, NEW YORK
PRINTED IN U.S.A.
NO. AMI 1000
(4-8286)

Figure 23. Excitation Spectrum For L345 (0.2 mole% Dy_2O_3) $\lambda_{fl} = 485$ nm.

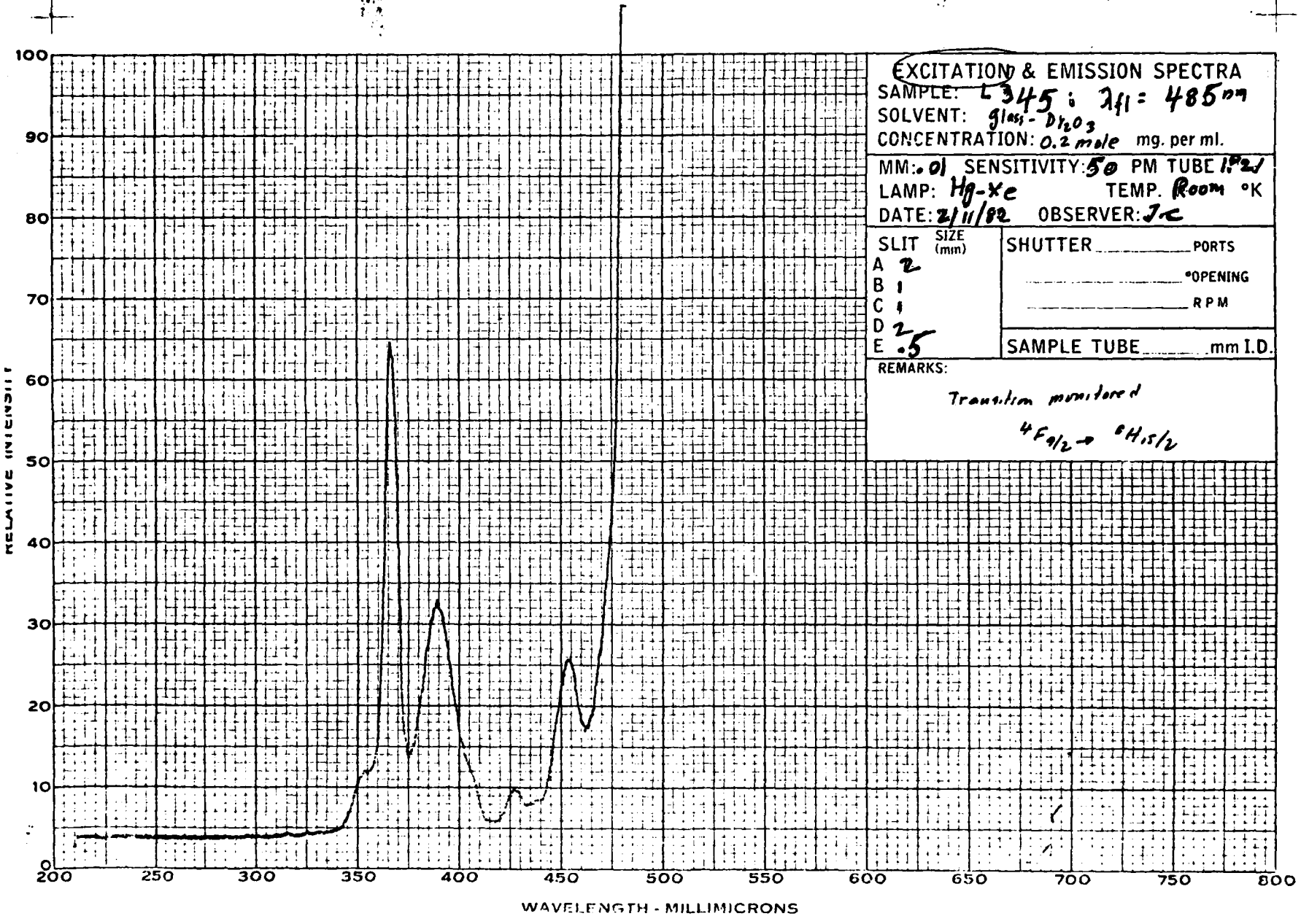

RECORDING CHARTS
GRAPHIC CONTROLS CORPORATION
BUFFALO, NEW YORK
PRINTED IN U.S.A.
No. AMI 1000
(4-8286)

Figure 2.6 Excitation Spectrum For L346 (0.5 mole % Dy_2O_3).
$\lambda_{51} = 575$ nm

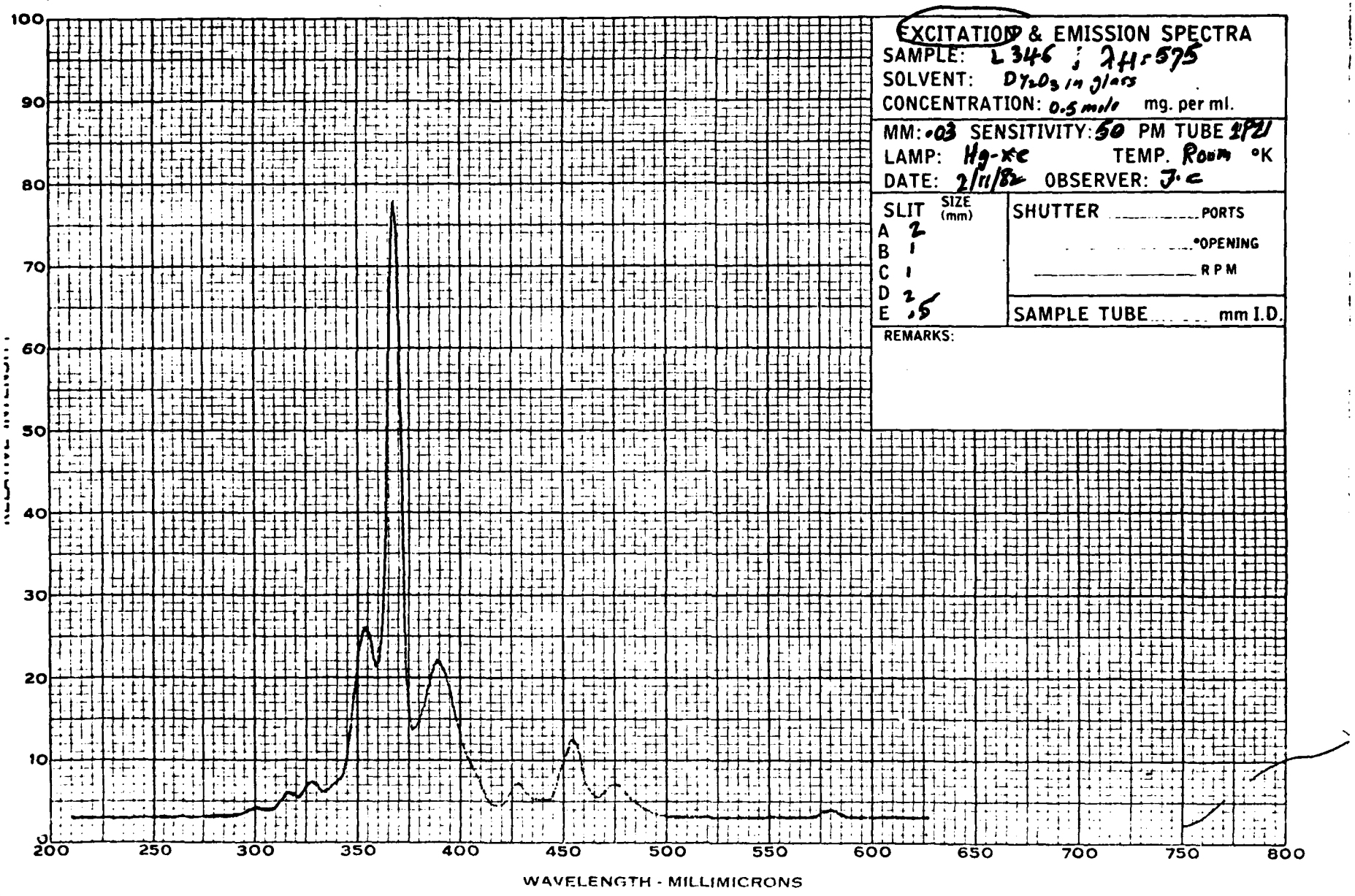

RECORDING CHARTS
PRINTED IN U.S.A.
NO. AMI 1000
(4-8286)

Figure 22. Excitation Spectrum For L346 (0.5 mole% Dy_2O_3)
λ_{Em} = 485 nm.

EXCITATION & EMISSION SPECTRA
SAMPLE: L346 ; λ_{Em} 485 nm
SOLVENT: Dy_2O_3 in glass
CONCENTRATION: 0.5 mole mg. per ml.
MM: .03 SENSITIVITY: 50 PM TUBE 4P21
LAMP: Hg-Xe TEMP. Room °K
DATE: 2/11/82 OBSERVER: J-C

SLIT	SIZE (mm)
A	2
B	1
C	1
D	2
E	0.5

SHUTTER ____ PORTS
____ °OPENING
____ RPM
SAMPLE TUBE ____ mm I.D.
REMARKS:

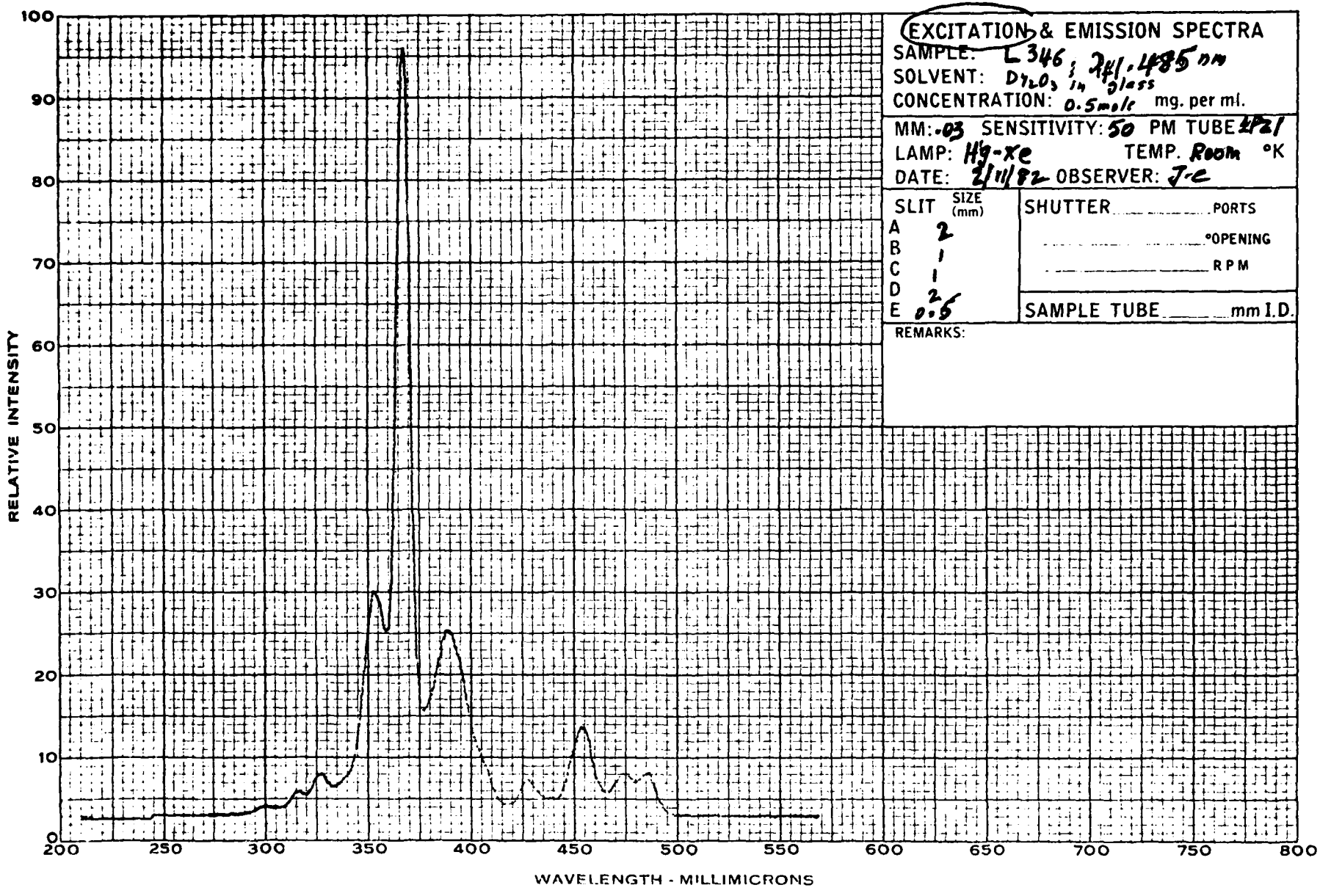

RECORDING CHARTS
GRAPHIC CONTROLS CORPORATION
BUFFALO, NEW YORK
PRINTED IN U.S.A.
No. AMI 1000
(4-8286)

Figure 23. Excitation Spectrum For L 351 (0.1 wt% UO_2). λ_{fl} = 520 nm.

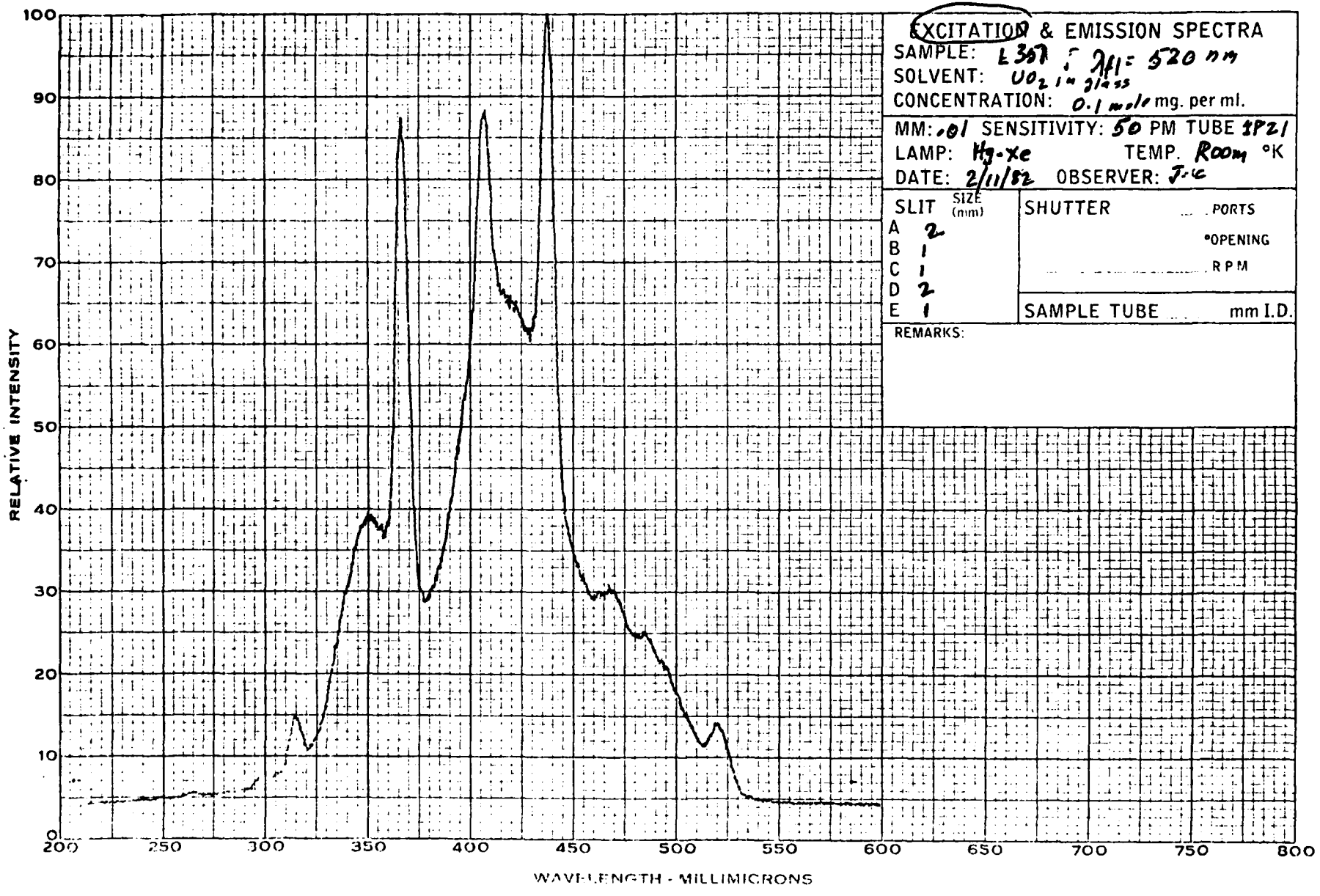

Figure 24. Absorbance Spectrum of Nd^{3+} in a Phosphate Glass Showing Location of Dy Emission Bands. (LLL Handbook of Nd-Doped Glass : Spectro. and Phy. Prop.)

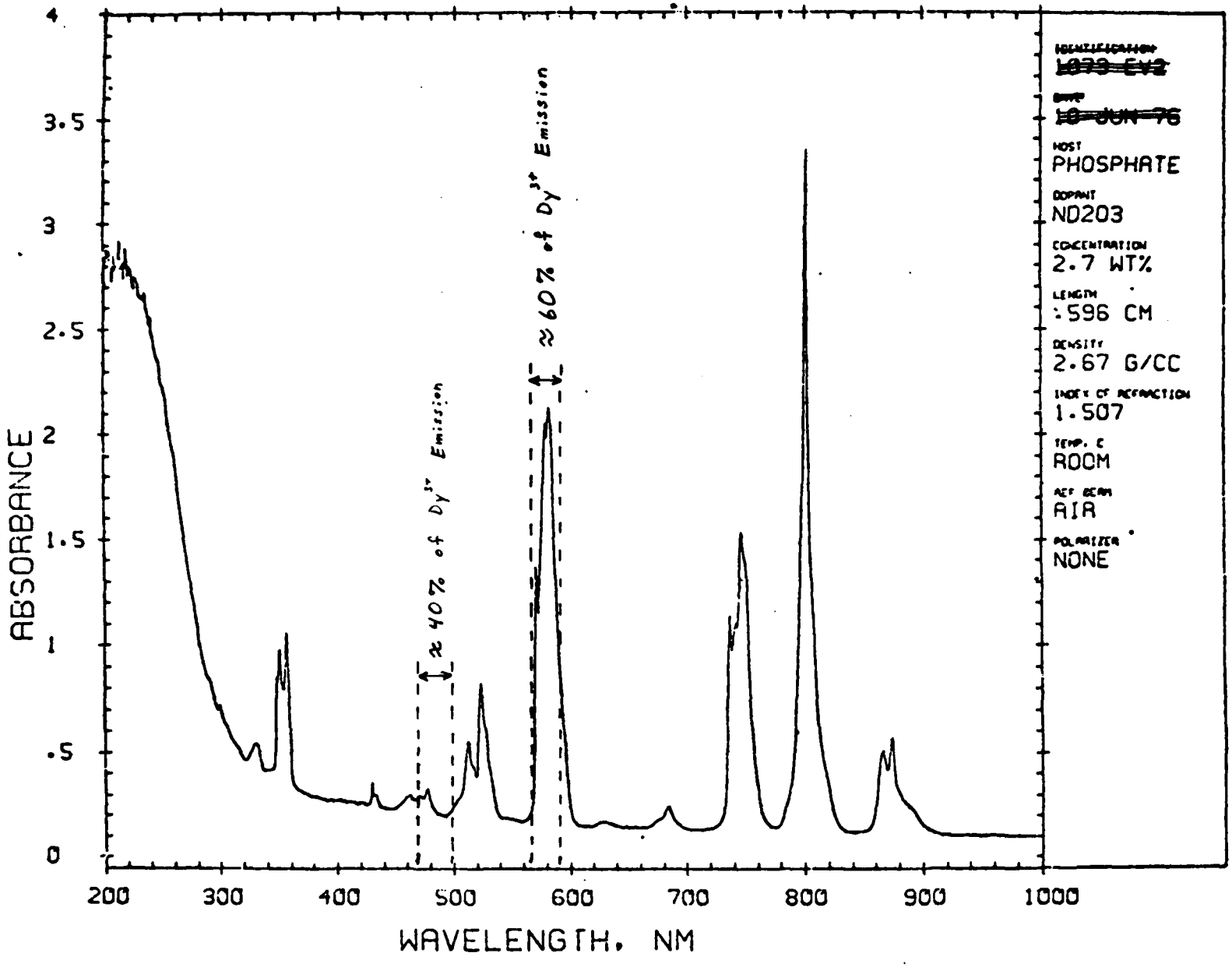

Figure 25. Energy Level Diagram of Trivalent Rare Earth Ions. Showing Location of Dy^{3+} Fluorescent Level. ~~(Refs.)~~
(From G. Dieke, Applied Optics, Vol 2, 1963)

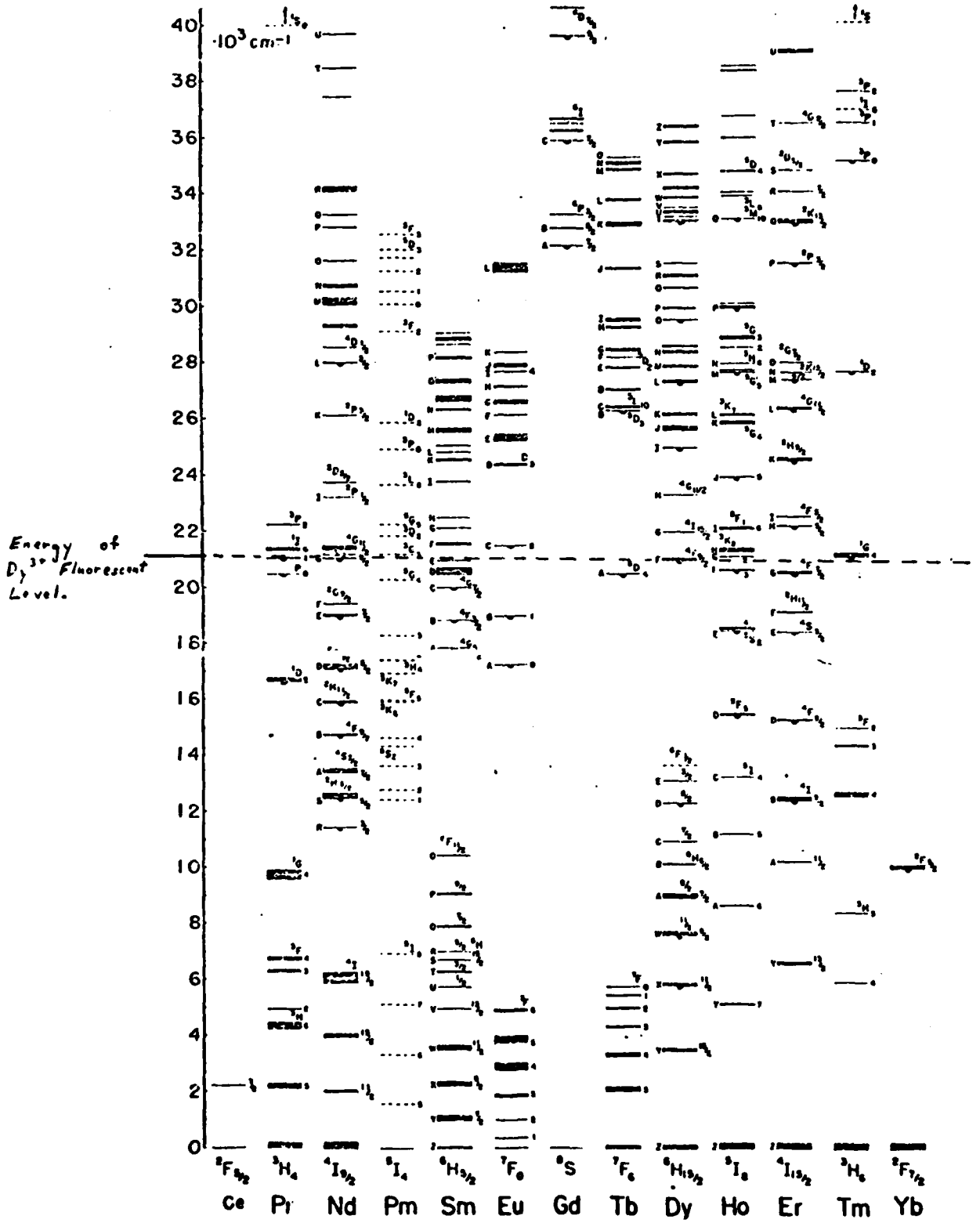

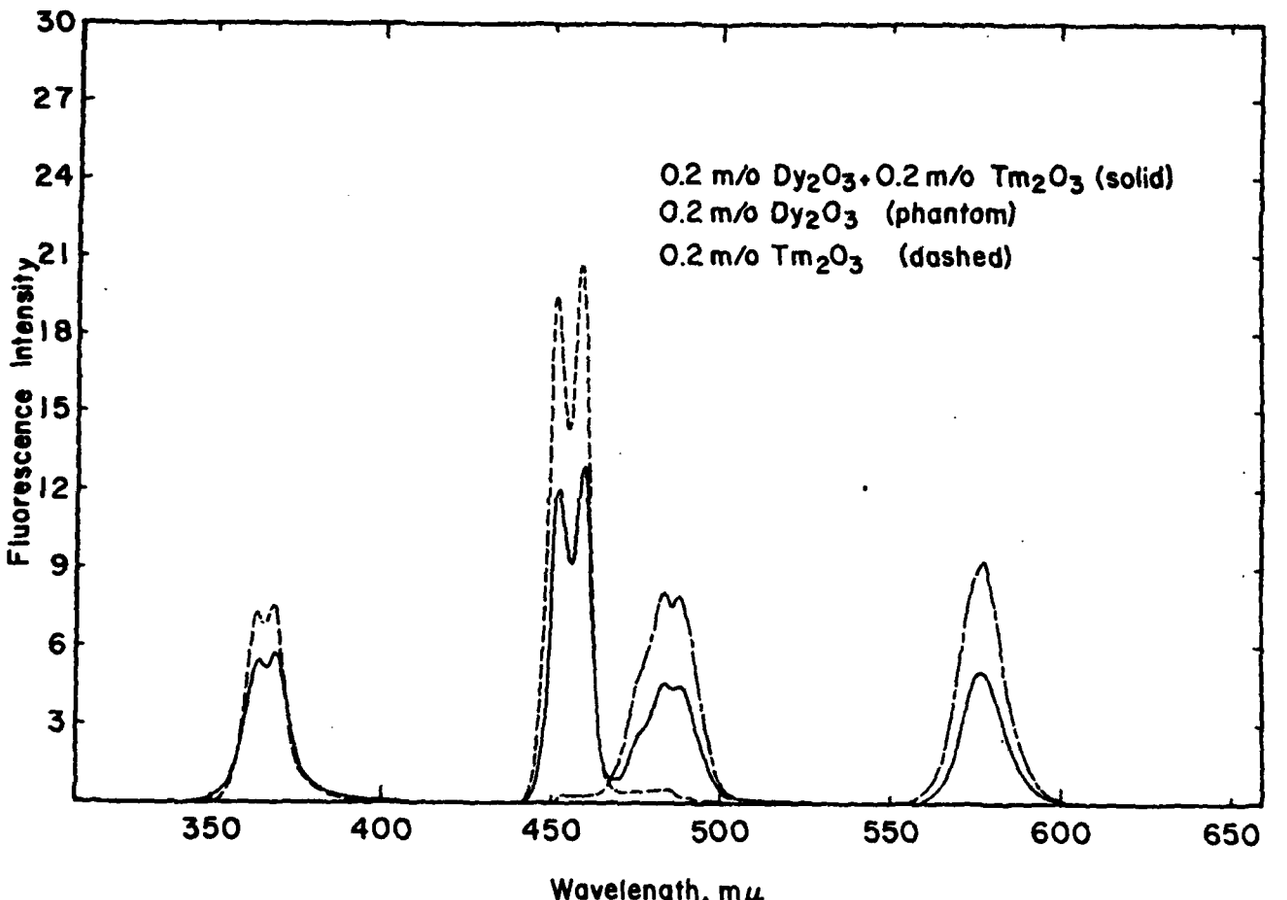

Fig. 26. Fluorescence of glass containing 0.2 m/o Dy_2O_3 + 0.2 m/o Tm_2O_3 compared to fluorescence of singly activated glasses.

(R.W. Dean and J.L. Drobnick, Presented at the American Ceramic Soc. 70th Annual Meeting, Glass Div., Chicago, Ill., 1968)

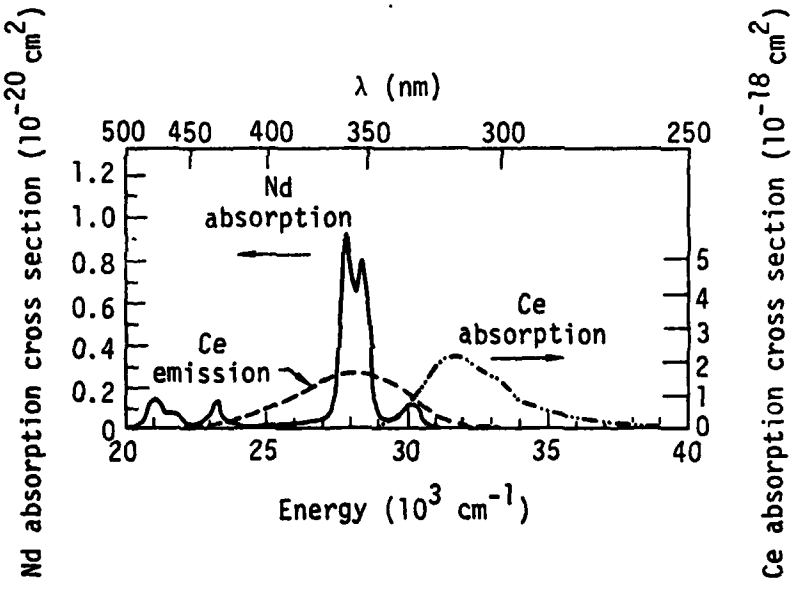

Figure 27. Absorption and Emission Spectra of Ce^{3+}.

(From R. R. Jacobs et. al., Journal of Applied Physics 47, 2020-2024 (1976))

TASK IV

Strengthening of Laser Rods

TASK IV

Strengthening of Laser Rods

Introduction and Summary

The basic factor limiting the average power output of lasers is the average power handling capabilities of the laser rod material. Owing to the heat absorbed by a pumped glass laser rod, a thermal gradient is created which produces a stress condition whereby the center of the rod is under compression and the surface in tension. When the thermal gradient reaches such a magnitude that the tensile stress at the rod surface exceeds the rupture strength of the glass, the rod fractures.

The most straight-forward procedure one can use to increase the power handling capabilities of glass lasers is to increase the rupture strength of the laser rod. With silicate laser glasses, improvements of rupture strength by factors of 4 or 5 are well within the state-of-the-art. The ion exchange processes usually used to accomplish the improvements in rupture strength are well known and easily available in literature.(1) Thermal-tempering of laser rods has also been attempted by the author. The same idea holds true, that is, the creation of a compressive layer of glass at the surface. However, in the thermal-tempered case, the pre-stressed compressive surface layer tends to be orders of magnitude thicker than in the well-controlled ion exchange case. Thus, the thermal-tempering process optically distorts the laser rod to such an extreme as to render it useless. Therefore, it would appear that the only avenue open to us to increase the rupture strength of Q-100 is to either develop a method of ion exchange suitable for phosphate glasses, or develop a silicate cladding glass for Q-100. In effect, we have chosen to explore both of these options. The research and development of an ion exchangeable silicate cladding of Q-100 is discussed in Task II of this report, along with the work on conventional cladding glasses. Studies and experimentation on ion exchanges suitable for phosphate glasses is reported in this section. Unfortunately, time and monies available for these efforts expired before either a suitable ion exchange process or a suitable silicate cladding glass could be developed. A synopsis of our efforts to develop an ion exchange for phosphate glasses is described in this section along with potential avenues for further research in this area.

(1) See for example: U.S. Patents 3,489,546, 3,484,224, 3,844,754, 3,502,454, and 3,687,799.

Preliminary Findings on the Ion Exchange of Phosphate Glasses

A significant improvement in the mechanical durability and power handling capability of glass laser rods can be obtained without changing the basic composition of the glass by means of an ion exchange process. This improvement is accomplished by forming a surface compressive layer. In such a process the ions of a glass are replaced within a 100μ surface layer with larger ions of a different specie. Because of the high viscosity, modulus of elasticity and relative hardness of silica glasses, conventional salts such as $NaNO_3$, $LiNO_3$, and KNO_3, work very well and can be readily used in different combinations, and at various temperatures to form a lasting compression layer on the glasses surface. The time involved for such treatments can vary from 3 to 5 days. However, phosphate glasses generally have a lower viscosity, modulus of elasticity, and hardness than silicate glasses. The relaxation time for the surface stress generated by such ion exchange processes are far less for phosphate glasses as compared to silicate glasses.

The basic problems encountered when trying to ion exchange a phosphate glass are as follows:

1. Excessive surface attack in molten salts.
2. Extremely low relaxation time and very short time needed to obtain a reasonable exchange.
3. Critically low bath temperatures - as a result of problem number 2 - impose a restricted choice and concentration of salts to be tried.

In order to overcome these problems, phase diagrams (see figure 4.1) of various NO_3^- and Cl^- salt combinations were used to reference which salts would stay molten within the strict temperature range in which the phosphate glass would retain it's surface integrity. In general the bath temperature could vary up to 220°C without excessive attack to the glass surface within a 30 minute treatment. However, the relaxation time is so low for phosphate glass that even at temperatures as low as 200°C the optimum exchange time is in the realm of 5 to 10 minutes (see figure 4.2 for time vs strength).

A doubling in thermal shock resistance of the phosphate glass was obtained by a 5 to 7 minute treatment in $AgNO_3$ and AgCl bath at 225°C. This was not satisfactory though as the Ag^+ ions oxidized, discolored, and blemished the rod surface. This layer could not be cleaned off without also taking the desired compression layer with it. Since an ion as large as the Ag^+ ion could indeed replace the Li^+ ion in the phosphate glass matrix, the Tl^+ and Cs^+ ions were also tried. A bath of $TlNO_3$ was used to treat Q-98 and Q-88 at various times and temperatures. The results were good for the Q-88 in a treatment for 2-5 minutes at 220-270°C but negligible for Q-98. Similar results were found for Q-98 and Q-88 in a $CsNO_2$-$LiNO_3$-$NaNO_3$-KNO_3 bath at 200°C for 10 minutes. Later it was found that a small amount of iron contamination had produced this effect. Most of the various samples tested were subjected to some degree of surface attack. After treatment, the rods which retained the 12μ or polished finishes with which they started, had very thin layers of compression. (less than .001".)

Buffers were added to the molten salts in an attempt to decrease the surface attack and increase the time of treatment and subsequent compression layer thickness. Again the choice of these different buffers was limited due to the solubility and temperature restraints already imposed. Most of the phosphate base buffers were insoluable or decomposed. One suspects that though silicate base buffers work well for the ion exchange of silicate glasses, the reaction mechanisms are not the same in the cases of phosphate ion exchange.

The $TlNO_3$ produced the best results, but only for phosphate glass which contains better than 20 mole % Li_2O. Although Thallium is quite expensive and very poisonous, its ion exchange abilities have some promise. Cesium is another cation which should be further investigated. The most astonishing find was that small amounts of Fe^{++} have a quite positive effect. This should definitely be looked into further. Small amounts on the order of a few ppm should be tried using various Fe^{++} compounds. There is a critical point where the Fe^{++} concentration will have no effect.

Promising Avenues of Future Investigation

Ion Exchange in Non-Molten Salt Mixtures

The restrictive temperature range involved when using molten salt mixtures led to the investigation of other mediums for ion exchange. A series of tests were performed on phosphate glass involving water, DMSO, and ethylene glycol in various combinations with Cs^+, Tl^+, Kg^+, Na^+, and Li^+ salts. The high reactivity of phosphates with water, and the added working temperature range made possible by DMSO and ethylene glycol makes this another avenue of research.

Ethylene glycol is presently used in the cooling systems of many solid state lasers to protect phosphate rods from water degradation. It has a relatively high boiling point of approximately 196^{o}C, and can be used to regulate water phosphate reactions.

DMSO, (Dimethylsulfoxide), (BP $\cong$ 189^{o}C) is miscible in both water and ethylene glycol, and has a noted ability to tie up the single valent cations we are trying to exchange.

$CsNO_3$ and $TlNO_3$ and some other salts have a pronounced ability to interfer with water phosphate reactions.

Coatings Applied by Sol-Gel Process

Another prospect appears to lie in the use of alkoxides to form a thin layer of silica glass on a phosphate glass surface. This opens up the possibility of AR coating, improving durability, and strengthening the glass in a single process. A SiO_2 layer can easily be incorporated into the phosphate glass surface by means of a dip coating process which employs tetraethoxysilane. If certain mixed metal alkoxides are used, the surface layer could be strengthened by conventional ion exchange methods. The glass coating which forms at low temperatures, (i.e. 25->100^{o}C) produce a silicon matrix which, when the organics are removed, becomes integrated into the phosphate glass matrix.

Summary

The limitations encountered when ion exchanging phosphate glass, as described on page 2, make the employment of different ion exchange mediums (other than molten salts) an attractive idea. This is not to say that buffers or metal catalysis can't be employed to compensate for the phosphates excessive reactivity in molten salts. The optimum exchange temperature in such processes is so critically low for phosphate glass and the surface attack so excessive that other non-traditional applications of + ions were also taken into consideration.

ADDITIONAL INVESTIGATION RESULTS

Further investigation subsequent to the expiration of this contract has led to the development of an ion exchangeable phosphate laser glass, designated Q-98. Although a complete analysis of Q-98's properties has not yet been undertaken, initial test results exhibit a five fold increase in rupture strength over Q-100. This increase in rupture strength was gained while sacraficing only 10% in efficiency and only a slight reduction in athernal properties.

Appendix

$NaNO_3$ $TlNO_3$

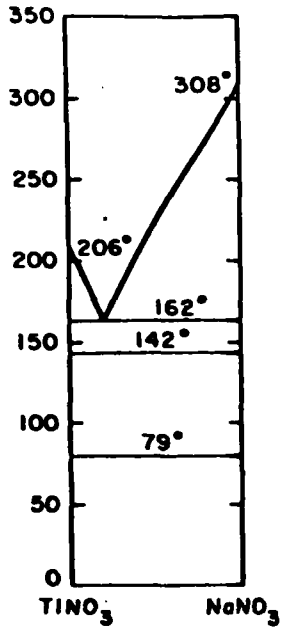

FIG. 1054.—System $NaNO_3$–$TlNO_3$.

C. van Eyk, *Z. physik. Chem.*, 51, 731 (1905).

KNO_3-$LiNO_3$-$NaNO_3$

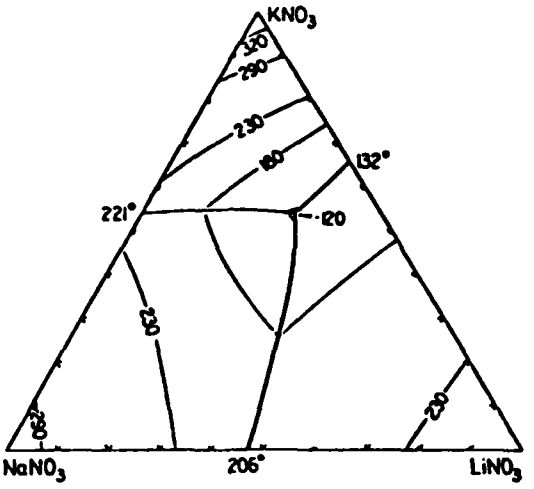

FIG. 1069.—System KNO_3–$LiNO_3$–$NaNO_3$.

H. R. Carveth, *J. Phys. Chem.*, 2, 216 (1898).

KNO_2-$NaNO_2$

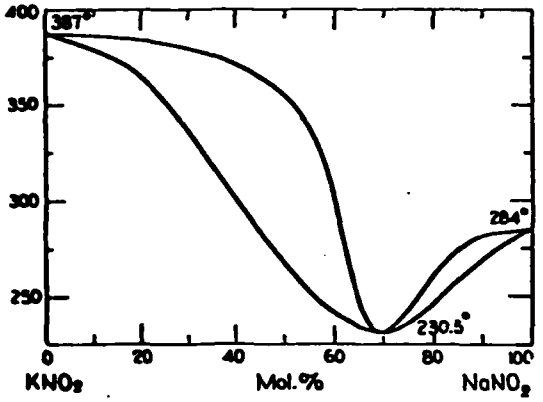

FIG. 1077.—System KNO_3–$NaNO_3$.

Von J. Ettinger, *Z. anorg. u. allgem. Chem.*, 206, 262 (1932).

$NaNO_2$-KNO_3

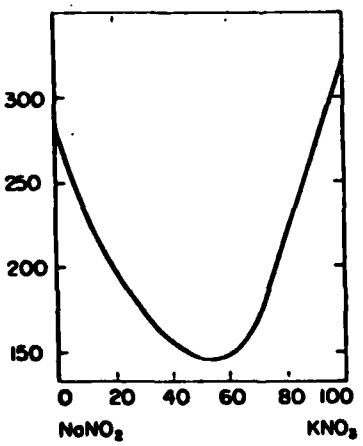

FIG. 1080.—System $NaNO_3$–KNO_3.

Kaoru Sakai, *Bull. Chem. Soc. Japan*, 27, 463 (1954).

Chlorides Only

KCl-$ZnCl_2$

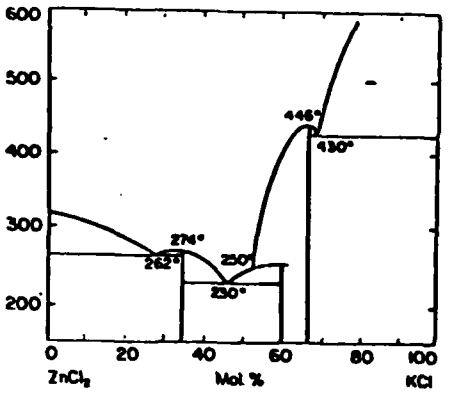

FIG. 1273.—System KCl–$ZnCl_2$.

Ya A. Ugai and V. A. Shatillo, *J. Phys. Chem. U.S.S.R.*, 23 [6] 745 (1949). See also F. R. Duke and R. A. Fleming, *J. Electrochem. Soc.*, 104, 253 (1957.)

Figs. 1063-1066

(b) Three Nitrates

$AgNO_3$-KNO_3-$TlNO_3$

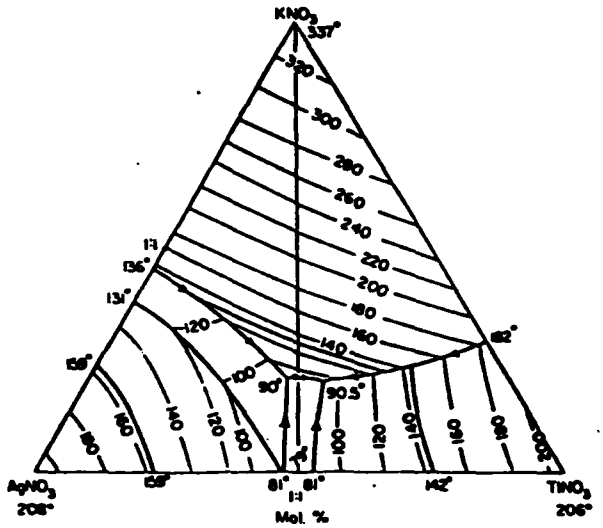

FIG. 1063.—System $AgNO_3$-KNO_3-$TlNO_3$.

V. A. Palkin, *Doklady Akad. Nauk S.S.S.R.*, 66, 72 (1949).

$AgNO_3$-$NaNO_3$-$TlNO_3$

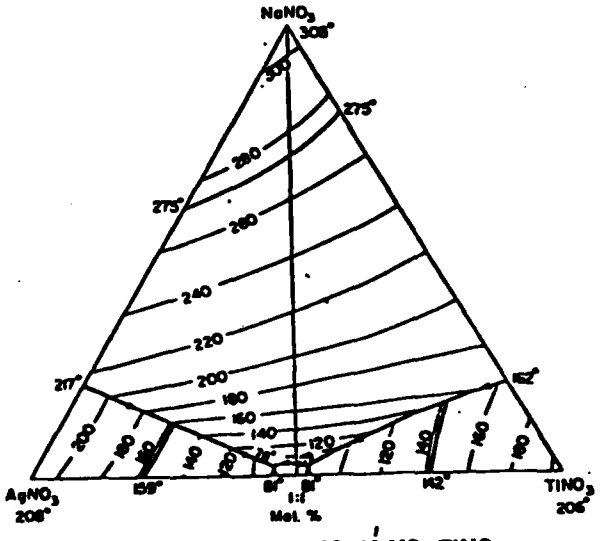

FIG. 1066.—System $AgNO_3$-$NaNO_3$-$TlNO_3$.

V. A. Palkin, *Doklady Akad. Nauk S.S.S.R.*, 66, 651 (1949).

Figure 4.1 (Cont'd.)

KCl-$AlCl_3$

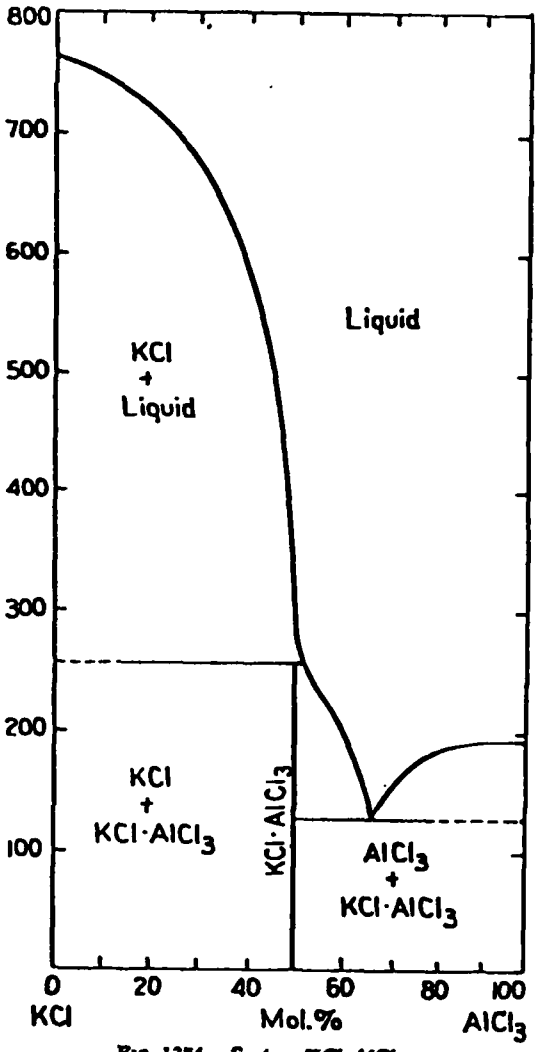

FIG. 1274 System KCl-$AlCl_3$.

U. I. Shvartsman, *J. Phys. Chem. (U.S.S.R.)*, 14, 254 (1940).

$AgCl$-$AgNO_3$

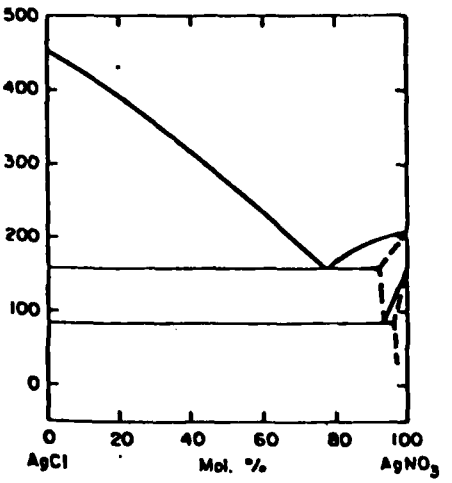

FIG. 1744.—System $AgCl$-$AgNO_3$.

Giuseppe Scarpa, *Atti reale accad. Lincei, Ser. II*, 22, 457 (1913).

Figure 4.2

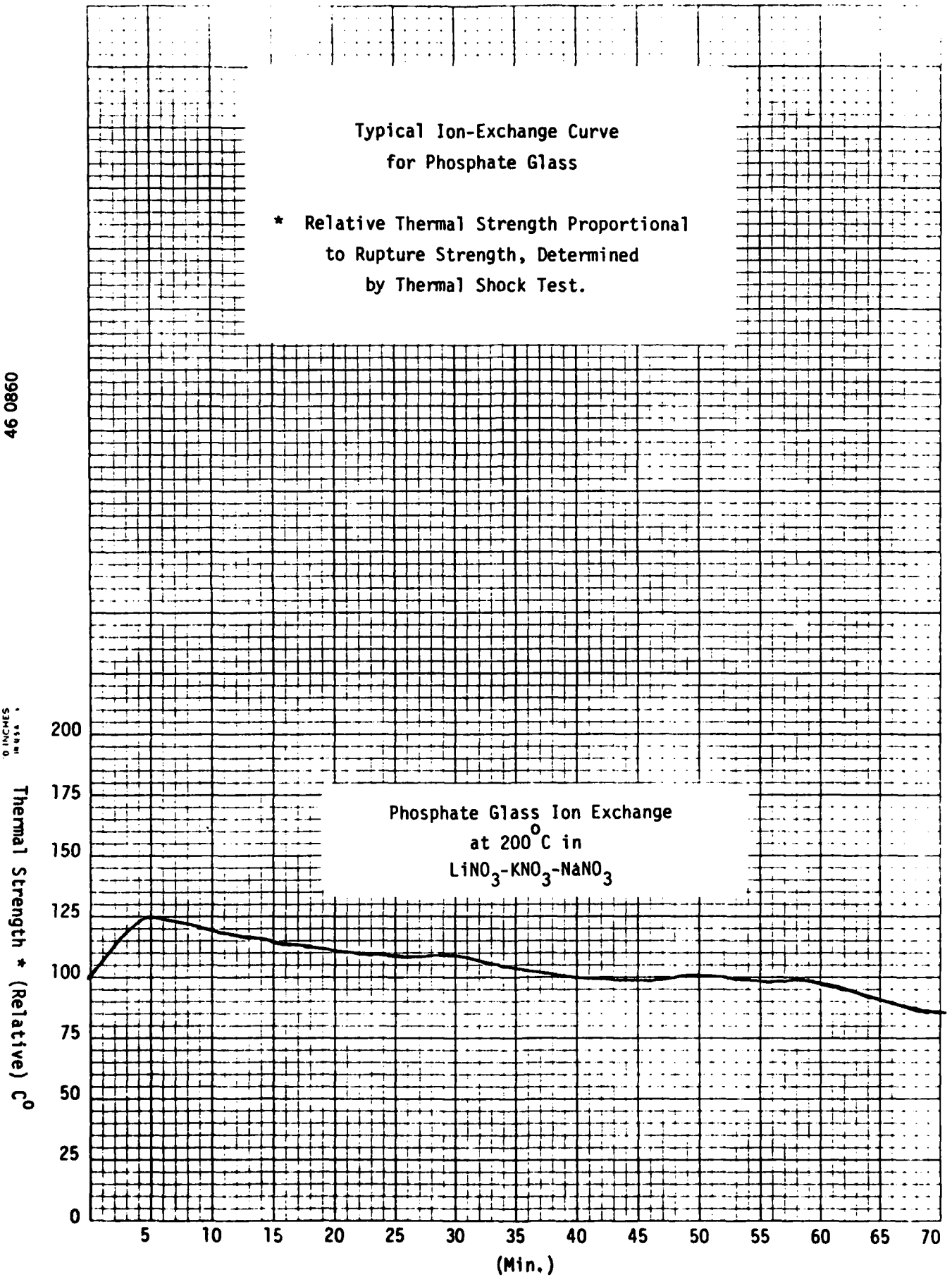

Figure 4.2

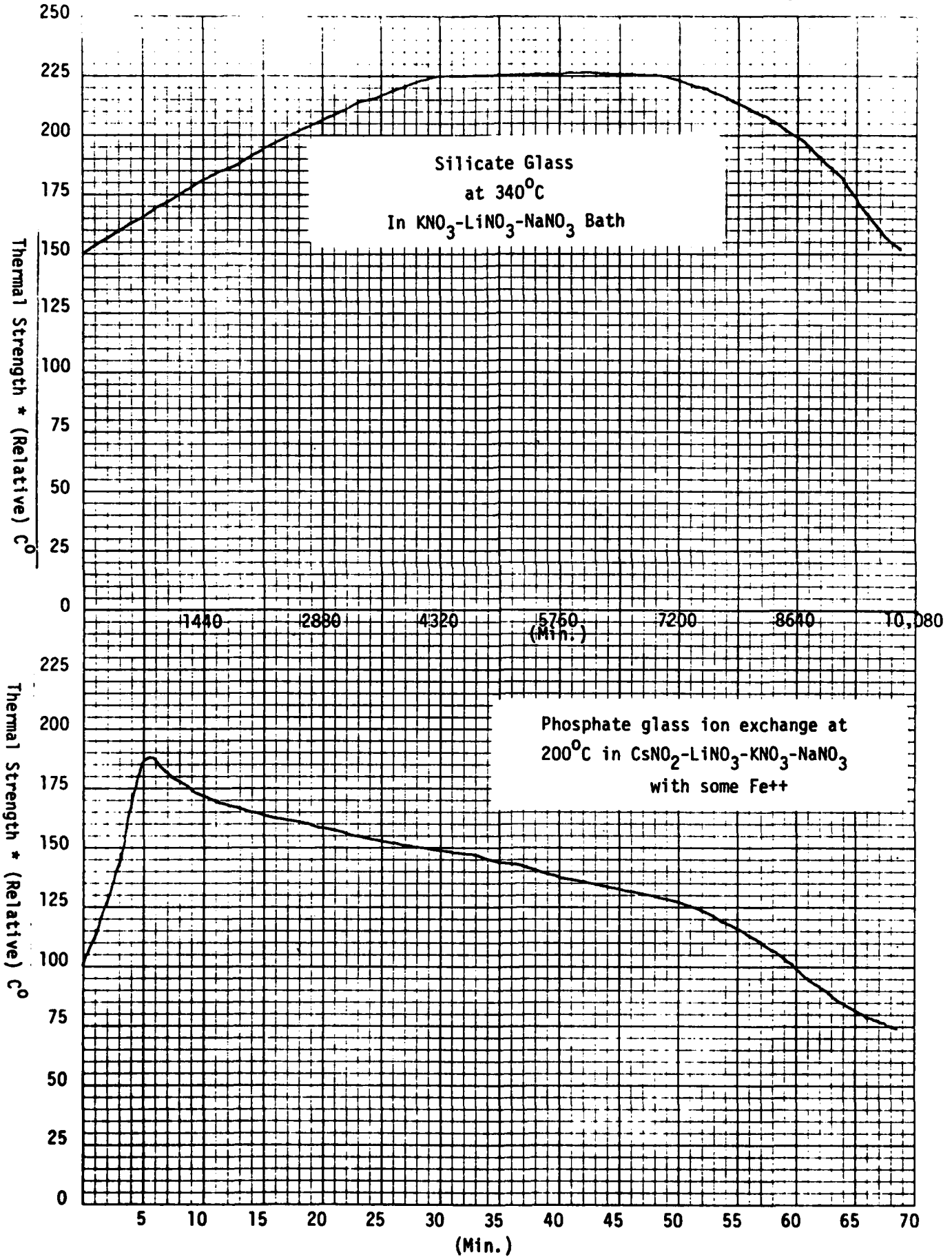
Silicate Glass
at 340°C
In KNO3-LiNO3-NaNO3 Bath
Thermal Strength * (Relative) C°
250
225
200
175
150
125
100
75
50
25
0
1440
2880
4320
5760
(Min.)
7200
8640
10,080
Phosphate glass ion exchange at
200°C in CsNO2-LiNO3-KNO3-NaNO3
with some Fe++
Thermal Strength * (Relative) C°
225
200
175
150
125
100
75
50
25
0
5
10
15
20
25
30
35
40
45
50
55
60
65
70
(Min.)

TASK V

Alternative Pump Sources

TASK V

Alternative Pump Sources

Introduction and Summary

After reviewing available literature on solid state laser pump sources, the only available alternative to Xenon flashlamps were cerium doped Krypton flashlamps.

At lower power levels, the Krypton flashlamp displayed a slightly better efficiency than the Xenon flashlamp probably due to a better overlap between the Krypton flashlamps line radiation and the Neodymium absorption spectrum.

At higher power levels the Xenon flashlamp exhibited a slightly better efficiency due to its ability to convert electrical energy to black-body radiation. Graps of input versus output for the Xenon and Krypton lamps are given in figure 5.1.

The Krypton lamp appeared to have a longer life with less fall-off, but did not improve overall efficiency.

Our findings seem to collaborate those made by ILC Technology of Sunnyvale, California. More elaborate research on this task was prevented by a lack of available funding.

Figure 5.1

FLASHLAMP

Test Data

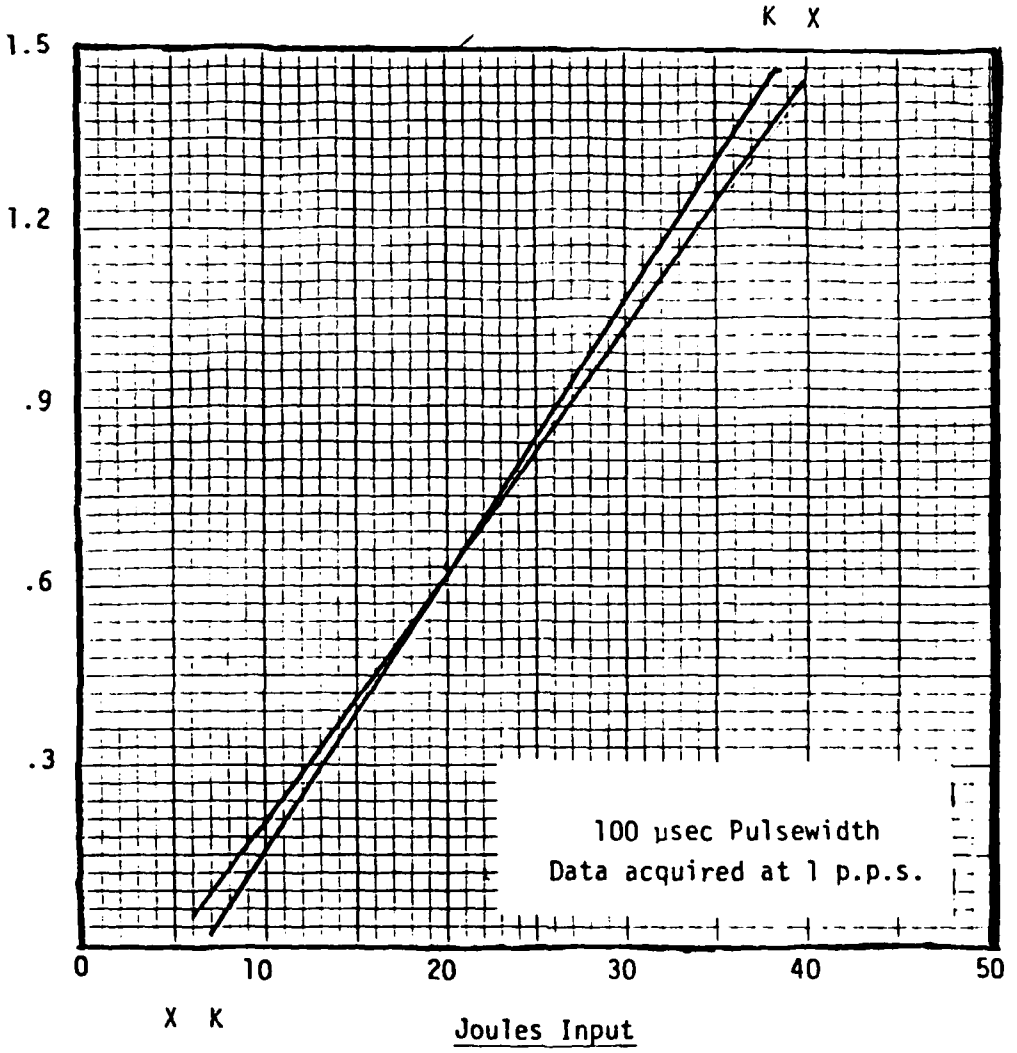

Rod: 1/4 x 3 1/4, Q-100, No Coatings

Output: 55% Reflector

Cavity: Kigre, Silver-Coated Ellipse

Coolant: H_2O

X: Xenon Flashlamp

K: Krypton Flashlamp